The Dissertation Committee for Shaoping Lu Certifies that this is the approved version of the following dissertation:

An Inverse Model Study of Abrupt Climate Change during Last Ice Age

Committee:

Charles S Jackson, Supervisor

Wendell Horton, Co-Supervisor

Harry L Swinney

Ernst-Ludwig Florin

Terrence M Quinn

An Inverse Model Study of Abrupt Climate Change during Last Ice Age

by

Shaoping Lu, B.S.

Dissertation

Presented to the Faculty of the Graduate School of

The University of Texas at Austin

in Partial Fulfillment

of the Requirements

for the Degree of

Doctor of Philosophy

The University of Texas at Austin

December, 2010

Dedication

To my parents

Acknowledgements

I have been enjoying my past six years of studying, working and living in Austin. I wish to thank my research supervisor Dr. Charles Jackson for getting me started on my PhD research and his selfless support to my research. Also, I would like to thank my academic supervisor Dr. Wendell Horton for his supervision and guidance of my education. Many thanks to the committee for their comments and review of my work.

I would like to thank Yurun Liu, Dr. Lindsey Gulden, Dr. Michael Tobis, Dr. Robert Scott, Dr. Brian Arbic and Dr. Frederick Taylor for the very helpful discussion in my research and friendship.

I want to thank Dr. Chaoshun Hu, Dr. Chunlei Chu, Dr. Tiancong Hong, Dr. Long Jin, Dr. Yang Liu, Siwei Li, Yi Tao, Xiaolei Song, Erick Leuro, Kun Yuan and all of my friends from ACCCF and USTC for their friendship and help. I am also thankful to Tongcang Li, who was my roommate through my graduate student life in the University of Texas.

My special thanks go to Dr. Mrinal Sen, Dr. Sergey Fomel, Dr. Alejandro Valenciano and Dr. Dan Whitmore who get me started on my career in petroleum industry as a Research Geophysicist.

The dissertation is dedicated to my parents for their love, encouragement and support.

An Inverse Model Study of Abrupt Climate Change during Last Ice Age

Publication No._____

Shaoping Lu, Ph.D

The University of Texas at Austin, 2010

Supervisor: Charles S Jackson

Co-Supervisor: Wendell Horton

Geologic records and climate model simulations suggest that changes in the meridional heat transport in the Atlantic Ocean were involved in the abrupt warming events – the so-called Dansgaard-Oeschger Interstadials (DOIs) – that punctuated an otherwise cold Greenland climate during the last glacial period. However, the role of Northern Hemisphere (NH) ice sheets in these events remains a subject of controversy. Here we report on the first attempt to combine quantitatively a paleo-temperature proxy with simplified ocean models, with the specific purpose of extracting information about the changes in mass balance of the NH ice sheets during the last glaciation. A Greenland paleotemperature record is combined with the climate models using Bayesian Stochastic Inversion (BSI) in order to estimate the changes that would be required to alter the Atlantic Ocean mass and heat transports between ~30 and 39 thousand years ago. The mean sea level changes implied by changes in NH ice sheet mass balance agree in

amplitude and timing with reconstructions from the geologic record, which gives some support to the freshwater forcing hypothesis. Our results are unaffected by uncertainties in the representation of vertical buoyancy transport in the tropical ocean, in large part because the global adjustments to high latitude freshening bypass the tropics and affect sinking rate in the opposite pole. However, the solutions are sensitive to assumptions about physical processes at polar latitudes. We find that the inversion reproduces the gradual changes in sea level and Antarctic temperature inferred from the independent evidence provided by proxy records. The Greenland warm event lasting over 3000 years (DOI 8) can be explained by sustained growth of NH ice sheet and reduced supply of icebergs to the North Atlantic. Our results indicate a more involved role of the NH ice sheets than previously thought, in which both collapse and subsequent growth would be required to explain the full series of the long (> 3000 years) warm events recorded in Greenland ice.

Table of Contents

List of Tables

List of Figures

Chapter 1 Introduction

1.1 Description of the problem

A fascinating problem in the physics of climate is the origin of the rapid climate changes of the last ice age. Paleotemperature records from Greenland ice cores (Figure 1.1) document a series of warm phases ("interstadials") that punctuated the background of glacial climate ("stadials") [*Dansgaard et al., 1982; Oeschger et al., 1984; Johnsen et al., 1992*]. The warm phases are frequently referred to as "Dansgaard-Oeschger" interstadials (DOI). The warming leading to DOIs was estimated to be 7-16^{o}C and occurred within a span of a few decades [*Johnsen et al., 1992; Severinghaus et al., 1998; Severinghaus and Brook, 1999; Lang et al., 1999*]. Sixteen DOIs have been identified during the marine isotope stage (MIS) 3 between 24.1-59.0ka BP, each of which last between 1~3 thousand years [*Johnsen et al., 1992; Dansgaard et al., 1993; according to MIS chronology of Martinson et al., 1987*].

Inferences of forcing to interpret the DOIs have come mainly from the observation, prior to DOIs, of layers of ice rafted debris (IRD) in North Atlantic sediments, such as Heinrich events (Figure 1.2) (for a review see Hemming [2003]). Heinrich layers consist of continent rocks, which can be easily distinguished from normal marine sediments (Figure 1.3). These continent rocks get incorporated into icebergs. They were presumably expelled from the Laurentide ice sheet during a period of ice sheet instability [*Alley and MacAyeal,* 1994; *MacAyeal,* 1993] (*The Laurentide Ice Sheet was a massive sheet of ice that covered hundreds of thousands of square miles, including most*

of Canada and a large portion of the northern United States, between 95,000 and 20,000 years before the present day). After the icebergs melted in North Atlantic, the continent sourced IRD got deposited to the ocean bottom and formed the Heinrich layers. In all, there are six Heinrich layers indentified and dated during the last ice age, and all of them deposited during the cold phases right before the major DOIs (Figure 1.2). Details of DO events and Heinrich events will be discussed in section 1.5 of this Chapter.

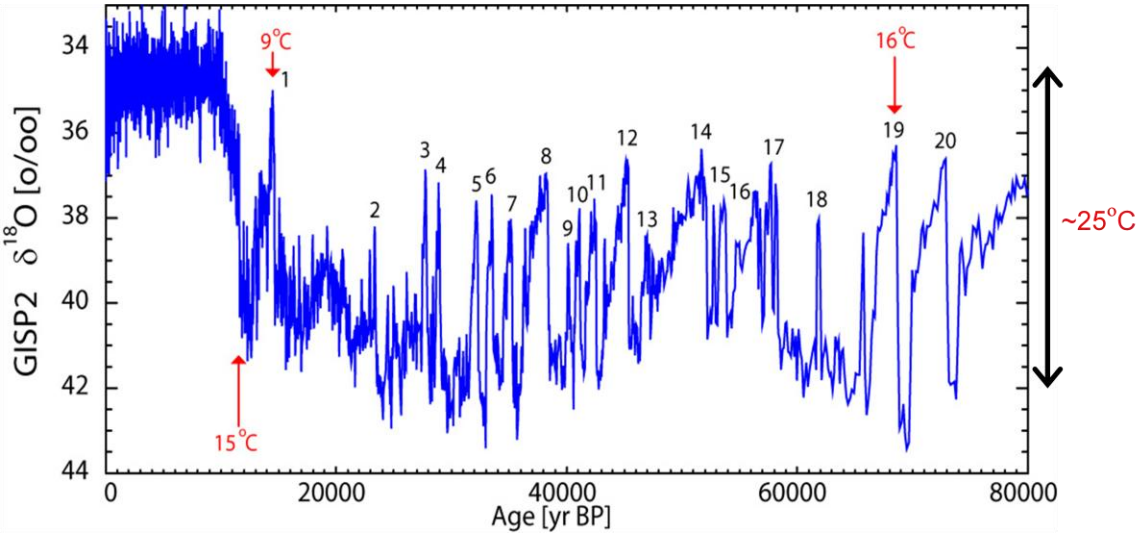

Figure 1.1 *The central Greenland GISP2 $\delta^{18}O$ record for the past 80kyr, interpreted as a proxy for air temperature [Grootes and Struiver, 1997]. DOIs have been numbered and amplitude of specific abrupt warmings estimated from measurements of N2 (+Ar) isotopes in trapped air is indicated [Severinghaus et al. 1998; Severinghaus and Brook, 1999; Lang et al., 1999]. The red numbers indicate warming jumps of 15, 9 and 16 ^{o}C, each within decades.*

1.2 Freshwater forcing hypothesis

From the observational DO events and Heinrich events, the freshwater forcing hypothesis has been proposed to interpret these events. The hypothesis proposes that anomalies in the freshwater supply to the North Atlantic Ocean caused abrupt climate change through their effects on the Atlantic Meridional Overturning Circulation (AMOC) and attendant poleward heat flux.

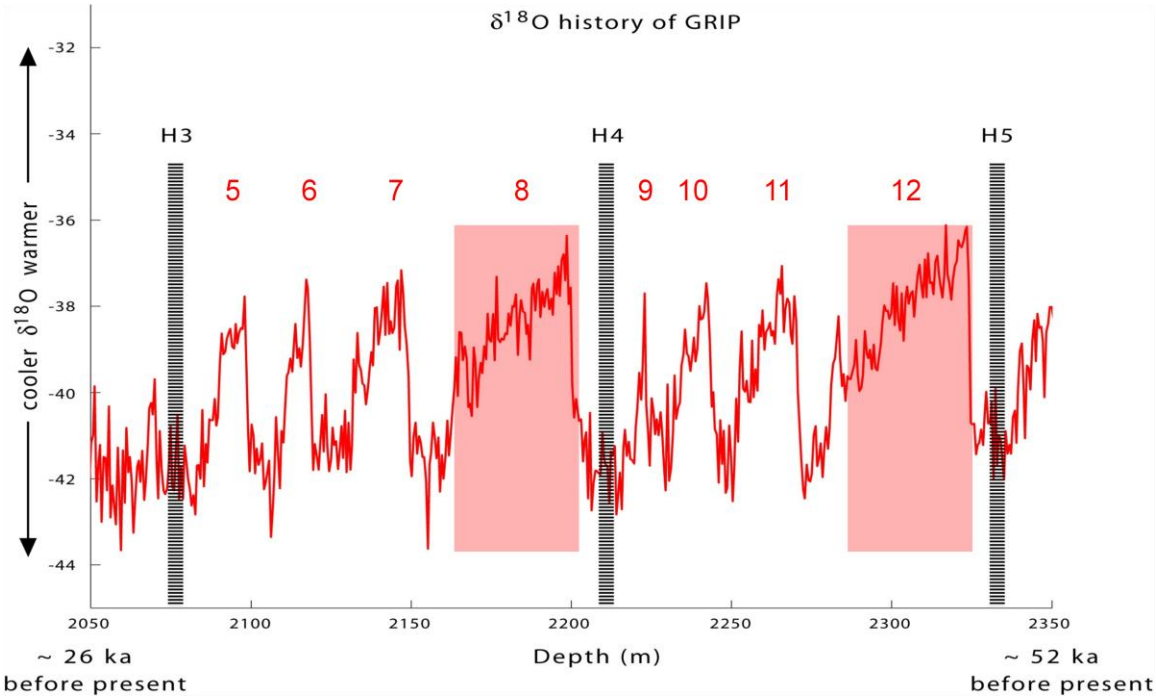

Figure 1.2 *DOIs during 26 ka~52 ka. Black stack bars denote the timing of Heinrich events, all of which were deposited during the cold phases right before the major DOIs (red shadow intervals). The red numbers refer to the DOIs.*

The large scale great ocean circulation pattern is displayed in Figure (1.4). In the Atlantic Ocean, the warm flux goes from south and low latitude to north ocean on the

ocean surface. After releasing heat to the atmosphere in the North Polar area, the salty cold dense water is sinking from ocean surface to ocean bottom. The cold saline current is coming back to south from the deep ocean. Upwelling from deep to surface almost happens everywhere in the Atlantic to close the AMOC. If huge amount of freshwater forcing is imposed into the North Atlantic Ocean, the AMOC would be perturbed.

The freshwater forcing hypothesis has been fueled by results from climate modeling. Panel (A) of Figure 1.5 displays the model simulated AMOC response to freshwater forcing perturbation in North Atlantic (refer to 4-box model in Chapter 2). The climate model exhibits multiple equilibrium circulation states for a given amount of steady freshwater input to the Northern Atlantic.

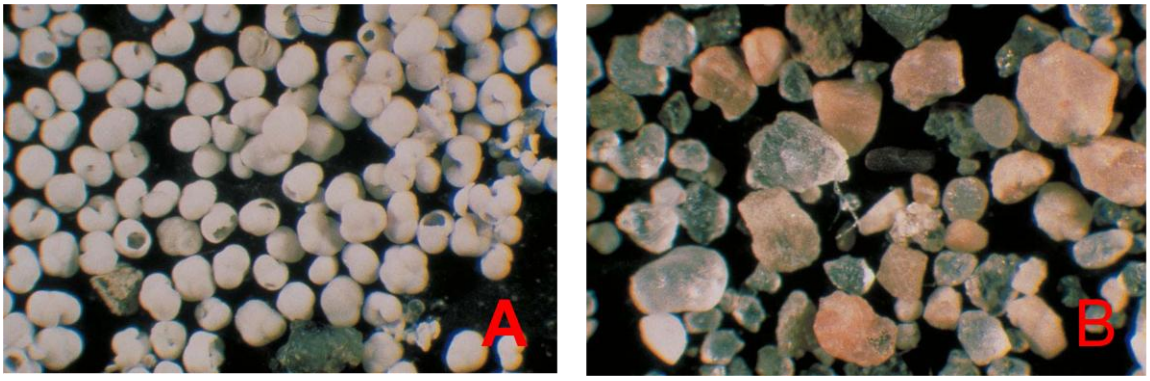

Figure 1.3 *Normal ocean sediments in panel (A); and Heinrich layers of ice rafted debris (IRD) in panel (B) from North Atlantic.*

1.3 Experiment results and conclusions

In the following chapters, I shall test the freshwater forcing hypothesis by inferring the timing and amount of ice sheet melt that would be required to reproduce the Greenland record of abrupt climate change. These solutions will be compared against multiple indicators of sea level change (which indicate the total mass of continental ice) as well as climate proxy records from Antarctica. My results show the importance of Northern Hemisphere ice sheet growth to sustain the long period of Greenland warmth.

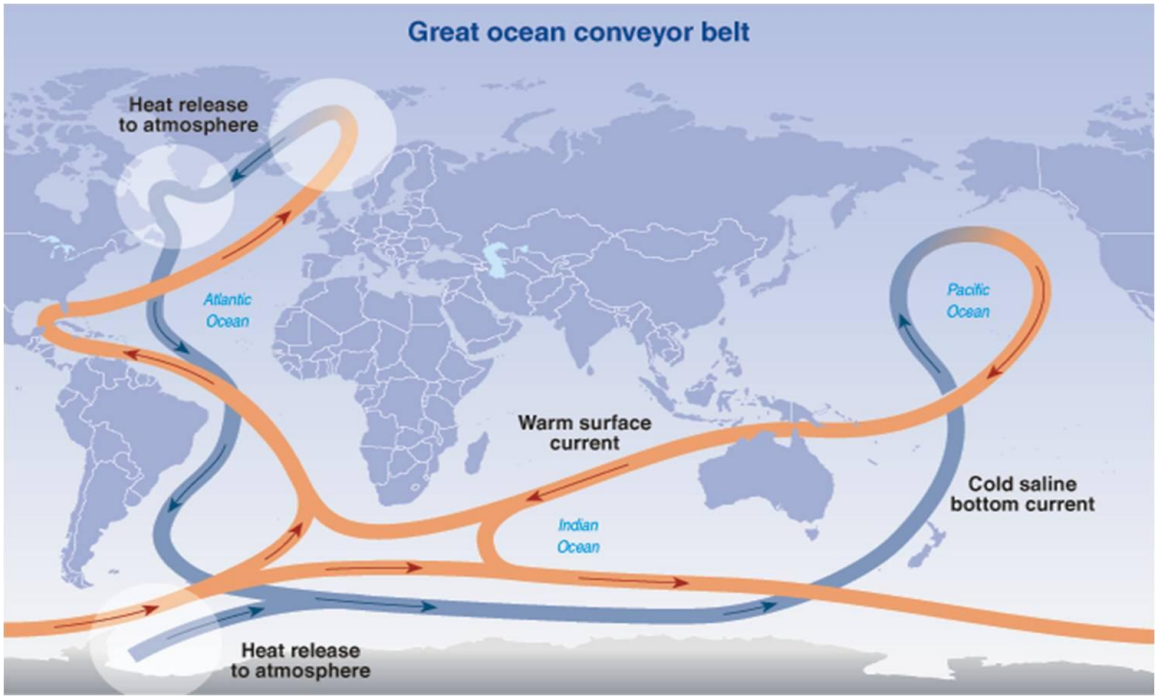

Figure 1.4 *Great ocean conveyor belt, [NRC 2002 summary of Broecker, 1991].Directions of warm surface current (orange) and cold current (blue) are denoted using arrows.*

This conclusion is significant. Without the inversion experiments, one way presume from the comparison of the model simulation (panel A) and observational DOIs (panel B) in Figure 1.5, that the climate system is a dual-mode system having a warm phase and a cold phase. In this view ice sheets are important as a trigger to flip the system from one state to the other. However, conclusion from inversion experiments emphasize the fact that the abrupt climate change DO events need to be maintained by a constant forcing: Northern Hemisphere continental ice sheet growth sustains warm periods, ice sheet retreat sustains cold periods. This conclusion contradicts to the general view of ice sheet melting due to warmth.

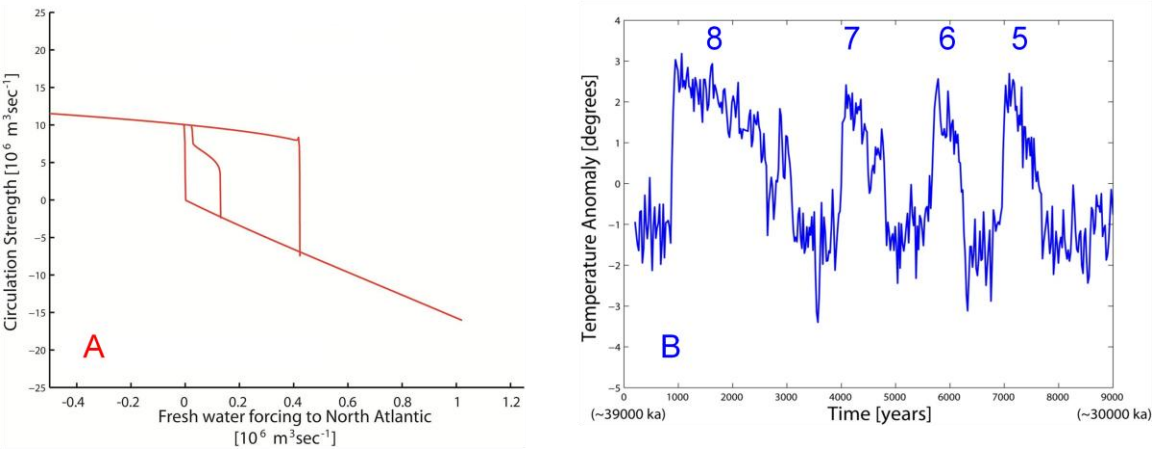

Figure 1.5 *(A) 4-box model simulated Atlantic Ocean Meridional Overturning Circulation response to freshwater forcing perturbation in North Atlantic. (B) Observational North Atlantic sea surface temperature anomaly during 30ka~39ka. The blue numbers refer to the DOIs.*

Two papers have been submitted from Chapter 2 [*Jackson et al. Paleoceanography*] and Chapter 4 [*Lu et al. Paleoceanography*]. A third paper is being prepared from the material in Chapter 3 for a submission [*Lu et al. Tellus A*].

1.4 Inversion approach of solving abrupt climate change problem

The observations and modeling results that exist do not provide an unambiguous interpretation of the origin of abrupt climate change. These data and models may be interpreted in potentially contradictory ways. As hypotheses concerning the origin of abrupt climate change accumulate, there is an increasing need to synthesize data and to develop methods for assessing their strengths and inconsistencies. Understanding the mechanisms of abrupt climate change is particularly challenging because of the uncertainties in the paleoclimate observations and in our knowledge of the physics of the climate system. Among the techniques that can be used to combine noisy observations with incomplete knowledge of a physical system are so-called inverse methods. In particular, Bayesian stochastic inversion (BSI) provides a way to account for the uncertainties in data and models and deal with the possibility of multiple solutions (inferences). Most notably, it can re-express the problem of abrupt climate change in terms of its implications for what we should see in observations if models provide adequate representation of the processes that exist in nature.

In Chapter 2, BSI is applied to a highly idealized "4-box" model of the ocean's meridional overturning circulation in order to estimate the changes in global sea level

implied by the combination of a Greenland ice core paleotemperature record during the last glacial period. This study allows us to investigate the effects of different assumptions concerning the importance of high latitude buoyancy forcing and low latitude vertical mixing processes on the meridional overturning circulation (MOC). These changes are then compared to changes in global sea level inferred from independent geologic records. The comparison provides a test of the consistency between the various datasets and a test of the hypothesis that anomalies in the freshwater supply to the North Atlantic Ocean caused abrupt climate change through their effects on the ocean meridional overturning circulation (MOC) and attendant poleward heat flux (freshwater forcing hypothesis).

In Chapter 3, I examine the 4-box model's transient adjustment progress by breaking the governing equations into a sum of component contributions to understand why the inversion solutions found in Chapter 2 are independent of uncertainties in the treatment of vertical mixing in the low latitude ocean and to interpret the freshwater forcing inversion experiments that favor the seemingly more fragile symmetric modes. Results from transient experiments show that the asymmetric circulation configuration is not plausible because either it can't sustain a reduced MOC circulation during phases of enhanced ice melt as is observed in paleo data (in northern sinking case), or it requires unreal amount of freshwater forcing (corresponding to ~120 meters sea level change) (in southern sinking case). For the most part, the importance of vertical mixing in low latitude ocean is not apparent in the 4-box model's transient behavior. This shows an inherent limitation of paleo data to help us test uncertainties of low latitude vertical

mixing physics in the real ocean.

In Chapter 4, I repeat the inversion but with a more complete model of the ocean's MOC. A Greenland paleotemperature record during the last glacial period is combined with a simple climate model (Bern model) using Bayesian Stochastic Inversion in order to estimate the changes in mass balance of the NH ice sheets that would be required to alter the Atlantic Ocean mass and heat transports. The implied changes in NH ice sheet mass balance and SH air temperature are then compared to independent evidence provided by proxy records of sea level and Antarctic air temperature. I find that the inversion reproduces the gradual changes in sea level and Antarctic temperature inferred from these records. Our results indicate a more involved role of the NH ice sheets than previously thought, in which both collapse and subsequent growth would be required to explain the full series of the long (> 3000 years) warm events recorded in Greenland ice.

1.5 Interpretations of Dansgaard-Oeschger Interstadials

Dansgaard-Oschger Interstadials (DOIs) are a series of apparent warm intervals first documented in Greenland ice core records that initiated abruptly and punctuated an otherwise cold glacial period during the last ice age. Interpretations of the origins and factors responsible for the DOIs has followed two tracks, 1) the refinement of observations of DOIs and 2) the development of models of physical processes perceived to be important to these events, particularly of the MOC in the Atlantic Ocean. Our

objective here is to make use of Bayesian stochastic inversion (i) to synthesize observational constraints on the freshwater forcing hypothesis for the origin of the DOIs, (ii) to document the effects of uncertainties in the representation of vertical mixing in the ocean which previous studies have shown to play a role in the stability of the MOC, and (iii) to estimate the uncertainties in mass balance of the NH ice sheets during the last glaciation inferred from observational paleoclimate records.

Our choice to focus on the freshwater forcing hypothesis to explain the DOIs in the Greenland record stems from numerous lines of observational evidence and model studies that invoke the susceptibility of the MOC in the Atlantic Ocean to glacial meltwater discharges from NH ice sheets [*Stouffer et al.*, 2006]. These lines of evidence are reviewed in the next section. There are significant uncertainties in each line of reasoning that leave open the interpretation that best explains abrupt climate change. Although I assume for testing purposes that the Greenland data primarily reflect changes in oceanic heat transport, we acknowledge that other components of the climate system could be important [*Wunsch*, 2003, 2006]. Other influences could include, for example, the changing size and shape of the Laurentide ice sheet [*Jackson*, 2000; Meissner et al., 2002], remote "teleconnections" to the tropical Pacific [*Cane*, 1998; *Cane and Clement*, 1999], and atmosphere-sea ice coupling [Gildor and Tziperman, 2003; Eisenman et al. 2009]. By making the assumption that the Greenland data solely reflect changes in ocean heat transport, we are likely ascribing too much of the observed variability to this single

mechanism. The calculation will merely suggest the extent to which observed DOIs can reasonably be related to the forcing and the physics included in our inversion.

1.5.1 Observational perspective

Abrupt warmings above Greenland during the last glacial period have first been postulated from ice core records of the oxygen isotopic composition ($\delta^{18}O$) of the ice and later supported by measurements on the isotopic composition of entrapped air [*Severinghaus and Brook,* 1998; *Lang et al.,* 1999; *Huber et al*., 2006]. A synthesis of the spatial extent of abrupt climate changes during this period is given by Voelker [2002]. Correlations with observations from marine sediments, such as the relative abundance of fossil shells of planktonic foraminifera and their oxygen isotopic composition, would suggest that the ocean was changing in concert with Greenland events, but with half the amplitude most likely due to feedbacks involving sea ice [*Bond et al.,* 1993; *van Kreveld et al.,* 2000; *Weinelt et al.,* 2003].

Inferences of forcing have come mainly from the observation, prior to DOIs, of layers of ice rafted debris (IRD) in North Atlantic sediments, such as Heinrich events (for a review see Hemming [2003]). This observation would fit the long-held notion that the MOC in the Atlantic Ocean could be reduced or even shut down if a sufficient amount of freshwater is supplied at the surface in the North Atlantic [*Broecker et al.,* 1990; *Clark et al.,* 2002].

Sudden changes in ice rafting inferred from paleoceanographic records are generally thought to reflect the evolving conditions of an ice sheet at its base, a place that is well insulated from external forcings. This has led some authors to postulate that DOIs originate from internal instabilities of the ice sheets that surrounded the North Atlantic Ocean [*MacAyeal,* 1993]. However, the apparent coordination of multiple ice sheets has called this hypothesis into question [*Bond and Lotti,* 1995], with the observed IRD record potentially explained as a response to observed climate variations [*Marshall and Koutnik*, 2006]. The significance of IRD layers in North Atlantic sediments remains unresolved in part because the presence or absence of IRD may have more to do with the mechanisms by which an ice sheet packages debris into bergs than it does about coastal berg production rates [*Alley and MacAyeal*, 1994; *Hulbe,* 1997; *van Kreveld et al.,* 2000].

Important sets of observations in this regard are records of relative sea level based on surface-dwelling corals [e.g., *Chappell,* 2002; *Thompson and Goldstein,* 2006], $\delta^{18}O$ records from deep sea sediments [*Waelbroeck et al.,* 2002], and $\delta^{18}O$ records from the Red Sea [*Siddall et al.,* 2003]. Reefs from the Huon Peninsula suggest that millennial scale changes in sea level were mainly coincident in time with Heinrich events [*Chappell,* 2002]. The largest Heinrich events are associated with a sea level rise in excess of 10 m, which is larger than the minimum sea level change of $\pm$ 3 m that may be theoretically resolvable by coral records [*Chappell,* 2002]. On the other hand, there is a lack of evidence, at least at the Huon Peninsula, and indeed from the other reconstructions as well, that non-Heinrich related DOIs were associated with significant changes in sea

level. Corals likely have the smallest uncertainties on past sea level and may be well constrained in terms of age, however, only a few observations exist.

The suggestion that changes in ocean circulation played a role in DOIs would be supported by other records from marine sediments. For example, records of benthic foraminiferal $\delta^{13}C$ suggest that the proportion of water masses from the northern North Atlantic and the Southern Ocean has varied during the last glaciation [e.g., *Curry et al.*, 1999]. Important changes in deepwater $\delta^{13}C$ can be simulated from changes in the MOC in the Atlantic Ocean [*Marchal et al.*, 1998, 1999a,b]. It has been difficult to draw a definitive picture of circulation changes from benthic $\delta^{13}C$ records [*Boyle*, 2000]. The events that are best recorded are those associated with massive IRD layers originating from the Laurentide ice sheet [*Boyle*, 2000]. This raises the question of how climate events in Greenland with apparently similar amplitude could result from different freshwater forcings (as suggested by coral records of sea level) and be associated with different water mass distributions in the deep Atlantic (as suggested by benthic $\delta^{13}C$ records).

1.5.2 Modeling perspective

The existence of multiple equilibria in ocean models provides support to the idea that the MOC must be playing a key part if not the dominant role in DOIs [for a review see *Weaver and Hughes*, 1992]. These models have demonstrated that the ocean can suddenly make rapid transitions from one equilibrium state to another given a change in surface freshwater balance. This behavior is apparent when the equilibrium strength of

the MOC is examined as a function of the strength of freshwater forcing. The corresponding hysteresis curve shows that the MOC can exhibit different states for the same transient or near-stationary forcing (e.g. Figure 2.2). These curves, however, do not give the whole sense of the non-linear behavior of the MOC, as they only describe a set of equilibrium states. For instance, model experiments have shown that the MOC is also sensitive to the rate of change of freshwater forcing [e.g., *Manabe and Stouffer*, 1994; *Marchal et al.*, 1999b; *Lucarini and Stone*, 2005a, 2005b].

Characterizing the sensitivity of ocean models to freshwater forcing is an important research topic, not only because of interest in past climate change, but also because of its potential relevance for global warming. Model studies show that the shape of the hysteresis curve that describes a model's sensitivity to high latitude freshwater input depends on a variety of factors such as i) assumptions about buoyancy mixing in the ocean [*Manabe and Stouffer*, 1999; *Schmittner and Weaver*, 2001], ii) the location where freshwater anomaly is introduced to the ocean [e.g. Saenko et al., 2007], and iii) the processes controlling the fluxes of heat and momentum at the sea surface [e.g., *Mikolajewicz and Maier-Reimer*, 1994; *Toggweiler and Samuels*, 1998; *Wunsch and Ferrari*, 2004]. The latter is particularly important to understanding why the MOC in the Atlantic Ocean may have behave differently during glacial epochs [*Ganopolski and Rahmstorf*, 2001; *Schmittner et al.*, 2002]. Also some, but not all, models are able to maintain a reduced state of the MOC without a persistent source of freshwater to the North Atlantic [*Stouffer et al.*, 2006]. The equilibrium solutions of coupled AOGCMs

appear to only be temporarily stable because of diffusive processes that undermine the reduced MOC state [Liu et al. 2009].

1.6 Methods

In this section I describe our strategy for testing the freshwater forcing hypothesis using Bayesian stochastic inversion. A 4-box model of the Atlantic Ocean is combined with a paleo-temperature record from a Greenland ice core in order to estimate a time series of freshwater flux anomaly in the North Atlantic and the attendant changes in the meridional transport of mass and heat, which would be required to explain a series of DOIs from 30 to 39 kyr B.P. The freshwater flux anomalies are converted into anomalies of global sea level, which are then compared with independent evidence from the geologic record. This exercise is repeated with different assumptions about vertical mixing in the model in order to address its influence of the response of ocean circulation to freshwater forcing [e.g., *Nilsson and Walin*, 2001]. Then a zonally averaged climate model including seasonality [Bern model Schmittner and Stocker, 2001] is used to estimate the time series of freshwater flux anomaly in the North Atlantic required to sustain the observational DOIs from 34 to 39 kyr B.P. The implied changes in NH ice sheet mass balance and SH air temperature are then compared to independent evidence provided by proxy records of sea level and Antarctic air temperature.

1.6.1 Bayesian Stochastic Inversion

Stochastic inverse modeling using Bayesian inference is a tool to interpret observational data in the presence of a model [*Gelman et al.*, 2004]. In particular it estimates the probability distribution of a forcing which permits a model to reproduce what is observed. It should be understood at the outset, however, that the solution is expressed as a conditional probability, meaning that all probability measures are relative to the best forcing identified to explain the data.

For instance, the time series of freshwater forcing that permits a climate model to reproduce a paleoclimate record from a Greenland ice core may be inferred by stochastically testing various forcing functions (scenarios) and quantifying the relative likelihood of each solution through a measure of model-data mismatch. Markov Chain Monte-Carlo (MCMC) provides sampling rules that both ensures sampling is not biased towards a particular region of solution space and improves efficiency by avoiding regions that are unlikely to provide an acceptable match to the Greenland data. However, standard MCMC approaches to stochastic inversion tend to be inefficient or impractical for applications that are computationally expensive. The solution to this challenge has been to create a statistical model of the physics-based numerical model, also called a "statistical emulator", which approximates the numerical model based on a limited number of sensitivity experiments [e.g. *Kennedy and O'Hagan,* 2001; *Higdon et al.*, 2004].

Here I take a different approach by keeping the physics-based model within a stochastic sampling algorithm, but relying on innovations in our sampling strategy for efficiently identifying optimal solutions and quantifying uncertainties. This alternate strategy is particularly useful with complex models, where there are strong non-linearities and multiple solutions are possible. Indeed, with such models, it is very difficult to guarantee that a traditional MCMC-type sampler can provide unbiased sampling [*Villagran et al.,* 2008]. Moreover, the solution may reside in a very narrow portion of solution space. In such cases, it would be very difficult to use Monte-Carlo to consider the problem of abrupt climate change forcing, as the chances of 'guessing' the correct sequence of freshwater forcing history would be extremely small.

The sampling strategy I use is referred to as Bayesian Stochastic Inversion (BSI) based on Multiple Very Fast Simulated Annealing (MVFSA) [*Jackson et al.,* 2004]. The basic idea of MVFSA is to strike a balance between the sometimes separate objectives of identifying the optimal solution, i.e., minimizing the mismatch between data and model on the one hand and estimating the probability distribution of the solutions (which provides information about uncertainties, multiple solutions, and any possible correlations between variables defining the solution) on the other hand. MVFSA proceeds by accumulating statistics about the shape of the solution space through multiple searches for the optimal solution.

1.6.2 Multiple Very Fast Simulated Annealing (MVFSA)

The objective of stochastic inversion using Bayesian inference is to estimate a joint-probability for selecting a set uncertain parameters (e.g. freshwater forcing) that allow a process model to approximate observations within the uncertainty of the observations and model. The result is known as *a posteriori* probability density function (PPD).

$$PPD\left(\mathbf{m} \mid \mathbf{d}_{obs}, g(\mathbf{m})\right) \propto \exp\left[-\frac{1}{2}\left(g(\mathbf{m})-\mathbf{d}_{obs}\right)^{T}\mathbf{C}_{noise}^{-1}\left(g(\mathbf{m})-\mathbf{d}_{obs}\right)\right]\cdot prior(\mathbf{m}) \qquad (1.1)$$

The data covariance matrix $\mathbf{C}_{noise}^{-1}$ quantifies the uncertainty in comparing model output to data and *prior*(**m**) represents prior probability for the freshwater forcing (i.e. a uniform probability from -0.3 to 0.3 Sv) independent of a new set of observations $\mathbf{d}_{obs}$ represented here by the scaled Greenland ice core proxy data. The quantity within the square brackets is typically referred to as the "cost" function or metric of errors in the model relative to what is observed with superscript (*T*) referring to the matrix transpose. Even with the Gaussian assumption for observational and modeling uncertainties, the PPD is generally not Gaussian because of nonlinearities represented in the ocean model g(**m**).

Equation (1.1) can only be estimated stochastically by selecting alternate freshwater forcing time series from the *prior*(**m**) distribution, simulating the combined effects of these parameters within the ocean model, and estimating the likelihood of this

selection by evaluating the cost function specified by *equation (2.4) in Section (2.3.4).* In general this requires a large number of experiments.

I use Multiple Very Fast Simulated Annealing (MVFSA) to select uncertain freshwater forcing time series [Sen and Stoffa, 1996; Jackson et al. 2004]. The rules for selecting samples is similar to a Metropolis/Gibbs sampler insofar as candidate parameter set values are either accepted or rejected (for stepping through parameter space) in proportion to a probability

$$P = \exp\left(\frac{-\Delta E}{T}\right), \tag{1.2}$$

where ΔE is the change in the metric of model-data discrepancies, also called the "cost function", for going from a model with parameter set values $\mathbf{m}_k$ to model with parameter set values $\mathbf{m}_{k+1}$. The selection of model parameters given an initial selection m_i within MVFSA are chosen such that

$$m_i^{k+1} = m_i^k + y_i(m_i^{\max} - m_i^{\min}), \tag{1.3}$$

$$y_i \in [-1,1], \tag{1.4}$$

and

$$m_i^{\min} \le m_i^{k+1} \le m_i^{\max} \tag{1.5}$$

where y_i is generated according to a Cauchy distribution

$$y_i = \mathrm{sgn}(RND - 0.5) T_k \left(\left(1 + \frac{1}{T_k} \right)^{|2RND-1|} - 1 \right). \quad (1.6)$$

Within equations (1.3-1.6), subscript (*i*) is the parameter number, (*k*) is the iteration number, *RND* is a random number generator with a uniform distribution between 0 and 1, and sgn is the sign operator. The cooling schedule at iteration (*k*) is

$$T_k = T_o \exp\left(-\alpha (k-1)^{1/NM} \right), \quad (1.7)$$

with *NM* equal to the number of parameters and α as a tunable parameter that can be tailored for particular problems. T_o is the initial annealing temperature and is equal to 3.5. The acceptance criterion for successive model selections is the same as for the Metropolis rule. The sampling process is stopped if successive iterations fail to reduce the cost function after a pre-determined number of experiments. This convergence criterion is 5.5 times the total number of uncertain parameters [*Jackson et al.*, 2004]. This algorithm has been applied to estimate the uncertainty in selecting parameters important to climate sensitivity within an Atmospheric GCM [*Jackson et al.*, 2004; *Jackson et al.*, 2008; *Jackson et al.*, 2009] as well as processes affecting the exchange of energy and moisture at the land surface [*Jackson et al.*, 2003].

1.7 Summary

In this thesis, I studied the abrupt climate change events of Dansgaard-Oeschger Interstadials (DOIs) during the last glacial period. Bayesian stochastic inversion is used to test the freshwater forcing hypothesis of abrupt climate change. A time series of freshwater flux anomaly in the North Atlantic Ocean between 30 and 39 kyr B.P. is inferred by combining a paleo-temperature record from a Greenland ice core with an ocean box model. Reconstructions of global sea level from independent geological records are then compared to the sea level changes implied by these anomalies. The comparison gives some support to the freshwater forcing hypothesis for the time interval from 30 to 39 kyr B.P. The largest drop in sea level present in observations and in our inversion is associated with ice sheet growth which enables sustained freshwater removal from the ocean and enhanced meridional circulation and heat flux to maintain the observed warmth during the long (~2.5 kyr) DOI 8. According to our results, the longer the period of warmth the larger the drop in sea level. Thus, both our results and observations show an approximately 15 to 20 m drop in sea level following Heinrich event 4 at 39 kyr B.P., the feature of greatest "commonality" (between model and observation).

Furthermore, I attempt to combine quantitatively a paleoclimate series with a climate model, with the specific purpose of extracting information about the changes in mass balance of NH ice sheets during the last glaciations. This study shows that paleoclimate records spanning a portion of the last glaciation and from different parts of

the globe (Greenland temperature, mean sea level, and Antarctic temperature) can be brought into consistency using a climate model of reduced complexity. The combination of the Greenland record with the model implies sea level changes between 34.3 – 39.3 kyr B.P. which are in accord with reconstructions based on corals and deep-sea sediments. Consequently, our results support a NH ice sheet forcing on abrupt climate change. In particular, they point to the importance of the period of NH ice sheet growth that follows a Heinrich Event to explain the long period of Greenland warmth. Our results are robust against differences in external climate forcing over this time interval Whereas they are encouraging, further investigation with a more comprehensive set of paleoclimate records and more complete climate models is probably desirable.

Chapter 2 A box-model test of the freshwater forcing hypothesis of abrupt climate change and the physics governing ocean stability

2.1 Introduction

In this chapter I will present the box model inversion experiment to test the adequacy of the freshwater forcing hypothesis to explain abrupt climate change. A 4-box model of the Atlantic Ocean is combined with a Greenland paleotemperature record using Bayesian Stochastic Inversion to infer changes in the mass balance of Northern Hemisphere ice sheets and in the meridional transport of mass and heat that would be required to explain a series of DOIs from 30 to 39 kyr B.P. The freshwater flux anomalies are converted into anomalies of global sea level, which are then compared with independent evidence from the geologic record. This exercise is repeated with different assumptions about vertical mixing in the model in order to address its influence of the response of ocean circulation to freshwater forcing [e.g., *Nilsson and Walin*, 2001].

2.2 Thermocline scaling theory for box model

As I discussed in the introduction chapter, the MOC which is thought to play a dominate role in DOIs, is sensitive to freshwater forcing. Characterizing the sensitivity of ocean models to freshwater forcing is an important research topic.

Nilsson and Walin [2001] use a box model of a single-hemisphere ocean to show that assumptions about vertical buoyancy transport are instrumental in the equilibrium response of the MOC to freshwater forcing. Consider vertical buoyancy transport as

being independent of vertical density stratification. Then simple scaling arguments for the oceanic thermocline show that increasing the surface density contrast between the equatorial and high latitude regions ($\Delta\rho$) increases the strength of the MOC , e.g.,

$$MOC \propto \Delta\rho^{1/3}. \qquad (2.1)$$

On the other hand, if vertical buoyancy transport increases with decreasing stratification – a plausible assumption – it is easier to generate vertical mass transport for the same amount of energy available for that transport when there is a reduced density contrast between the surface and deep oceans. Since the density contrast between the surface and deep oceans at low latitudes scales with the density contrast between the equator and the high latitudes at the surface ($\Delta\rho$), increasing $\Delta\rho$ would decrease the strength of the MOC,

$$MOC \propto \Delta\rho^{-1/3}. \qquad (2.2)$$

This is what *Nilsson and Walin* [2001] termed the freshwater "boosting" hypothesis. Numerical solutions of a single hemisphere box model replicate their arguments (see Appendix 2). These arguments are also supported by numerical experiments with ocean circulation models [*Nilsson et al.*, 2003; *Mohammad and Nilsson*, 2004; *Marchal et al.*, 2007]. However, they may not apply in a straightforward way to a two-hemisphere basin with competing polar regions (water sinking in northern and southern hemispheres) [*Saenko and Weaver*, 2003; *Mohammad and Nilsson*, 2006; *Marchal et al.*, 2007]. In

particular, Marzeion et al. [2007] found there were additional feedbacks within a more realistic global AOGCM (CLIMBER-3α) that weakens the effects of freshwater forcing into the North Atlantic Ocean for producing a reduced stratification that is the basis for the "boosting" regime. Also, they describe equilibrium responses and may therefore be of limited value to understand transient changes of the MOC [e.g., *Marchal et al.*, 2007].

Box models also make the assumption that the MOC is related in a simple way to meridional density gradients through geostrophy and the thermal-wind relation. De Boer et al. [2010] provided several counter examples where the relationship between the MOC and the meridional density gradient relationship may be affected by remote influences from the Southern Ocean winds and the Antarctic Bottom Water formation.

2.3 4-box model inversion experiment

2.3.1 Ocean box model

The present work considers a box model of the Atlantic Ocean (2 Hemispheres). The fluxes of heat, salt, and mass between different oceanic boxes are parameterized. A whole hierarchy of box models has been used to explore aspects of the MOC. Here I use a model that can exhibit several modes of the MOC broadly corresponding to some of the multiple equilibria found in ocean general circulation models [e.g., *Manabe and Stouffer*, 1988; *Marotzke and Willebrand*, 1991].

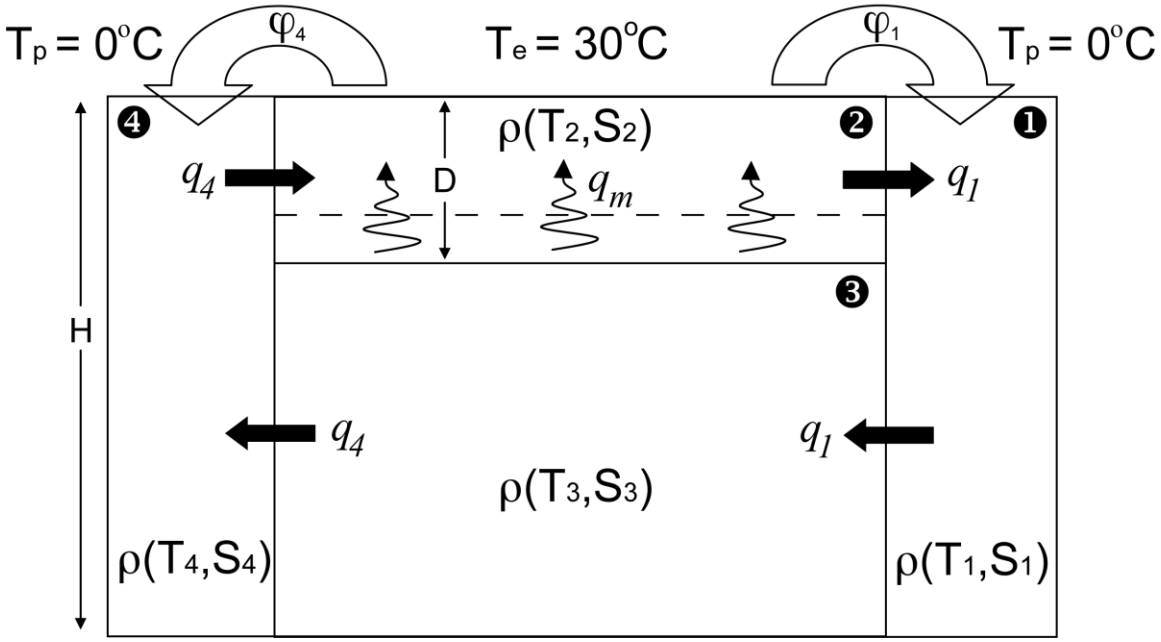

Figure 2.1 Diagram of two-hemisphere 4-box model of the Atlantic Ocean (northern sinking case). The density (ρ) is a linear function of temperature (T) and salinity (S). The depth of the thermocline at low latitudes (D) is set by a balance between the horizontal volume fluxes q_1, q_4, the vertical volume flux q_m, and the atmospheric freshwater volume fluxes φ_1 and φ_4. Volume fluxes q_1 and q_4 alter the depth of box 2 (D) without moving mass from box 3 to box 2. The volume flux q_m moves mass from box 3 to box 2 by altering the depth of box 2.

The model includes i) two high latitude boxes (one in each hemisphere) and ii) two low-latitude boxes, one for the warm thermocline water and one for the cold sub-thermocline water (Figure 2.1). The effects of the Southern Ocean on the Atlantic's MOC

are not included (see Section 2.5.3 for an investigation of these effects). Details about the box model are reported in Appendix 1.

Several versions of a box model are considered with different parameterizations of vertical volume transport between the two low-latitude boxes. In general, this vertical volume transport (q_m) is a function of the density contrast between the two boxes ($\rho_3 - \rho_2$) and the depth of the thermocline (D),

$$q_m = q_{mr}\left(\frac{\rho_{3r} - \rho_{2r}}{\rho_3 - \rho_2}\right)^{\zeta}\left(\frac{D_r}{D}\right)^{\eta}. \qquad (2.3)$$

Physically this relationship means that the mass flux that is required to maintain an advective – diffusive equilibrium is smaller if there is a greater density contrast and/or larger depth to the thermocline. The latter relationship implies less diffusive mass fluxes with deeper, more gradual density gradients. The exponents ζ and η in equation (2.3) can be set to represent different mixing assumptions [*Nilsson and Walin*, 2001]. For instance (ζ = 0, η = 1) represents constant mixing, (ζ = 0.5, η = 0.5) represents a stability-dependent mixing, and (ζ = 1, η = 1) represents constant mixing energy. The model parameters are listed in Table A1.

The equilibrium sensitivity of the model to poleward moisture fluxes φ_1 and φ_4 shows the same qualitative differences to different mixing assumptions as its single-

hemisphere version (Figure 2.2, and see Appendix 2). The scaling laws (1-2) apply for our two-hemisphere model only when there is strong sinking in the north. In this case, the flow through the polar box in the Southern Hemisphere (box 4) has no influence. Interestingly, the critical point that determines the circulation flips between northern sinking and southern sinking is very sensitive to the mixing formulation. There is also a class of solutions that does not exist for the single-hemisphere model (Appendix 2). Namely, there are symmetric solutions with sinking in both the northern and southern polar boxes, which is balanced by upwelling in the equatorial zone. For these solutions, an increase in sinking in one hemisphere is balanced by a decrease in sinking in the opposite hemisphere. All symmetric solutions respond in a similar way to changes in freshwater input. The circulation, once it has migrated to one of the asymmetric sinking states, does not easily transit back to the equatorially symmetric flow with sinking in both hemispheres. Thus, these asymmetric solutions are unstable only to large freshwater perturbations.

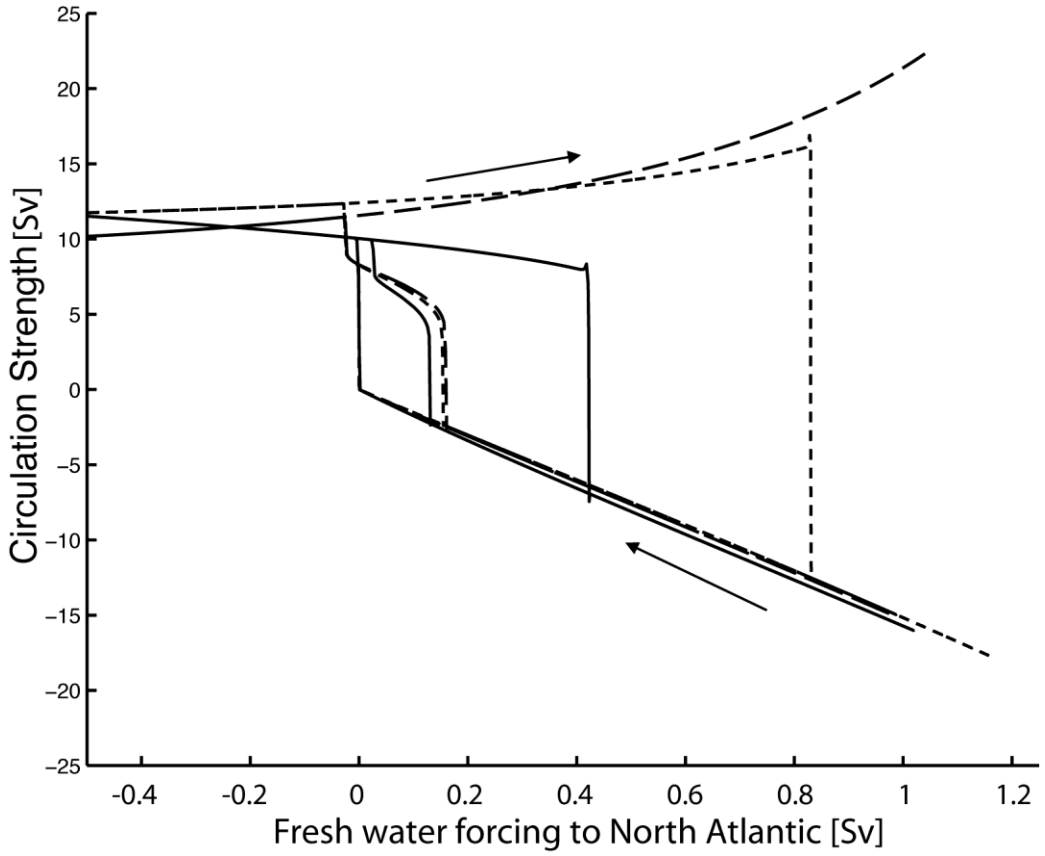

Figure 2.2 Equilibrium solutions of the 4-box ocean model. The meridional overturning circulation in the northern hemisphere (q_1) is shown as a function of the meridional moisture transport in the atmosphere (φ_1). Arrows indicate the direction of hysteresis. The different lines refer to different assumptions about vertical buoyancy transport: constant vertical mixing (solid line), stability dependent mixing (short dashed line), and constant mixing energy (long dashed line).

2.3.2 Experiment design

I use stochastic inversion to identify scenarios (time series) of freshwater forcing that permit the 4-box ocean model to approximate a paleo-temperature record from a Greenland ice core between 30 and 39 kyr B.P. [*Grootes and Struiver,* 1997]. This time interval is chosen because it includes a prominent sequence of DOIs beginning after Heinrich event 4 at 39 kyr B.P. The length of inversion is constrained by the number of freshwater anomalies that one can realistically estimate given our choice to use stochastic inversion (see section 1.3.1 in Chapter 1). The freshwater forcing scenarios are tested using reconstructions of sea level during this time interval based on $\delta^{18}O$ records from deep-sea sediments [*Waelbroeck et al.,* 2002], corals [*Thompson and Goldstein,* 2006], and $\delta^{18}O$ records from the Red Sea [*Siddall et al.,* 2003]. Here these sea level records are assumed to reflect changes in the volume of the Northern Hemisphere ice sheet melt or calving to the North Atlantic Ocean. Because model solutions may depend on assumptions about vertical buoyancy transport at low latitudes, I repeat this exercise with the three different assumptions about this transport

2.3.3 Cost function

The stochastic inversion searches for freshwater forcing scenarios that minimize a cost function with two contributions. A first contribution quantifies the mismatch between predicted and observed sea surface temperatures in the polar region in the North Atlantic. A second contribution ensures that sea level is not appreciably altered by the end of the experiment. The reason for the latter constraint is discussed below. The ocean

model predicts a volume-average temperature for each box . I presume that the fluctuations of ice $\delta^{18}O$ in the Greenland record [*Grootes and Stuiver*, 1997] are related in a simple, linear way to variations in sea surface temperature in the polar region in the North Atlantic (i.e. to temperature in box 1). This is likely only qualitatively correct [*Landais et al.*, 2004; *Huber et al.*, 2006]. To be specific, I presume that a 15 ℃ warming above Greenland [e.g. *Landais et al.*, 2004] corresponds to a 4 ℃ warming of the northern polar ocean box [*Bond and Lotti*, 1995]. The cost function is thus defined as,

$$E(\mathbf{m}) = \frac{1}{1101}\sum_{t=1}^{1101}\frac{\left(\left(T_1(t)-\overline{T}_1\right)-\left(T_{obs}(t)-\overline{T}_{obs}\right)\right)^2}{\left(1^\circ C\right)^2} + \frac{(\Delta MSL)^2}{(30m)^2}. \qquad (2.4)$$

Here T_1 is the model temperature in the northern polar box and T_{obs} is the temperature interpreted from the Greenland record. The overbar indicates a time average (1101 evenly spaced points between 30 and 39 kyr B.P.). Note that I have not smoothed the Greenland temperature estimates. The error in making this model – data comparison has an assumed uncertainty of 1 ℃. Finally, ΔMSL is the change in mean sea level at 30 kyr B.P..

The second contribution to the cost (equation 2.4) constrains the net change in mean sea level by the end of the inversion to ± 30 m, although most solutions considered with that constraint are within a few meters of zero change. This choice reflects an interpretation of sea level reconstructions which show that the continental ice sheets were not growing or shrinking appreciably between 30 and 39 kyr B.P.. This constraint helps

the inversion reject unrealistic freshwater forcing scenarios. Indeed, I found that without this constraint, the inversion preferentially selects solutions that require global ice volume to grow and shrink by more than the equivalent of 120 meters sea level on millennial time scales. Note that this constraint does not specify what sea level must do between the beginning and end of the experiment. It merely specifies that all changes must approximately cancel.

2.3.4 Freshwater forcing

The stochastic inversion estimates a time series of freshwater forcing (*ff*) at 81 evenly spaced intervals from 39 to 30 kyr B.P.. A continuous time series is made by linear interpolation between these points. Candidate values of *ff* are selected from a uniform "prior" distribution with a minimum of -0.3 Sv and maximum of 0.3 Sv (1 Sv = 10^6 m^3 s^{-1}). As discussed in Section (2.4), the choice of this range does matter. The stochastic inversion takes a random step between these minimum and maximum values for each of the 81 unknown forcing values, with a variable average step size that is determined by the MVFSA algorithm. This step size gradually becomes smaller through the course of the inversion. Although the fresh water forcing values are selected individually, their effect on the model is only evaluated as a whole through the impact of the time series on the cost function. This selection process takes into account possible non-linear dependencies in the selection of the best candidate solutions.

2.3.5 Solution averaging

The inversion consists of 400 independent attempts to minimize the cost function, with each attempt involving approximately 3600 experiments. The best performing experiment in each attempt is then systematically averaged together, only combining experiments that result in a further reduction in the cost function. This process tends to reduce the noise or random component that may exist in each of the individual solutions. There were multiple groups of solutions that were identified through this selection and averaging process. Within each attempt to minimize the cost function, I selected the solution with the smallest cost value for analysis.

2.4 Results

A set of three freshwater forcing scenarios are obtained through inversion of the Greenland paleo-temperature record, one for each configuration of the 4-box model representing constant vertical mixing, stability-dependent mixing, and constant mixing energy (Figure 2.3b). These forcing scenarios modify the meridional overturning circulation and poleward heat transport in such a way as to recreate features observed in the Greenland record (Figure 2.3a). The periods of sustained warmth correspond to periods of (i) freshwater removal from the ocean (growth of continental ice sheets) and (ii) increased meridional flow in the NH (q_1), and (ii) decreased meridional flow in the SH (q_4) (Figure 2.3c).

Uncertainties in vertical mixing, which had such a dramatic effect on the equilibrium MOC (Figure 2.2), have very little effect on the solutions that reproduce the transient sequence of abrupt climate change (Figure 2.3). Section 2.5.1 summarizes the reasons why different assumptions about vertical buoyancy transport are not important to these solutions.

A time integral of the freshwater forcing obtained from the inversion solutions provides predictions of global sea level anomalies that we assume are related to the decay or growth of the NH ice sheets. Again, the differences in mixing formulation make little difference to the predicted sea level anomalies (Figure 2.4). The sea level anomalies obtained from the three freshwater forcing scenarios are compared against the three independent estimates of sea level change from 39 to 30 kyr B.P. based on corals and $\delta^{18}O$ records (Figure 2.4). The feature that is in broad agreement among the modeled and observed sea level anomalies is the initial drop of sea level of 15 to 20 m. It corresponds to the longest period of sustained warmth in the Greenland paleo-temperature record following Heinrich event 4 at 39 kyr B.P.. According to our inversion, the subsequent interstadial events with shorter duration can be explained by smaller variations in sea level (less than 5 m). The general relationship that emerges is that the duration of Greenland warmth is approximately proportional to the amount of ice sheet growth (or sea level fall), with ratios ranging from 112 years to 167 years sustained warmth for every meter of sea level fall. Given the uncertainties in the sea level data, we cannot draw firm inferences about model-data disagreement for the shorter DOI events.

Given the crudeness of our ocean model, the level of agreement between the various estimates of sea level and the model predictions is perhaps surprisingly good. The agreement is independent of the uncertainties in vertical mixing formulation as indicated by the relatively minor differences among the three modeled curves of sea level anomaly (Figure 2.4).

In another inversion (not shown) I select candidate freshwater forcing values from a wider range of possible values (-0.4 Sv to 1.3 Sv). The inversion in this case tends to favor temperature jumps on the order of 9 ℃ (not the 4 ℃ jumps that I imposed as the "target") and required sea level variations on the order of 60 m. The ocean circulation remains equatorially asymmetric. In contrast, the solutions with the smaller (-0.3 Sv to 0.3 Sv) freshwater forcing (Figure 2.3) come mainly from the equatorially symmetric circulation state (sinking at both poles). I infer that a threshold exists for freshwater forcing values in excess of 0.3 Sv that makes it difficult for the inversion to identify the symmetric-only solutions. We know from equilibrium experiments that the asymmetric states are particularly stable. With regards to the realism of the symmetric solutions, they were required to obtain a match to the observational data, which, admittedly, could be occurring for the wrong reasons. On the other hand, very little is known of the circulations and balances that close the global ocean circulation. The symmetric solutions allow a kind of seesaw response between northern and southern sinking rates which is consistent with higher dimensional OGCMs [*Knutti et al.*, 2004].

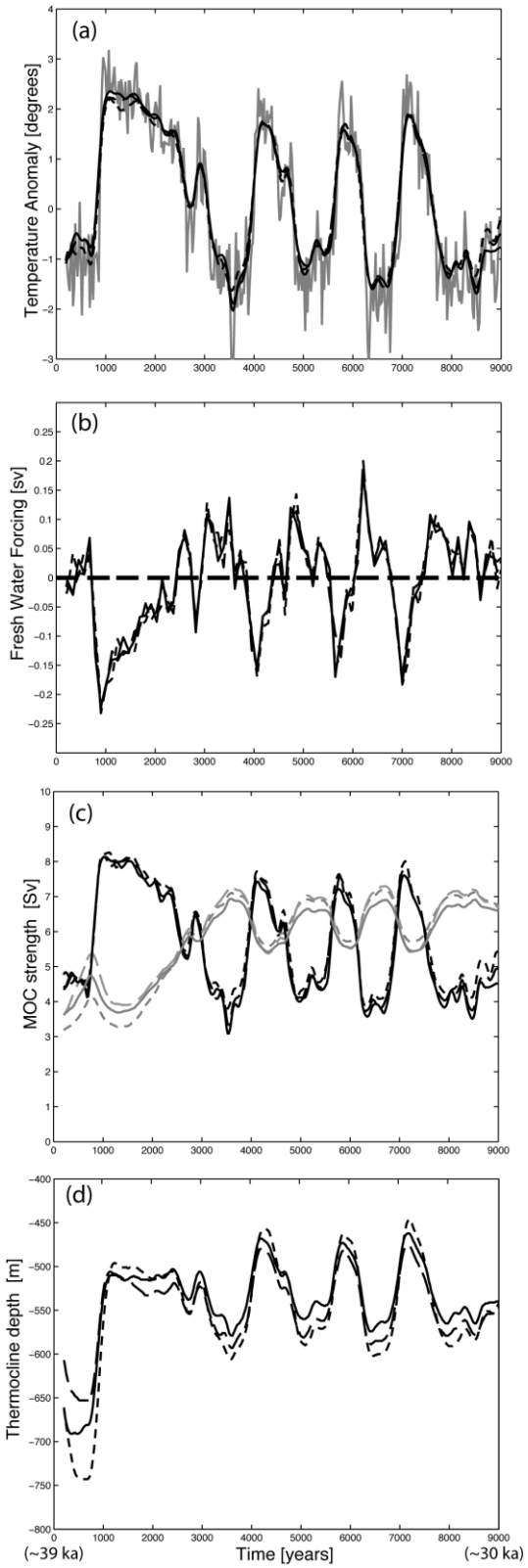
(a)
Temperature Anomaly [degrees]
(b)
Fresh Water Forcing [sv]
(c)
MOC strength [Sv]
(d)
Thermocline depth [m]
(~39 ka)
Time [years]
(~30 ka)

Figure 2.3 Inversion solutions: Panel (a) compares the temperature of the polar northern box (black lines) with the sea surface temperature inferred from the Greenland record (gray lines) [Grootes and Struiver, 1997]. Panel (b) shows the changes in surface freshwater forcing for the polar northern box. Panel (c) shows the changes in the northern (black) and southern (gray) components of the ocean's meridional circulation. Panel (d) shows the changes in thermocline depth. The solid, short, and long dashed lines correspond to different assumptions about vertical mixing: constant vertical mixing (solid line), stability dependent mixing (short dashed line), and constant mixing energy (long dashed line).Model inputs: freshwater forcing time series in panel (b); model outputs: North Atlantic sea surface temperature in panel (a), AMOC in panel (c), thermocline depth in panel (d).

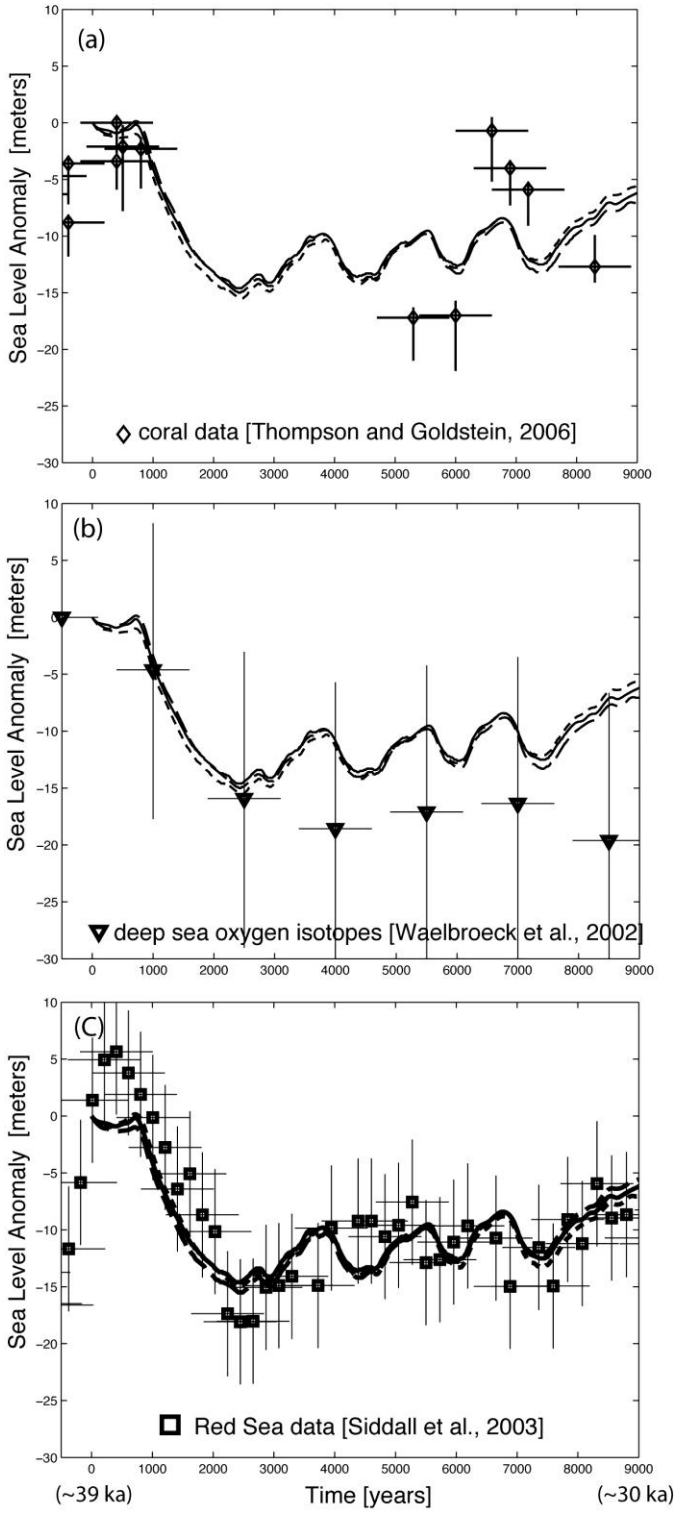
(a)
Sea Level Anomaly [meters]
◊ coral data [Thompson and Goldstein, 2006]
(b)
Sea Level Anomaly [meters]
▽ deep sea oxygen isotopes [Waelbroeck et al., 2002]
(C)
Sea Level Anomaly [meters]
Red Sea data [Siddall et al., 2003]
(~39 ka)
Time [years]
(~30 ka)

Figure 2.4 Comparison between sea level anomalies inferred from the Greenland record and estimated from (a) coral records [Thompson and Goldstein, 2006], (b) $\delta^{18}O$ records from deep-sea sediments [Waelbroeck et al., 2002], and (c) $\delta^{18}O$ records from Red Sea sediments [Siddall et al., 2003]. The Red Sea data has been smoothed by a three point running mean. The uncertainty of ±5.5 m (1-σ) indicated for the Red Sea data reflects a smoothing of about 500-yr which removes some of the inter-sample variability [Siddall et al., 2003; Rohling et al., 2004]. The solid, short, and long dashed lines correspond to different assumptions about vertical mixing: constant vertical mixing (solid line), stability dependent mixing (short dashed line), and constant mixing energy (long dashed line).

2.5 Discussion

2.5.1 Insensitivity to formulation of vertical mixing

Vertical mixing at low latitudes is important to setting the stability thresholds of the meridional overturning circulation in ocean models [e.g., *Prahl et al.*, 2003; *Dijkstra and Weijer*, 2005]. However, these results mainly pertain to the equilibrium states of the MOC. The insensitivity of our inversions to vertical mixing formulation highlights one of the primary shortcomings of scaling arguments derived for the steady state and of inferences drawn from model experiments on equilibrium response of MOC to slowly evolving freshwater forcing. Indeed, the hysteresis obtained from such experiments has been used as a conceptual model of abrupt climate change (e.g., Figure 2.2). The MOC, however, can have a transient response to a sudden change in freshwater forcing that is quite different from its equilibrium response. Moreover, the stability thresholds may

depend on the rate of change in freshwater forcing in addition to its amplitude [e.g., *Manabe and Stouffer*, 1994; *Marchal et al.*, 1999b; *Lucarini and Stone*, 2005a, 2005b].

To illustrate this point, Figure 2.5 shows the adjustment to equilibrium of the ocean model to a 0.3 Sv step increase in fresh water forcing that starts at year 500. The initial model state is an asymmetric circulation with northern sinking. Initially all versions of the model, no matter which formulation of vertical mixing is assumed, show decreasing overturning strength in the Northern Hemisphere (Figure 2.5a). Only after ~600 years do the different mixing assumptions lead to divergent responses. The increase in overturning strength with increased freshwater forcing, which occurs for the stability-dependent and fixed mixing energy assumptions, does not occur until 500 years after the freshwater forcing is initiated (Figure 2.5a).

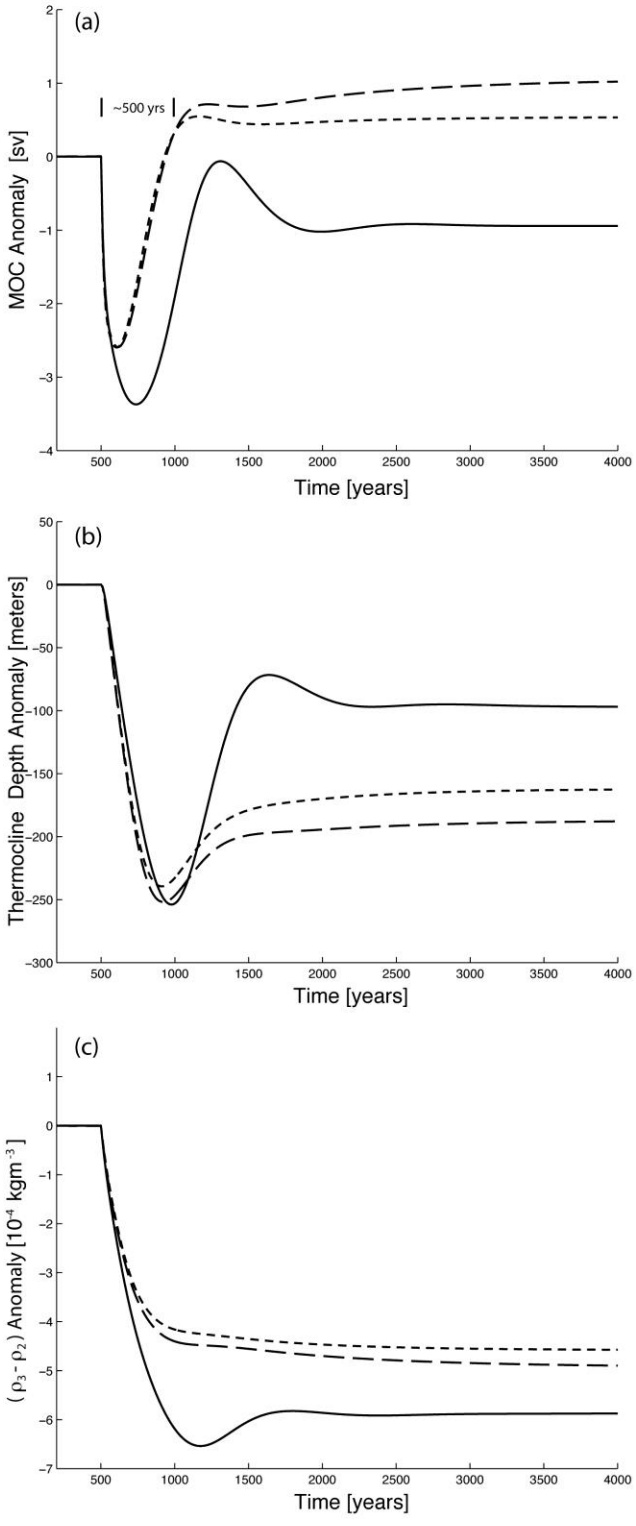
(a)
~500 yrs
MOC Anomaly [sv]
Time [years]
(b)
Thermocline Depth Anomaly [meters]
Time [years]
(c)
(ρ3 - ρ2) Anomaly [10-4 kgm-3]
Time [years]

Figure 2.5 Adjustment of the 4-box ocean model to a 0.3 Sv step increase in poleward moisture transport (φ_1) starting at year 500 and maintained for the duration of the experiment. Shown are the anomalies relative to the values prior to year 500. Panel (a) shows the northern sinking volume flux (q_1). Panel (b) shows the depth of the thermocline (D). Panel (c) shows the bottom (box 3) to surface (box 2) density difference (ρ_3-ρ_2). The solid, short, and long dashed lines correspond to different assumptions about vertical mixing: constant vertical mixing (solid line), stability dependent mixing (short dashed line), and constant mixing energy (long dashed line).

The above results are interpreted as follows. With the reduction in overturning strength, less mass is exported from the surface equatorial box and the thermocline quickly deepens (Figure 2.5b). There is virtually no difference in the time evolution of thermocline depth among the different mixing assumptions until after 1000 years of the initiation of freshwater forcing. The similarity of the initial response of the model for all mixing assumptions is due to the fact that the adjustment is dominated within the first 500 years by changes in the horizontal flow in the NH (q_1), with virtually no change in vertical flux at low latitudes (q_m). It is this latter flux that leads to different equilibrium sensitivities for the different assumptions. The vertical flow (q_m) responds slowly because the effect of a deepening thermocline (from reduced horizontal flow q_1) (Figure 2.5b) counteracts the effect of a reduced density stratification in the initial stage of the adjustment (Figure 2.5c). After ~500 years, however, the latter effect overcomes the

former for the cases with stability-dependent mixing and constant mixing energy. The model then approaches the 'boosting' equilibrium state [*Nilsson and Walin*, 2001].

The above analysis pertains to a comparison of results for the asymmetric circulation mode with northern sinking. Thus, one may question its applicability to the solutions in Figure 2.3, which are mostly for the equatorially symmetric circulation state. I find, however, that the different mixing assumptions have little impact on inversion solutions that require transitions among asymmetric circulation states (not shown). In particular, if I change the inversion target to find solutions for a larger temperature jumps of 9℃ (instead of 4℃) , requiring the model to transit among its asymmetric states, nearly identical freshwater forcing scenarios are found.

2.5.2 Role of ice sheets

The presumption has been that ice sheets were mainly important to abrupt climate change as a source of freshwater [*Broecker et al.*, 1990; *MacAyeal*, 1993; *Clark et al.*, 2002]. This is logical given their main contribution to the geologic record is in the form of ice rafted debris observed during the cold phases between DOIs [*Bond et al.*, 1993; *Alley and MayAyeal*, 1994; *Bond and Lotti*, 1995]. Our inversion results, however, emphasize the importance of ice sheet growth to sustaining the observed warmth of the DOIs. According to our results, ice sheet collapse is important for shutting down the MOC. But without the subsequent ice sheet growth and reduced freshwater input to the ocean, the MOC would not be able to prolong the warmth at high northern latitudes.

Thus, the longer the warmth the larger the predicted drop in global sea level. The coral and $\delta^{18}O$ records of sea level change from 39 to 30 kyr B.P. tend to support this inference: they consistently show ~15 to 20 m drop after the Heinrich event 4 at 39 kyr B.P., with smaller variations during the subsequent series of shorter DOIs.

Heinrich event 5, at around 46 kyr B.P., was followed by a ~ 2 kyr long warming similar to Heinrich event 4 described above [*Grootes et al*., 1993; *Meese et al.,* 1997]. There is very little change in the deep-sea $\delta^{18}O$ record [*Waelbroeck et al.*, 2002], which may be a consequence of the data smoothing applied to this record. Although existing coral records are not ideal to identify the amplitude of sea level change between 48 and 39 kyr B.P., they do suggest the possibility of a 30 m drop in sea level between 48 and 44 kyr B.P. (near the end of the interstadial warming). The sea level record from the Red Sea [*Siddall et al.,* 2003, not shown] is consistent in timing and amplitude with features in the Greenland $\delta^{18}O$ record following Heinrich events 4 and 5. A recent review of sea level estimates generally supports our primary finding that periods of sustained warmth are correlated with falling sea levels [*Siddall et al.*, 2008].

One of the important implications of our results is the suggestion that abrupt climate change appears to be more of a forced phenomenon than one that is triggered and maintained by the existence of multiple circulation states in the ocean. Given the uncertainties in sea level data, I can only make this inference for DOI 8 (starting at 38 kyr B.P.) and not necessarily for DOIs 7, 6, and 5 which can be explained

by much smaller changes in freshwater forcing. A different and intriguing interpretation of the role of ice melt is to regulate the periodicity of DOI events undergoing self-sustained relaxation oscillations with less ice melt corresponding to longer duration interstadial events [Schulz et al., 1999; Schulz 2002; Schulz et al., 2002; Timmermann et al. 2003; Sima et al., 2004]. Because the 4-box model does not exhibit internal instability behavior, we cannot test this hypothesis without building upon or altering the model to include this possibility.

This interpretation is also supported by several other studies that requires a sustained reduction of the hydrologic balance of the North Atlantic to explain interstadial warmth. The AOGCM modeling work of Knutti et al. (2004) summarize the relationship between modeled Greenland temperature and anomalous freshwater forcing to the North Atlantic Ocean with a fairly simple relationship $T_n \propto \tanh(s \cdot ff)$ and was able to fit a "thermal-freshwater seesaw" conceptual model to simultaneously connect Greenland and Antarctic temperature anomalies with benthic $\delta^{18}O$ sea level proxy record between 60 to 25 kyr B.P.. While the 4-box model does not have as simple a relationship between temperature anomalies in the Northern box (1) and freshwater flux (Figure 2.6a), the differences do not make a lot of difference to the implied sea level anomalies (Figure 2.6c). Liu et al. (2009) was only able to simulate the Greenland record of the Bolling-Allerod warming around ~14.5 kyrs B.P. with a large and sudden reduction in freshwater supply to the North Atlantic, which also allowed favorable comparison with proxy records from the Cariaco Basin, Iberian Margin, and Antarctica.

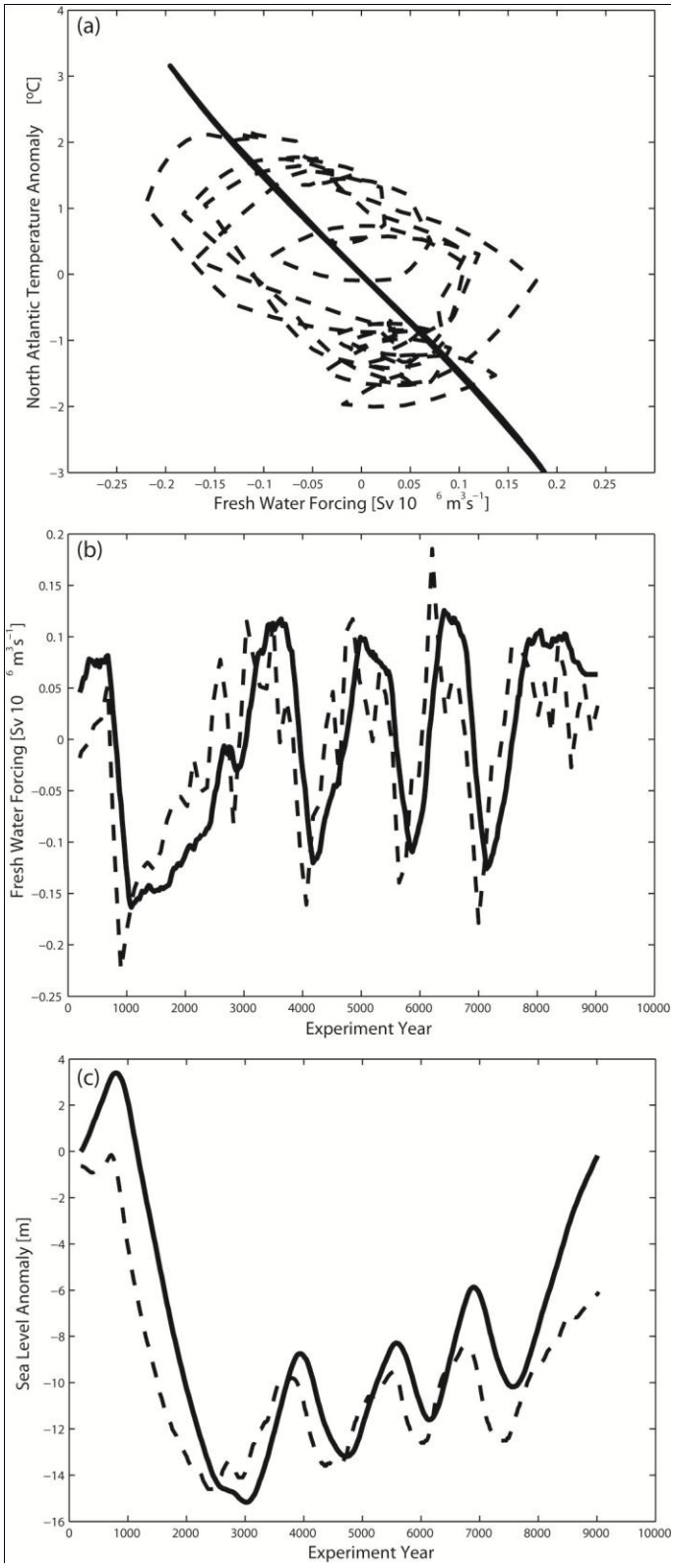
(a)
North Atlantic Temperature Anomaly [°C]
Fresh Water Forcing [Sv 10 6 m3s−1]
(b)
Fresh Water Forcing [Sv 10 6 m3s−1]
Experiment Year
(c)
Sea Level Anomaly [m]
Experiment Year

Figure 2.6 Comparison between solutions from 4-box model inversions (dashed) and results of Knutti et al. [2004] (solid). Knutti et al [2004] found a simple relationship between Greenland temperature anomalies (T_n) and freshwater anomalies (ff) to the North Atlantic given by $T_n \propto \tanh(s \cdot ff)$ *where (s) is sensitivity scaling parameter that would be model dependent,. Panel (a) shows freshwater forcing versus box sea surface temperature anomalies, (b) time series of inferred freshwater forcing, and (c) implied sea level anomalies.*

Inferences of the amount of ice melt during Heinrich event 4 from surface ocean oxygen isotopes estimate the event is the equivalent of 2 m ±1 m, an amount that is roughly consistent with the amounts associated with observed IRD thicknesses [*Alley and MacAyeal,* 1994] While these results are consistent with our results in that little or no freshwater forcing was required to shut down the MOC at the beginning, presumably it is the collapse of an ice sheet that allows for an extended period of ice growth. Thus it is not clear to us how we could then explain a sustained 15 to 20 drop in sea level that seems to be required by multiple sea level records without a larger collapse of the ice sheet during the Heinrich event. This question could be better addressed with an coupled climate-ice sheet model.

2.5.3 Sensitivity to modeling assumptions

The Nilsson and Walin (2001) scaling arguments that form the basis of the 4-box model presents a set of hypotheses for the balance of buoyancy and vertical mixing

processes that govern the strength of the MOC. In addition, I present the results of two additional experiments that test the effects of different sets of modifications to the model that explore alternate hypotheses for processes that govern the global MOC. Given the specialized derivation of the 4-box model, it is not entirely clear that these modifications make the model more realistic. Nevertheless, the experiments present an opportunity to use paleoclimate proxy archives to evaluate the plausibility of different modeling assumptions.

2.5.3.1 Southern Ocean. Our two-hemisphere box model is equatorially symmetric and does not represent the Southern Ocean. In order to test the potential importance of the Southern Ocean on our results, I parameterized its dynamical influences according to the scaling arguments presented by *Gnanadesikan* [1999] (see also *Sanko and Weaver* [2003]). It is important to emphasize, however, that the role of the Southern Ocean to powering the Atlantic's overturning circulation is an open question [*Bugnion et al.*, 2006a-b; *Kuhlbrodt et al.*, 2007].

Following *Gnandesikan* [1999], the surface volume flux q_4 from the Southern Ocean to the equator would be driven by zonal wind stress and transient eddies. With the parameterization of the dynamical influences of these effects in our model, I found that the MOC tends to be stabilized, such that the model becomes fairly insensitive to freshwater forcing at high latitudes in the NH (Figure 2.7). Note in particular that the model lacks a symmetric circulation state that was important to the inversion solutions

discussed previously. The stochastic inversion fails to find any freshwater forcing scenario that replicates the Greenland paleo-temperature record and does not come close to predicting observed changes in sea level (Figure 2.8).

These results may be taken to mean that inferences of freshwater forcing as attempted here can depend strongly on the treatment of the Southern Ocean. Clearly, this assertion would need to be tested with more realistic ocean models.

2.5.3.2 High-latitude convection. Our model lacks a series of potential feedbacks introduced by the stratification when the polar box is flooded with freshwater, such as an increase in sea ice cover, a reduced heat flux from the ocean to the atmosphere, and an increase of precipitation over evaporation, all of which reinforce a polar halocline catastrophe [*Welander* 1982; *Marotzke and Willebrand*, 1991]. While the model represents a kind of polar halocline catastrophe, it does so largely without any of these other feedbacks.

The box model is extended to represent polar stratification by subdividing each polar box into a surface box (of 500 meter depth) and a deep box (3500 m depth) (Welander 1982). When the density difference between the surface and deep boxes results in stable stratification, no mixing is specified between these boxes. In contrast, when density in the surface box exceeds that of the deep box, a bi-directional mixing is

prescribed at a fixed rate of 5 Sv (I also tested the results with a fixed rate of 1 Sv.) All other aspects of the model remain unchanged.

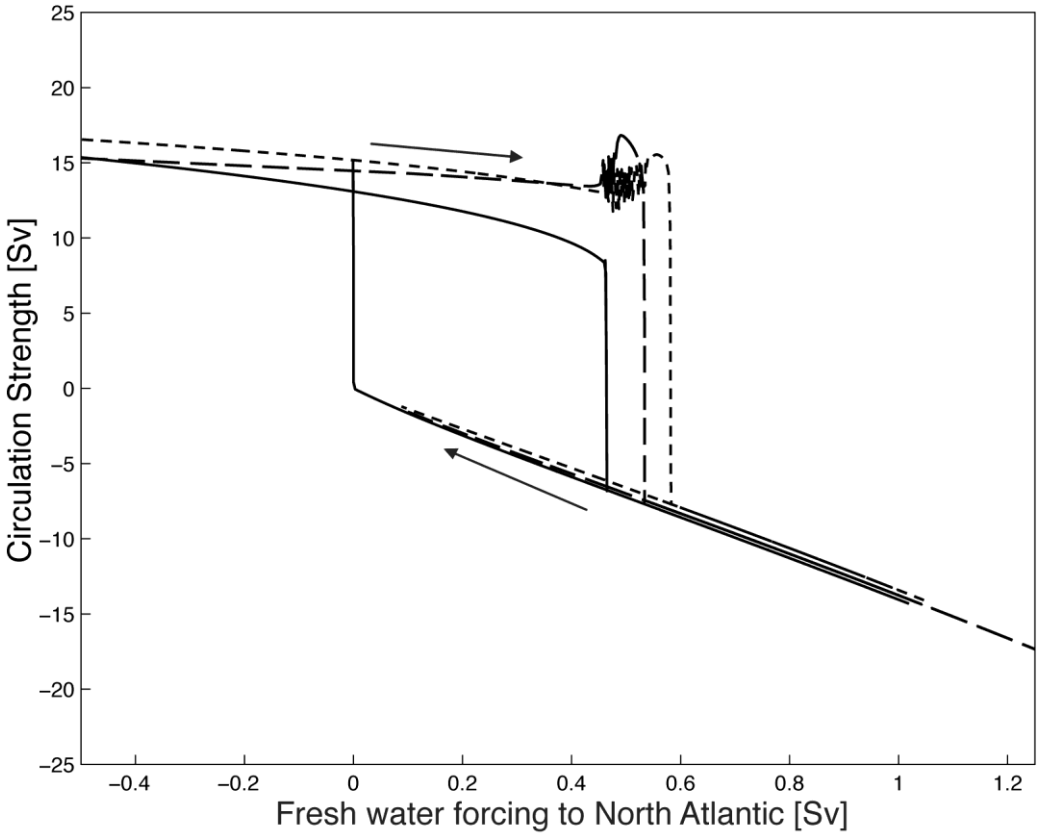

Figure 2.7 Equilibrium solutions of the 4-box ocean model with a parameterization of the Southern Ocean according to Gnanadesikan [1999]. The meridional overturning circulation in the northern hemisphere (q_1) is shown as a function of the meridional moisture transport in the atmosphere (φ_1). Arrows indicate the direction of hysteresis. The different lines refer to different mixing assumptions: constant vertical mixing (solid line), stability dependent mixing (short dashed line), and constant mixing energy (long dashed line).

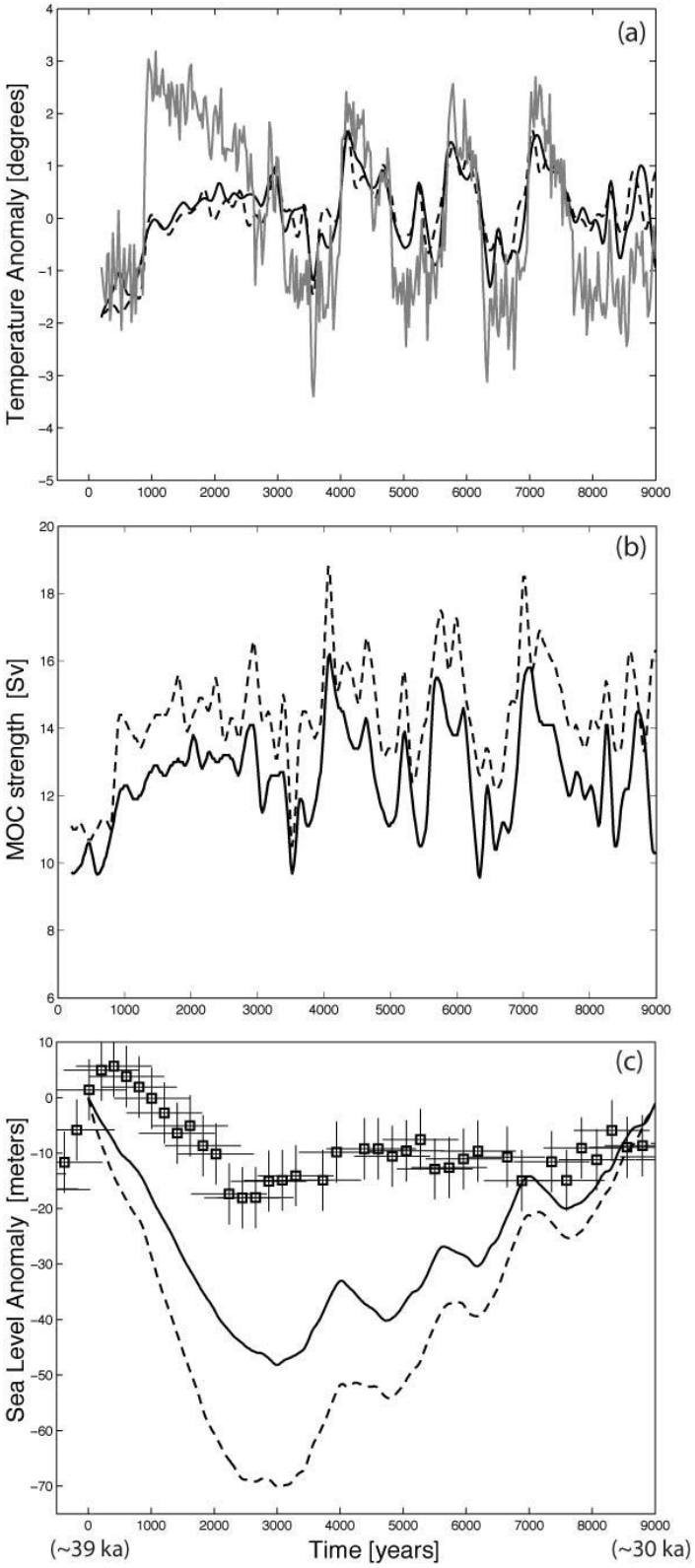
(a)
Temperature Anomaly [degrees]
(b)
MOC strength [Sv]
(c)
Sea Level Anomaly [meters]
(~39 ka)
Time [years]
(~30 ka)

Figure 2.8 Inversion solutions for the 4-box model with a representation of the Southern Ocean. Panel (a) compares the model solutions for temperature for the polar northern temperature (black lines) to the scaled Greenland record (gray lines) [Grootes et al., 1993; Meese et al., 1997]. Panel (b) gives the corresponding solutions for MOC strength [Sv], Panel (c) compares sea level anomalies inferred from the Greenland record and estimated from $\delta^{18}O$ records from the Red Sea [Siddall et al., 2003]. The solid, short, and long dashed lines correspond to different assumptions about vertical mixing: constant vertical mixing (solid line), stability dependent mixing (short dashed line), and constant mixing energy (long dashed line).

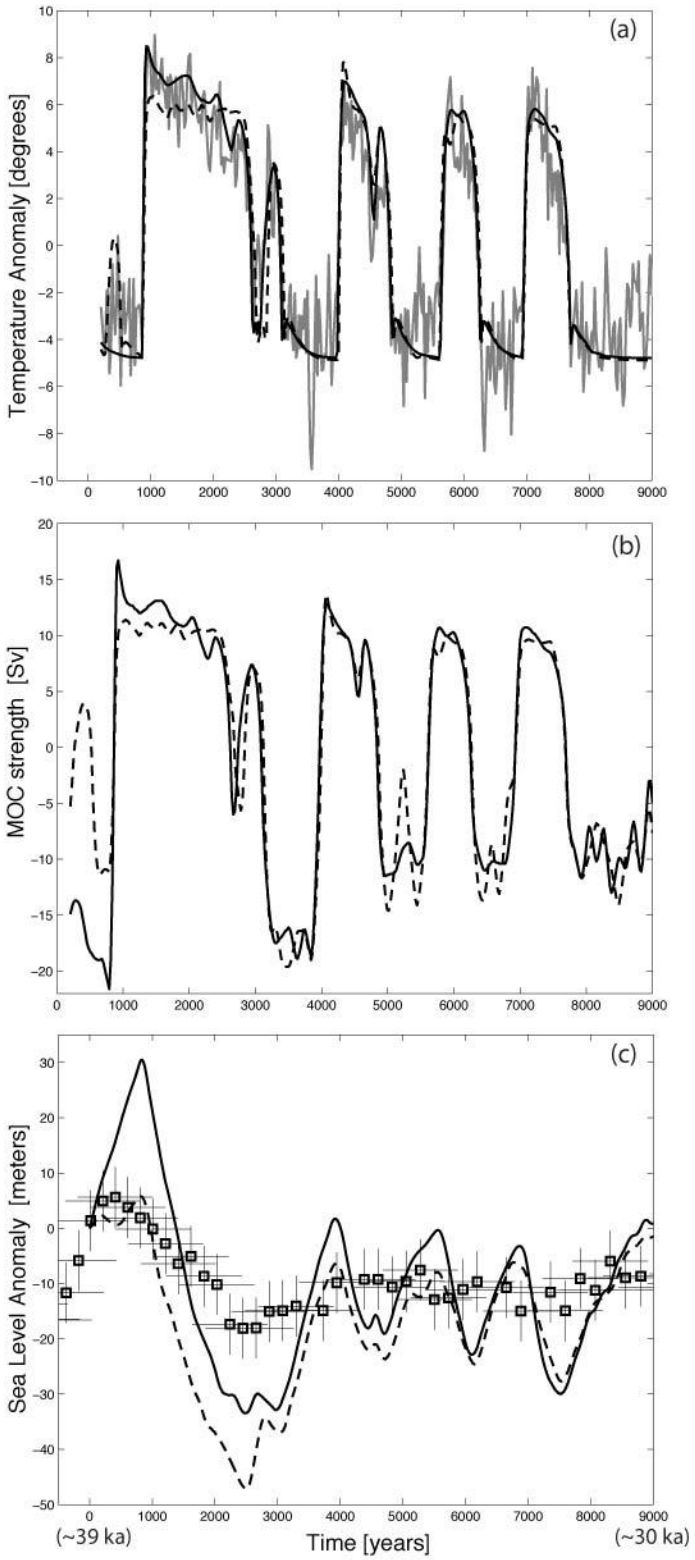
(a)
Temperature Anomaly [degrees]
(b)
MOC strength [Sv]
(c)
Sea Level Anomaly [meters]
(~39 ka)
Time [years]
(~30 ka)

Figure 2.9 Inversion solutions for the 6-box model, with two boxes in each polar region and a stability threshold for deep convection in these regions. Panel (a) compares the solutions for the polar northern temperature (black lines) to the scaled Greenland record (gray lines) [Grootes et al., 1993; Meese et al., 1997]. Panel (b) gives the corresponding estimate for MOC strength. Panel (c) compares sea level anomalies inferred from the Greeland record and estimated from $\delta^{18}O$ records from the Red Sea [Siddall et al., 2003]. The solid dashed lines correspond to different rates of deep convection: 5 Sv (solid) and 1 Sv (dashed).

With polar stratification inversion solutions indicate that a much larger amount of freshwater is required to force abrupt transitions in meridional overturning circulation as compared to the 4-box model and sea level records (Figure 2.9). Equilibrium sensitivity of the MOC to freshwater forcing indicates the absence of equatorially symmetric solutions that were so important to the 4-box model solutions. Thus, processes at high latitudes (Southern Ocean or polar stratification) lead to significantly different inferences about freshwater forcing from the Greenland record. However, whether these processes can aptly be represented in a box model is unclear.

2.5.3.3 *Higher-dimensional model*. The fluxes of mass, heat, and salt are represented very crudely in an ocean box model. The extent to which this crudeness influences our results, in particular our estimate of freshwater forcing, warrants therefore further consideration. In an effort to assess the accuracy of our results, the freshwater forcing derived from the

4-box model inversion of the Greenland data (e.g., Figure 2.3b) is used as boundary conditions for a more physically realistic, zonally averaged climate model [*Schmittner and Stocker*, 2001]. This model comprises three components: (i) an ocean circulation model with three basins (Atlantic, Pacific, and Indian Oceans) connected to a Southern Ocean [*Wright and Stocker*, 1992]; (ii) a zonally averaged energy and moisture balance model of the atmosphere [*Stocker et al.*, 1992], and (iii) a thermodynamic model of sea ice [*Wright and Stocker*, 1993]. After tuning, the model is able to capture important features of observed modern climate such as the seasonal variations in surface air temperature, the meridional circulation in different oceanic basins, and the meridional heat and moisture fluxes in the ocean and atmosphere [*Schmittner and Stocker*, 2001; *Stocker et al*., 1992].

I find that the climate model, when forced with the freshwater water anomalies deduced from the combination of Greenland data and the box model, reproduces the paleo-temperature record from the Greenland ice core to a reasonable degree (Figure 2.10). This result provides some additional support to the relevance of the box model to interpret the Greenland data. Use of the zonally averaged model for the purpose of inferring freshwater forcing from these data is the subject of a separate study [*Lu et al.*, submitted].

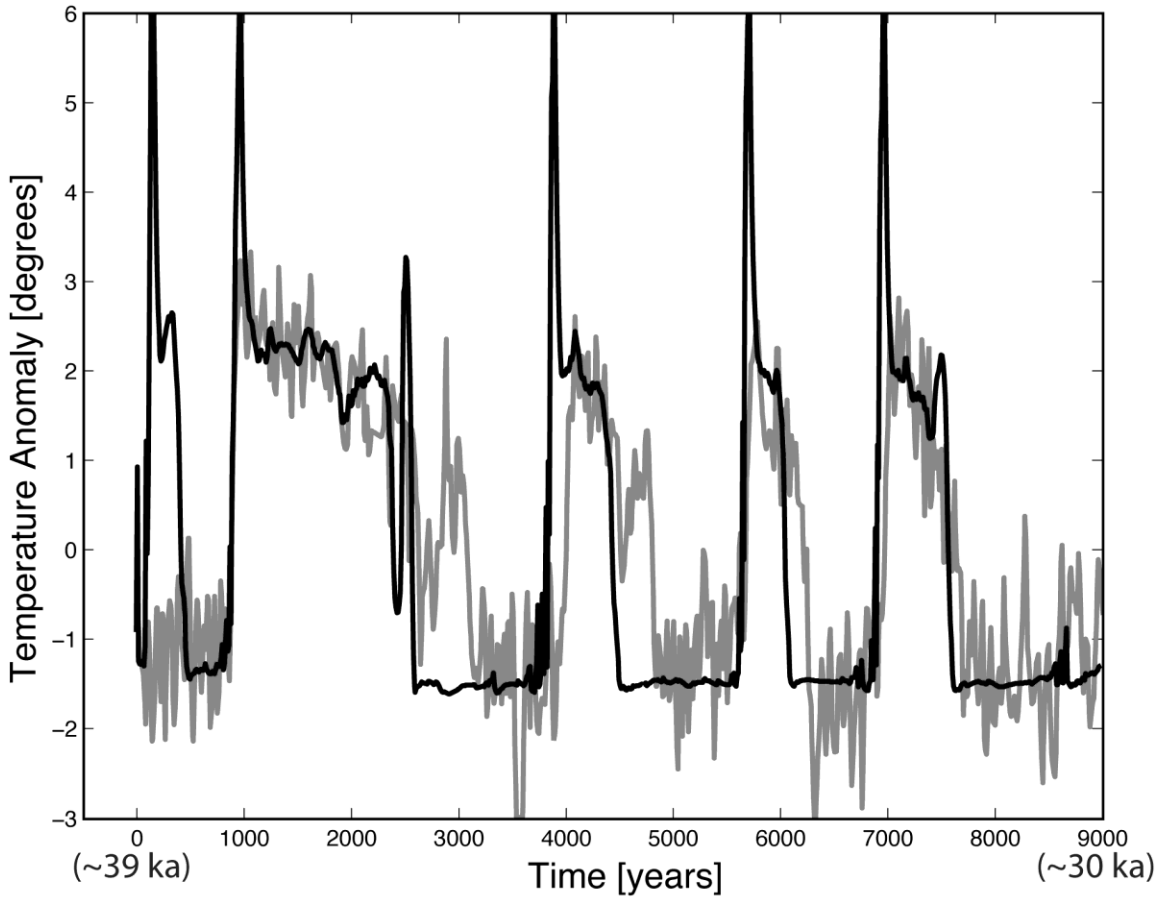

Figure 2.10 Response of a zonally averaged climate model [Schmittner and Stocker, 2001; see text] to freshwater forcing solutions found through inversion of the Greenland record with the 4-box model (i.e. those in Figure 2.3b). Shown is time series of sea surface temperature at 72°N in the Atlantic Ocean as compared to the temperature inferred from the Greenland record [Grootes et al., 1993; Meese et al., 1997].

2.6 Conclusions

Bayesian stochastic inversion is used to test the freshwater forcing hypothesis of abrupt climate change. A time series of freshwater flux anomaly in the North Atlantic Ocean between 30 and 39 kyr B.P. is inferred by combining a paleo-temperature record from a Greenland ice core with an ocean box model . Reconstructions of global sea level from independent geological records are then compared to the sea level changes implied by these anomalies. The comparison gives some support to the freshwater forcing hypothesis for the time interval from 30 to 39 kyr B.P. The largest drop in sea level present in observations and in our inversion is associated with ice sheet growth which enables sustained freshwater removal from the ocean and enhanced meridional circulation and heat flux to maintain the observed warmth during the long (~2.5 kyr) DOI 8. According to our results, the longer the period of warmth the larger the drop in sea level. Thus, both our results and observations show an approximately 15 to 20 m drop in sea level following Heinrich event 4 at 39 kyr B.P., the feature of greatest "commonality" (between model and observation). They also show agreement in sign, but not necessarily in amplitude, for the other DOIs. The significance of the discrepancies warrants further investigation.

I have considered three fundamentally different assumptions about vertical buoyancy transport at low latitudes corresponding to constant vertical mixing, stability-dependent mixing, and fixed mixing energy. These different assumptions produce, for the steady state, qualitatively different sensitivities of meridional mass transport to

freshwater forcing, including the possibility that an increase in freshwater forcing leads to an increase in the transport. Our inversion results, however, are robust against these assumptions. Thus, the sensitivity to the nature of vertical mixing is most apparent for circulation states at equilibrium and much less so for the adjustment of circulation to time-dependent freshwater forcing.

Some of the major limitations of this work should be stressed. For example, it is assumed that the Greenland paleo-temperature record reflects changes in oceanic poleward heat transport and that an equatorially symmetric 4-box ocean model can represent this transport adequately. More realistic ocean models would be required to test other potentially important assumptions such as the treatment of the Southern Ocean and polar stratification.

Chapter 3 4-Box Model Perturbation Analysis

3.1 Introduction

In the last chapter, the 4-box model is used to test the ice sheet freshwater forcing hypothesis of abrupt climate change by inferring the quantity of continental ice sheet melt to northern polar box1 (Figure 2.1) that can reproduce the Greenland ice core temperature proxy record. I found that the inversion solutions were independent of uncertainties in the treatment of vertical mixing in the low latitude ocean, despite the importance of these treatments to the model's equilibrium sensitivity to freshwater forcing. Also, I found that the inversion solutions remain in a symmetric circulation configuration, which is curious as the symmetric state only exists for a small range of freshwater forcing perturbations than the asymmetric mode. The 4-box model used in Chapter 2 was formulated based on scaling arguments of Nilsson and Walin (2001) applicable to long-term balances in a single hemisphere context. The possibility that freshwater forcing could increase MOC flow illustrated the potential importance of non-local factors (i.e. vertical mixing at low latitudes) over buoyancy forcing to the high latitudes in contradiction to most thinking and modeling studies on the subject (*Huang*, 1999; *Nilsson*, 2003; *Mohammad and Nilsson*, 2004). Till now it has been clear that the NW's scaling theory is plausible in single hemisphere models, in which the return flow is entirely governed by low latitude vertical mixing. However, it has not been clear that such arguments would apply to two-hemisphere ocean, including a study by Marzeion et al (2007), who did not find that vertical mixing was as important a factor in determining the MOC response to freshwater forcing in an OGCM.

Of the various 4-box model equilibrium state responses to freshwater forcing, NW's scaling theory is only applicable in the northern sinking asymmetric case; while it is not true for the symmetric regime that has sinking in both polar regions. I find that vertical mixing is not important in our inversion experiment. This may be due to the transient nature of the forcing or possibly from the fact that the inversion solutions only make use of the symmetric modes of the circulation.

Here I will address the question of why the NW's scaling theory fails in the 4-box model symmetric regime and the apparent unimportance of the vertical mixing to the box model inversion solutions. Although the box model is highly idealized, it affords us the opportunity to analyze more precisely the balance of factors that control its behavior. Here I shall examine the transient adjustment progresses by breaking the governing equations into a sum of component contributions. Answers to these questions may also help interpret the freshwater forcing inversion experiments that favor the seemingly more fragile symmetric circulation modes.

3.2 Methods

Below I address questions concerning the similarity and differences between two versions of the 4-box model that either assume a coefficient of vertical diffusivity that is independent of vertical density stratification ("constant diffusivity") or a coefficient of diffusivity that scales inversely with vertical density stratification ("constant energy").

An understanding of factors controlling model behavior comes from a perturbation analysis of the governing equations in which I subdivide contributions to the total flow into 0th, 1st, 2nd, and 3rd order terms for the poleward flow (q_1 and q_4 in Figure 2.1; see Appendix 3). I evaluate the terms dominating the model's stability by considering the transient and long-term response of q_1 and q_4 to a step increase in poleward moisture transports φ_1. Differences in vertical mixing formulation may affect q_1 and q_4 by governing the depth and mass transport into the low latitude shallow box2.

3.3 4-box model asymmetric AMOC perturbation analysis

The asymmetric MOC occurs when the column average density of the low latitude boxes is smaller than one polar box and larger than the other polar box. When this occurs, a small amount of upwelling is maintained in the light polar box through poleward moisture fluxes that dominate over radiative cooling effects to the polar atmosphere. In our equilibrium constant diffusivity case with sinking in the northern and upwelling in the southern, $\rho_1 = \rho_3 =$ 1.0269 (g/cm^3), $\rho_2 =$ 1.0249 (g/cm^3), $\rho_4 =$ 1.0265 (g/cm^3). For the constant energy case, $\rho_1 = \rho_3 =$ 1.0267 (g/cm^3), $\rho_2 =$ 1.0249 (g/cm^3), $\rho_4 =$ 1.0263 (g/cm^3). q_1 is governed to 0th order by the density contrast between the surface and deep low latitude boxes (term $q_{10A} \propto (\rho_{3eq} - \rho_{2eq})$) (equations A3.1.3-A3.1.4). The other 0th order term is negligible as the density of the deep low latitude box 3 is the same as the sinking polar box1 thus eliminating a role for term $q_{10B} \propto (\rho_{1eq} - \rho_{3eq})$. In contrast to q_1, both 0th order terms are important for q_4 in box4.

However because the density of the box4 is less than the bottom tropical box3, effects of term $q_{40B} \propto (\rho_{4eq} - \rho_{3eq})$ is negative and more than counters the positive effects of $q_{40A} \propto (\rho_{3eq} - \rho_{2eq})$ (Figure 3.1).

The response of the southern box circulation q_4 to a 0.2Sv step increase in the northern poleward atmospheric moisture transport φ_1 is minimal (< 0.5Sv) for both the constant diffusivity and constant energy configurations (Figure 3.2). It is this minimal response that permits the 4-box model to retain NW's scaling arguments. I use the perturbation analysis to look more closely at why this can be. The most important balances for q_1 and q_4 are in the first order terms equations (A3.1.5-A3.1.8). For q_4, all first order terms contribute significantly to the overall response, giving rise to a complex transient behavior because of the different adjustment time scales, but ultimately nearly cancel each other (Figure 3.3). The two factors that would tend to increase the negative high-to-low latitude density gradient and make q_4 more negative, namely increases in the shallow tropical box salinity and decreases in the southern polar box salinity, are undermined by a deepening thermocline (caused by reductions in northern polar sinking q_1 and/or increases in tropical upwelling q_m) and a freshening of the deep tropical box3. Within these four terms governing the evolution of q_4, the two terms that are perhaps the least obvious to explain involve a difference between two perturbation terms (i.e. terms $q_{41B} \propto (d\rho_4 - d\rho_3)$ and $q_{41C} \propto (d\rho_3 - d\rho_2)$). In the case of q_{41B}, it is important to note that the decreased density for the deep low-latitude ocean box3 mimic

those of the northern polar box1 and has a larger amplitude as compared to the southern polar box4. Term q_{41C} is dominated by a large increase in shallow low-latitude ocean box2 salinity that is a factor of 3 to 4 times smaller than the deep low-latitude ocean box3.

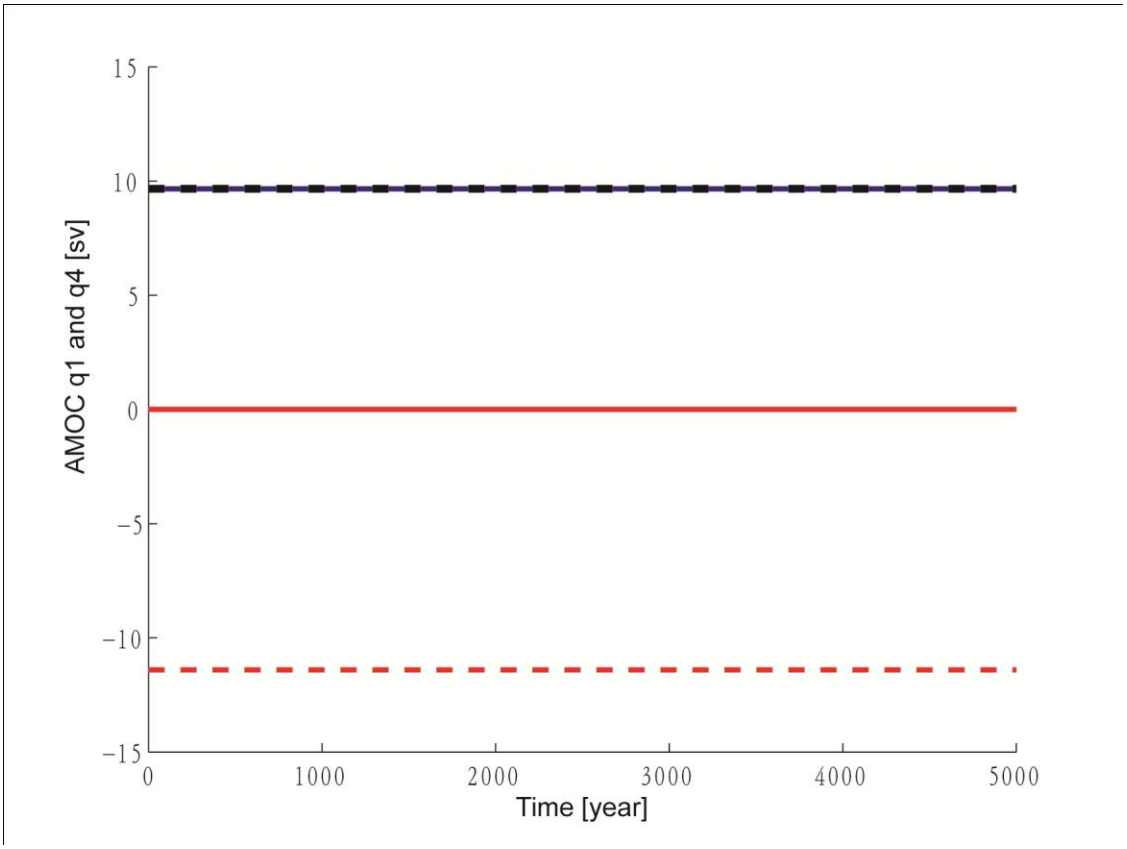

Figure 3.1 The four 0^{th} order terms for q_1 and q_4 for an asymmetric circulation state. Two positive terms are from $q_{10A} = q_{40A} \propto (\rho_{3eq} - \rho_{2eq})$ (dashed black and solid blue lines). The remaining two terms are $q_{10B} \propto (\rho_{1eq} - \rho_{3eq})$ (solid red), which is negligible, and $q_{40B} \propto (\rho_{4eq} - \rho_{3eq})$ (dashed red), which nearly cancels $q_{40A} \propto (\rho_{3eq} - \rho_{2eq})$.

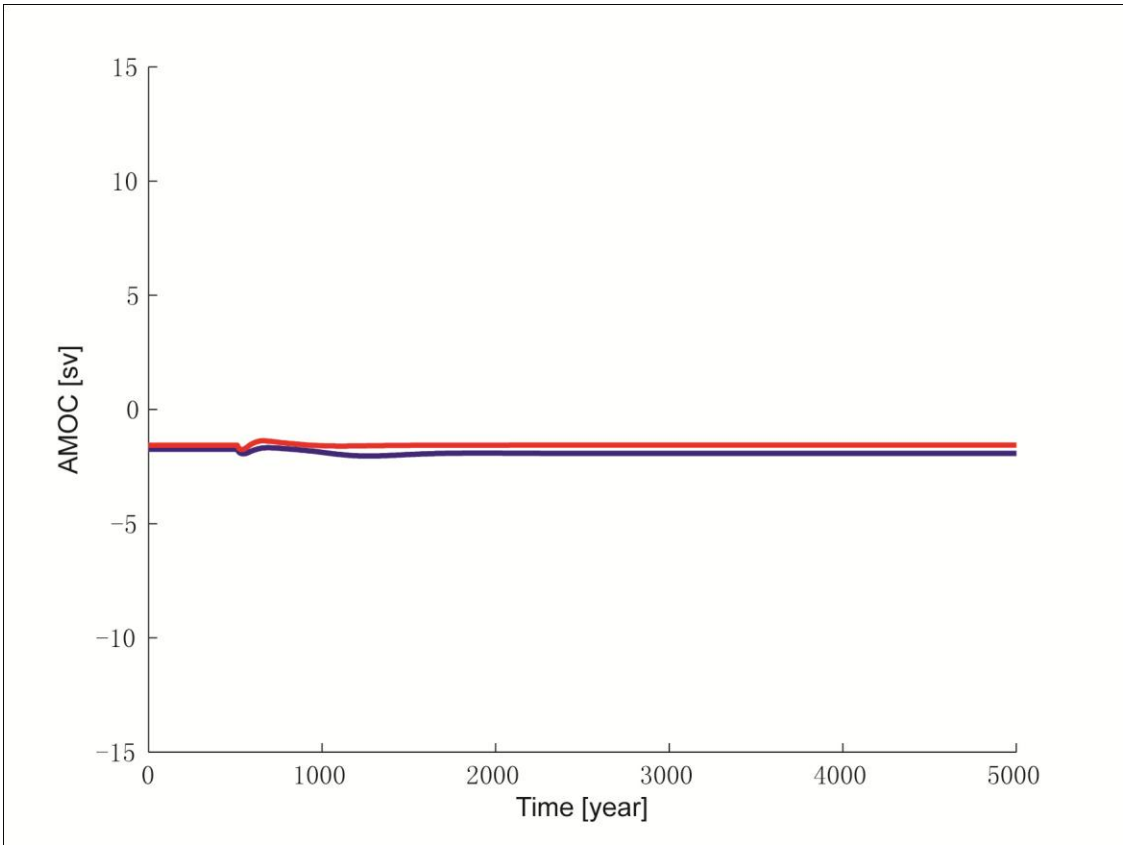

Figure 3.2 The response of the southern box circulation q_4 to a 0.2Sv step increase in the northern poleward atmospheric moisture transport φ_1 , under the constant diffusivity (blue) and constant mixing energy (red) assumptions.

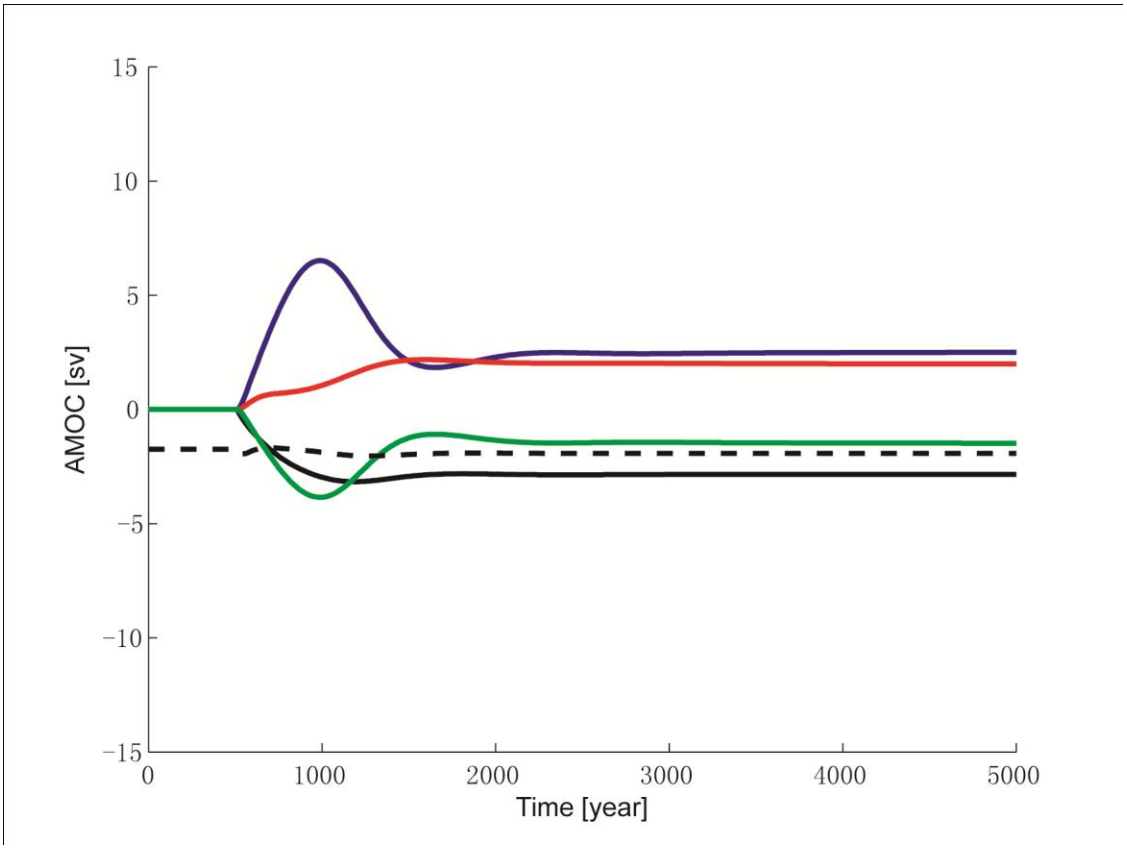

Figure 3.3 The response of the four 1st order terms of q_4 *(solid) and* q_4 *total (dashed) to a 0.2Sv increase in northern poleward moisture transports* φ_1 *. Terms* $q_{41A} \propto (\rho_{3eq} - \rho_{2eq})dD$ *(blue) and* $q_{41D} \propto (\rho_{4eq} - \rho_{3eq})dD$ *(green) follow the same thermocline depth anomalies, but result in nearly opposite contributions to overall flow. Terms* $q_{41B} \propto (d\rho_4 - d\rho_3)$ *(red) increases because of reductions in box4 density from freshening that oppose* $q_{41C} \propto (d\rho_3 - d\rho_2)$ *(black), which becomes more negative from large increase in box2 density from increasing salinity.*

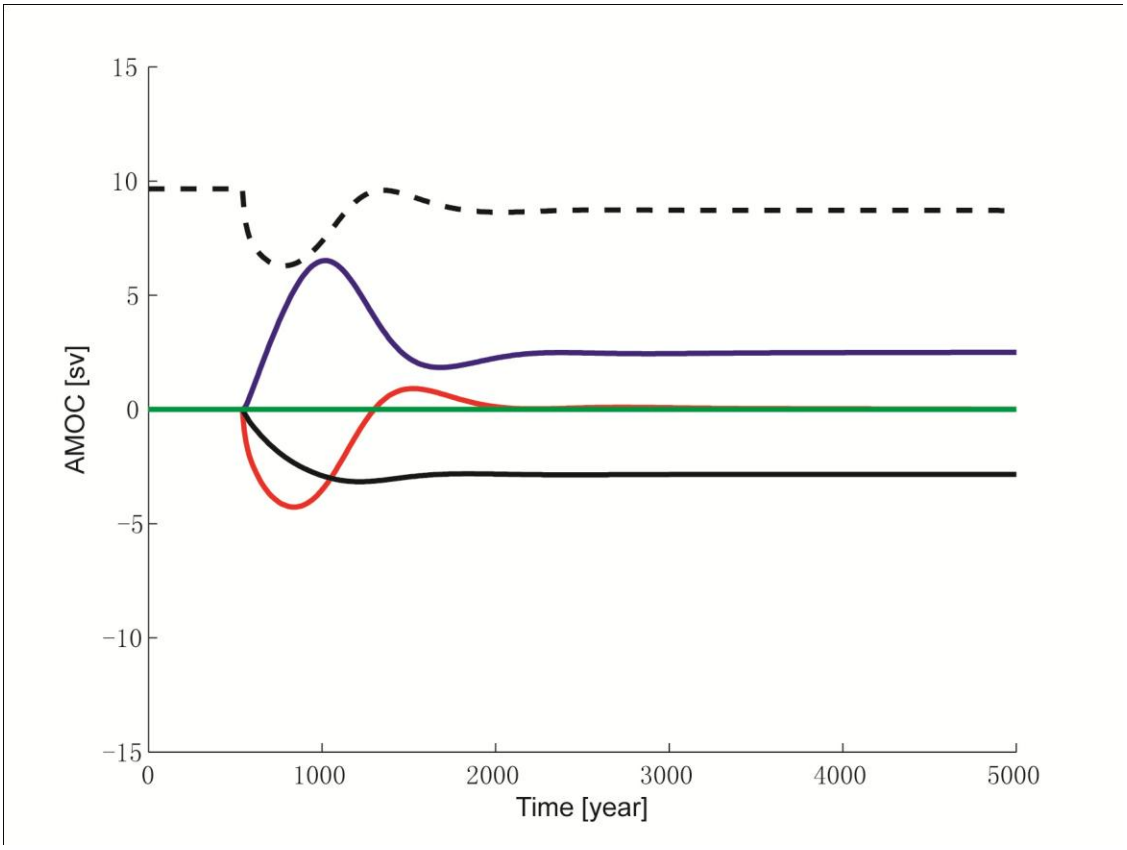

Figure 3.4 The response of the four 1st order terms of q_1 *(solid) and* q_1 *total (dashed) to a 0.2Sv increase in northern poleward moisture transports* φ_1 *. Term* $q_{11A} \propto (\rho_{3eq} - \rho_{2eq})dD$ *(blue) follows the thermocline depth anomalies, becoming more positive; term* $q_{11C} \propto (d\rho_3 - d\rho_2)$ *(black) becomes more negative from large increase in box2 density from increasing salinity; term* $q_{11D} \propto (\rho_{1eq} - \rho_{3eq})dD$ *(green) is negligible; term* $q_{11B} \propto (d\rho_1 - d\rho_3)$ *(red) reduces because of reduction of box1 density from freshening.*

3.4 4-box model symmetric AMOC perturbation analysis

The symmetric regime with sinking in both polar regions is stable when the 4-box model is initialized as two (south/north) similarly dense polar columns as compared to a less dense low latitude column (Figure 2.1). In the equilibrium constant mixing case, $\rho_1 = \rho_3 = \rho_4 = 1.0271$ (g/cm^3), $\rho_2 = 1.0250$ (g/cm^3); and constant mixing energy case, $\rho_1 = \rho_3 = \rho_4 = 1.0270$ (g/cm^3), $\rho_2 = 1.0249$ (g/cm^3). As is the case with the asymmetric mixing, the q_1 is governed by two 0^{th} order terms in equations (A3.1.3-A3.1.4) (Appendix 3). Because the density of the deep low-latitude box3 is the same as the sinking polar box1, the role of the term $q_{10B} \propto (\rho_{1eq} - \rho_{3eq})$ is eliminated (Figure 3.5). To 0^{th} order q_1 and q_4 only depend on the low latitude vertical density contrast $q_{10B} \propto (\rho_{3eq} - \rho_{2eq})$, which is not related with northern polar box density. This allows for the 4-box model to maintain its symmetric polar sinking circulation states.

In the symmetric regime with sinking in both polar regions, the equilibrium response of the 4-box model to a 0.01Sv step increase in the northern poleward atmosphere moisture transport φ_1 is independent of low-latitude vertical mixing assumptions. (Note the small forcing is required as the symmetric states are less "robust" than the symmetric states.) Perturbed by variations of φ_1 , the overturning sinking branches in southern and northern polar boxes respond in opposite ways (one increases while the other decreases) (Figure 3.6).

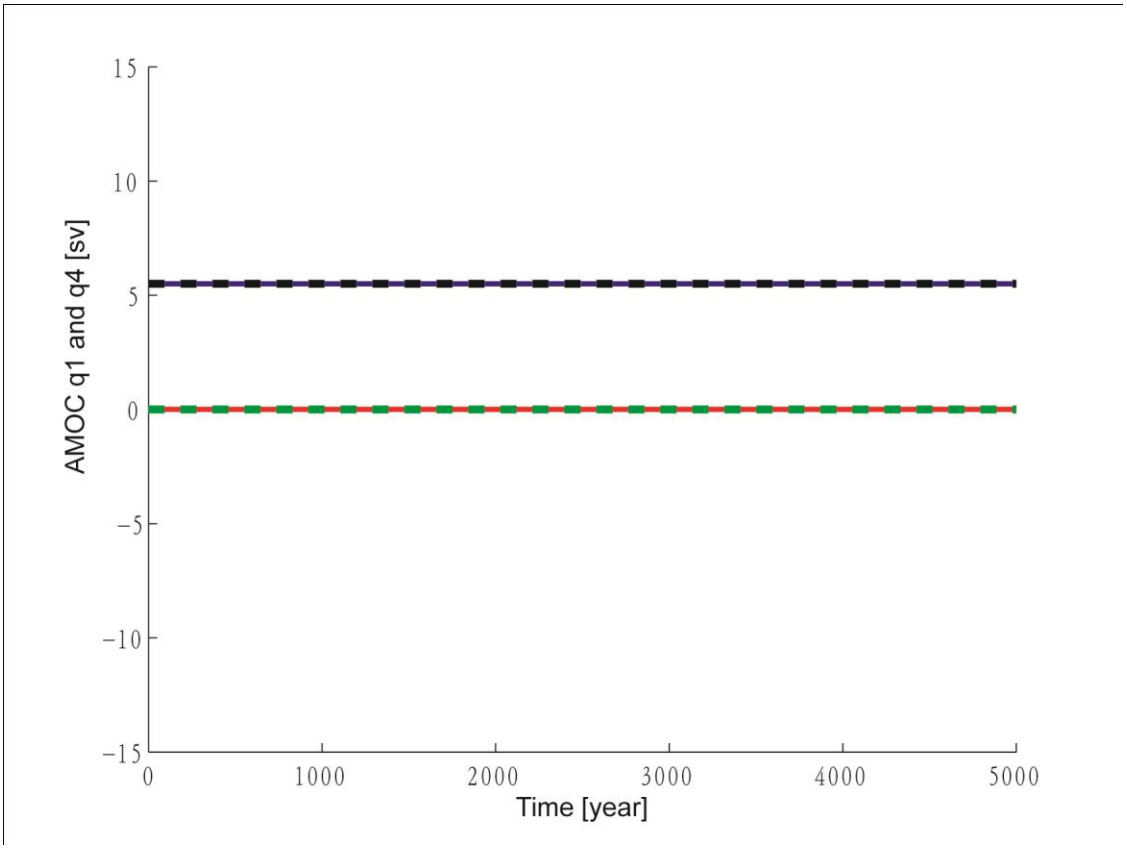

Figure 3.5 The four 0^{th} order terms for q_1 and q_4 in symmetric circulation state. Two positive terms are from $q_{10A} = q_{40A} \propto (\rho_{3eq} - \rho_{2eq})$ (dashed black and solid blue lines). The remaining two terms are $q_{10B} = q_{10A} \propto (\rho_{1eq} - \rho_{3eq})$, which are zero.

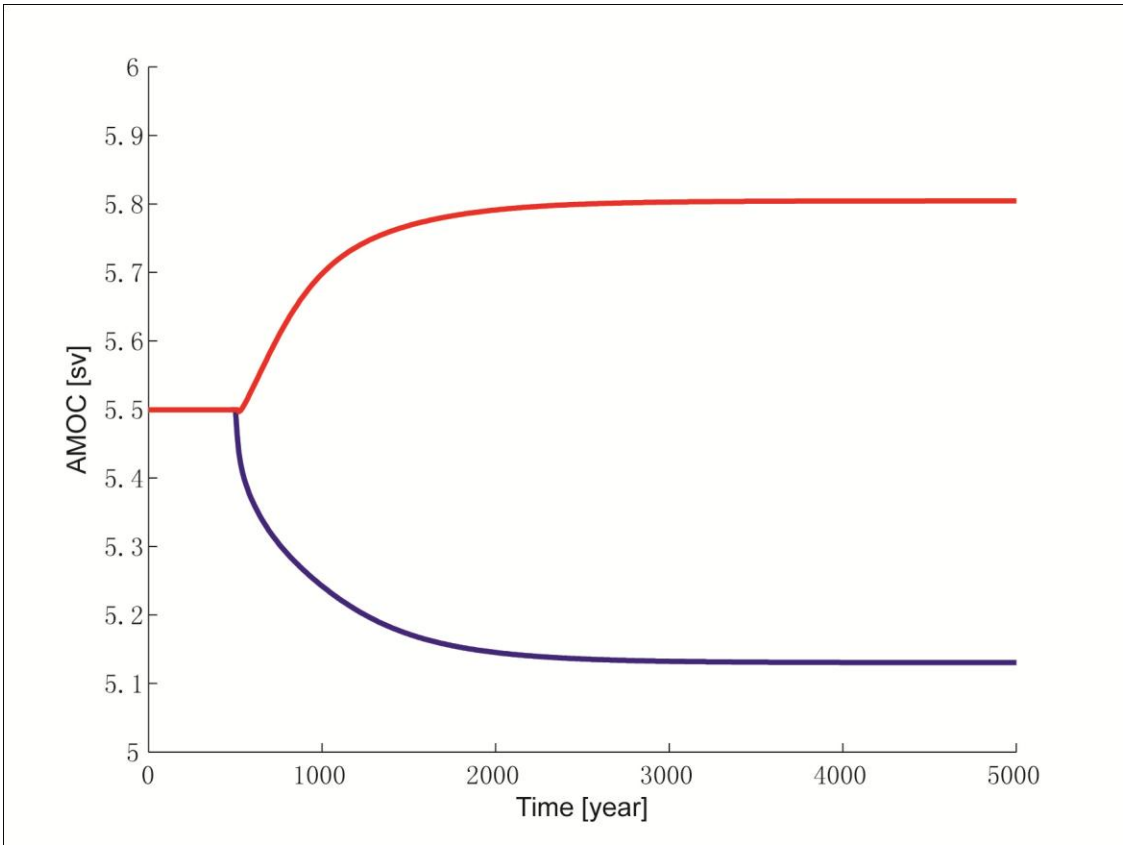

Figure 3.6 The responses of northern sinking q_1 *(blue) and southern sinking* q_4 *(red) to a 0.01Sv increase in northern poleward moisture transports* φ_1 *in symmetric circulation configuration.*

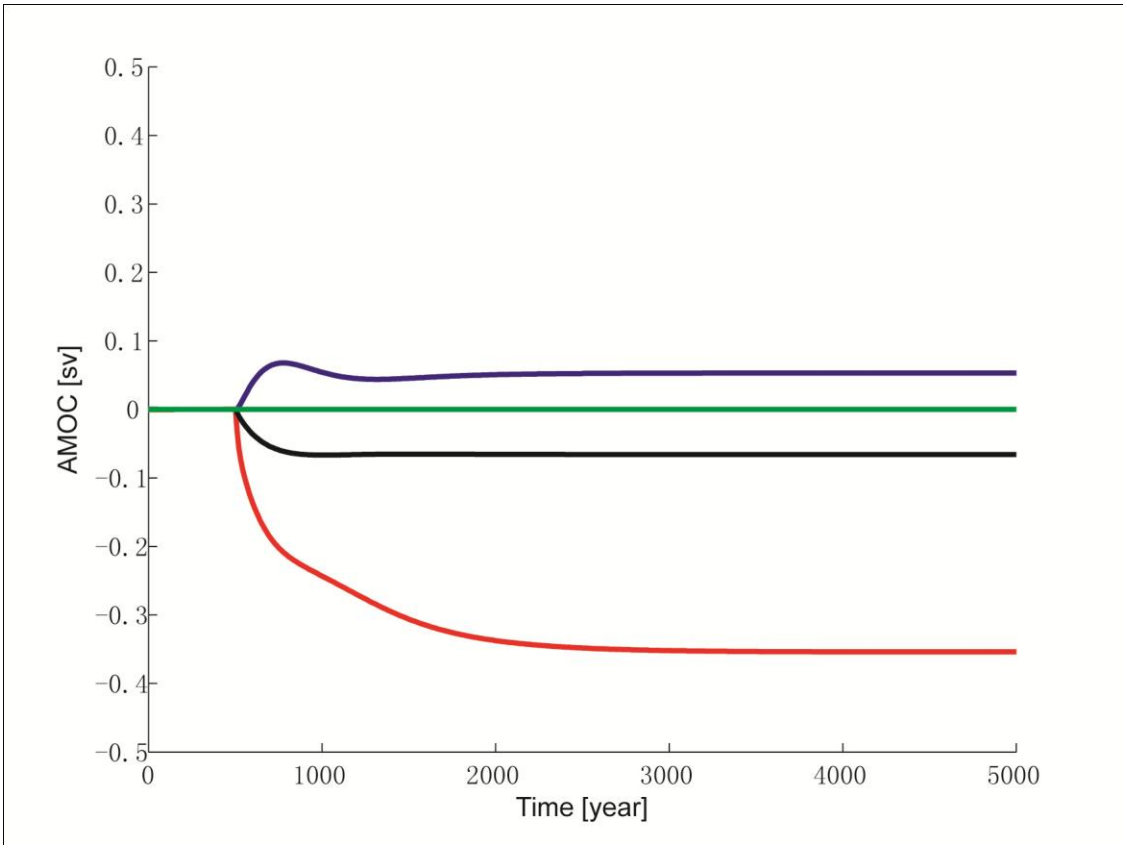

Figure 3.7 The response of the four 1st order terms of q_1 *to a 0.01Sv increase in northern poleward moisture transports* φ_1*. Term* $q_{11A} \propto (\rho_{3eq} - \rho_{2eq})dD$ *(blue) follows the thermocline depth anomalies, becoming more positive; term* $q_{11C} \propto (d\rho_3 - d\rho_2)$ *(black) becomes more negative from large increase in box2 density from increasing salinity; term* $q_{11D} \propto (\rho_{1eq} - \rho_{3eq})dD$ *(green) is negligible; term* $q_{11B} \propto (d\rho_1 - d\rho_3)$ *(red) reduces because of reduction of box1 density from freshening.*

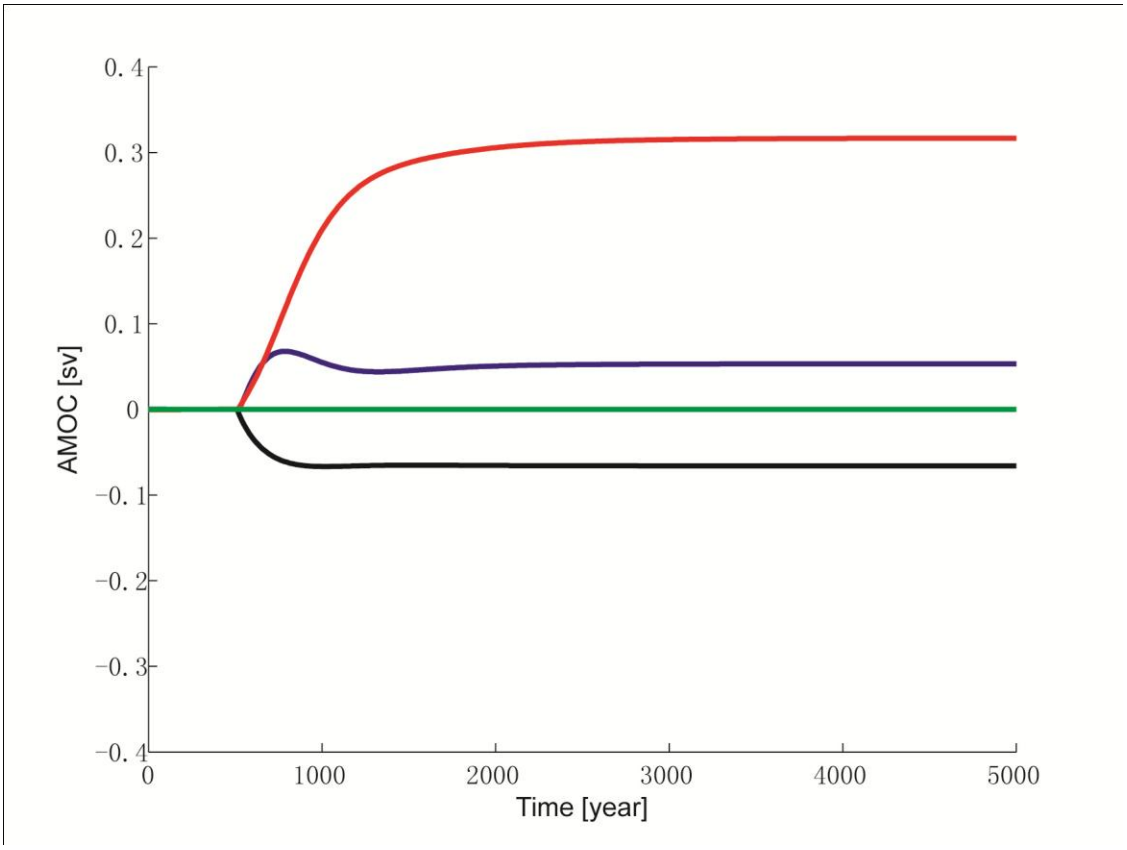

Figure 3.8 The response of the four 1st order terms of q_4 to a 0.01Sv increase in northern poleward moisture transports φ_1. Term $q_{41A} \propto (\rho_{3eq} - \rho_{2eq})dD$ (blue) follows the thermocline depth anomalies, becoming more positive; term $q_{41C} \propto (d\rho_3 - d\rho_2)$ (black) becomes more negative from large increase in box2 density from increasing salinity; term $q_{41D} \propto (\rho_{4eq} - \rho_{3eq})dD$ (green) is negligible; term $q_{41B} \propto (d\rho_4 - d\rho_3)$ (red) increases because of incensement of box4 density from low latitude saltier q_4.

The dominant effects from the northern poleward atmosphere moisture transport φ_1 on q_1 and q_4 are mostly explained by the 1st order terms (equations A3.1.5-A3.1.8). For each mass flux q_1 and q_4 three terms contribute, but two of them nearly cancel; the "A" $\propto dD$ (q_{11A} and q_{41A}) terms act to reduce the low latitude column density due to deepening thermocline (Figure 3.7 and Figure 3.8) and is undermined by the "C" $\propto (d\rho_3 - d\rho_2)$ (q11C and q41C) terms, which is dominated by increasing ρ_2 through salinity increases.

The "B" terms (q_{11B} and q_{41B}) dominate the circulation mass flux q_1 and q_4; and they are nearly equal and opposite: $q_{11B} \propto (d\rho_1 - d\rho_3)$ in q_1 compensates $q_{41B} \propto (d\rho_4 - d\rho_3)$ in q_4. Unlike in the asymmetric case, where the response of q_4 was minimal, the circulation changes induced by changes in poleward moisture fluxes φ_1 are amplified by changes in the low latitude. When more freshwater is pumped from low latitude surface box2 to northern polar box1 via atmosphere poleward moisture flux φ_1, the strength of mass flux q_1 from box2 to box1 is reduced. Both effects make the low latitude surface box2 more salty. Without considering changes in q_4, the extra salinity in box2 would be communicated to the southern polar box4, allowing it to become more dense. This increased density between low and high latitudes further increase q_4 . In contrast to "asymmetric" case, this same feedback is "negative" due to the upwelling q_4 in southern polar box4, in which case instead of q_4, the vertical mixing in low latitude

ocean is "forced" to compensate the northern sinking q_1. It turns out that the very small changes of the vertical mixing rate in low latitude ocean from changes in poleward moisture transport φ_1 does not allow the 4-box model to be sensitive to the details of its uncertainty physics.

3.5 Discussion

3.5.1 Why there may be limited information in paleo proxy data to test ocean mixing physics.

In the asymmetric circulation configuration, response to high latitude freshening, the transient MOC follows the variation of high-low latitude density contrast in northern hemisphere (equation A3.1.6). Because the high latitude ocean gets freshening first and low latitude ocean gets freshening later, the MOC has a transient "U" type response (Figure 3.4). This "U" type transient response is largely independent of low latitude vertical mixing.

In the symmetric circulation configuration, which is relevant to the inversion solution, the transient MOC response to high latitude northern ocean freshening follows the variation of high-low latitude density contrast in northern hemisphere (equation A3.1.6). This NH event leads to more dense water being pushed to the southern ocean. When the high latitude southern ocean is in the sinking mode (and in the symmetric configuration), this "denser" effect enhances its sinking strength, and occurs in proportion to the reduction in the northern sinking branch. (This southern ocean feedback

to northern freshening is negative to the southern ocean upwelling in the asymmetric circulation regime.) In symmetric circulation configuration, the southern-northern ocean tele-connection via density variation makes the 4-box model MOC be independent of vertical mixing in low latitude ocean, which is true in both dynamic and equilibrium world.

Other modeling studies have noted that Nilsson and Walin (2001) scaling argument may not apply in two-hemisphere model (*Marzeion et al.,* 2007; *De Boer et al.*, 2009). One study reports a "U" response to a steady freshwater forcing implies that it is consistent with NW's argument (*Ottera et al.*, 2003). However, that type of response was seen in our 4-box model without stability dependent vertical mixing.

With the minimal differences in the transient symmetric or asymmetric configuration responses to perturbation, I conclude that there is limited information in paleo data for testing ocean vertical mixing physics. This is because the 4-box model's transient response to northern high latitude freshening is independent of low latitude vertical mixing, which is true for both symmetric and asymmetric circulation configurations. It is only in the asymmetric equilibrium response to high latitude freshening does the 4-box model become sensitive to vertical mixing physics.

3.5.2 Why "symmetric" solutions appear to match paleo data better

Paleo data inferred freshwater forcing only allows the 4-box model to remain in the symmetric circulation configuration, because the asymmetric circulation can't sustain the cold stadials in the paleo data due to the delayed freshwater forcing boosted regime in the model's dynamic response.

If I compare the 4-box model steady-state hysteresis (Figure 1.1) and freshwater forcing solutions (Figure 2.3b), it would seem possible that the overturning circulation should transit to an asymmetric circulation configuration. However, this did not happen (Figure 2.3c). The 4-box model remains in the symmetric circulation configuration. The resolution to this question is that the model is sensitive to both the freshwater forcing rate and forcing amplitude (Figure 3.9). Or in other words, the parameter that matters in the model response to freshwater forcing is the total amount of freshwater forcing, which is a combination of forcing rate and amplitude. This dependence of model overturning circulation to freshwater forcing amount is not strictly linear (Figure 3.10).

Given enough amount of freshwater forcing (e.g. three times big), the 4-box model will transit to the asymmetric circulation configurations. The asymmetric solutions show its characteristic transient "U" response during the period immediately follows an increase in high latitude freshening. If this had happened to the real ocean, I would have seen a much shorter stadial (cold) climate than is shown in the Greenland data (years 3000~3500 and years 4800~5200 in Figure 3.11). In the southern sinking case, the model

predicts the cold phase successfully (years 6200~6700 Figure 3.11), however that requires huge amount of forcing (~120m sea level change), which contradicts to the sea level paleo records.

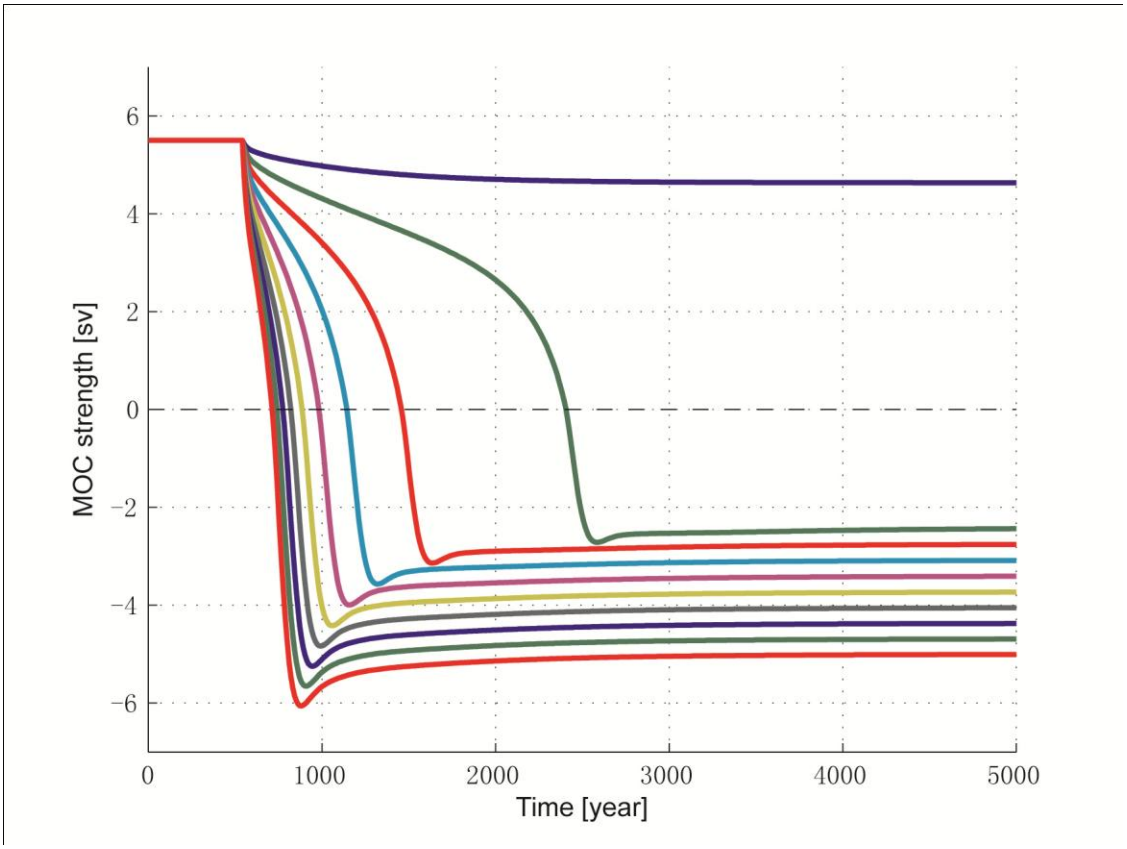

Figure 3.9 4-box model circulation mode sensitivity to freshwater forcing, q_1 response to a step increase in northern poleward moisture transport φ_1 . Top to bottom the forcing is from 0.02 to 0.20Sv with the increment of 0.02Sv.

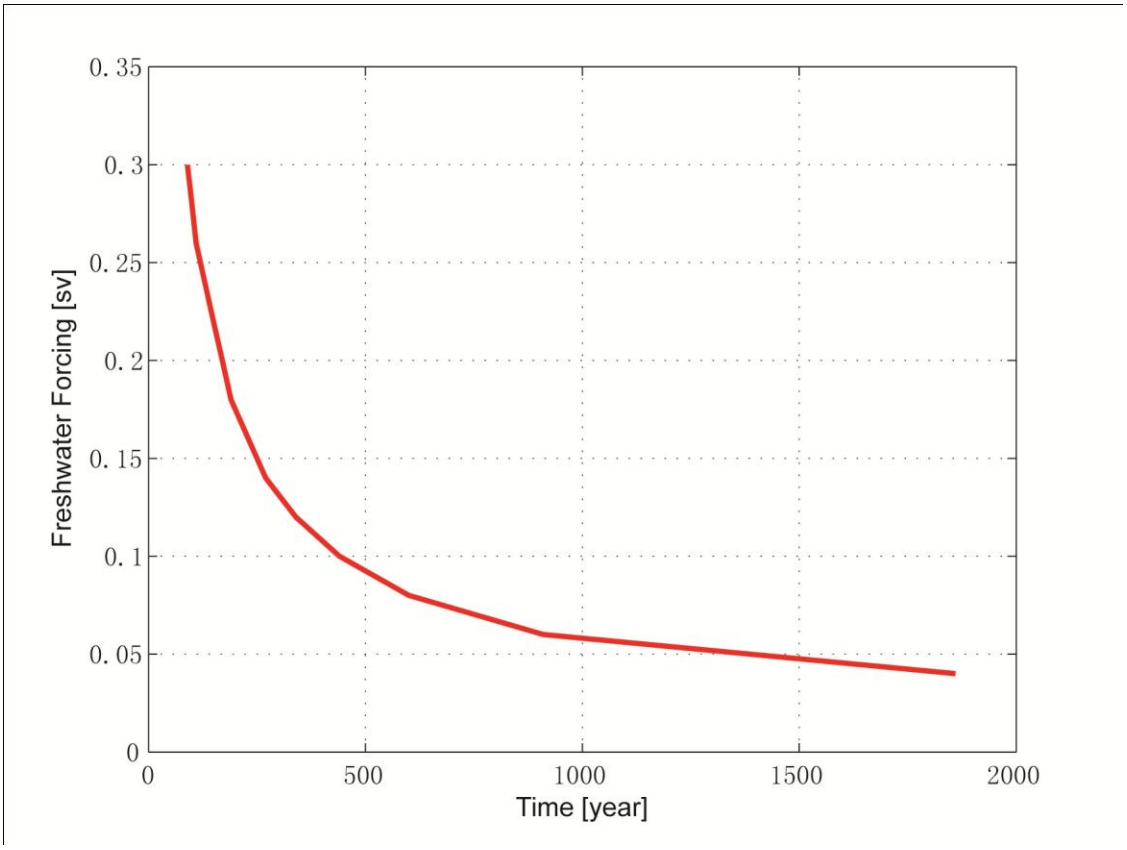

Figure 3.10 Perturbation of increase in poleward moisture transport φ_1 that cause 4-box model to transit to the asymmetric circulation.

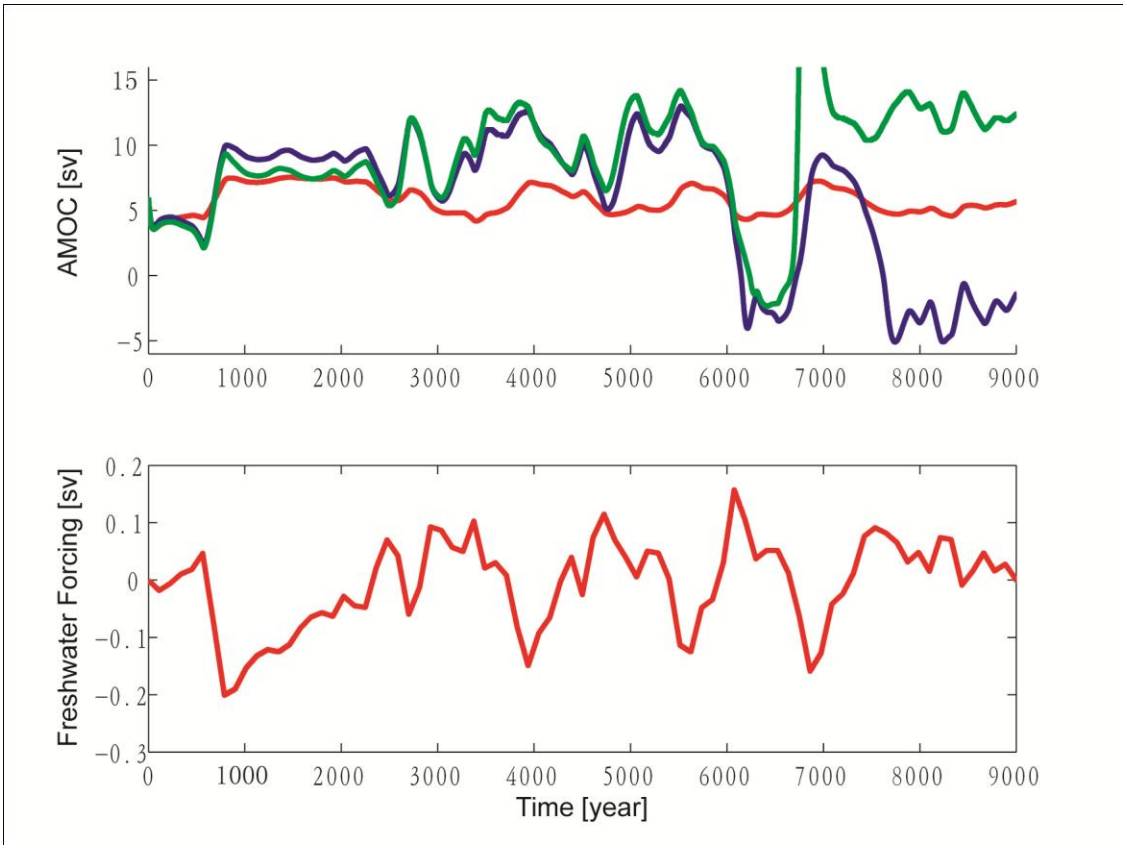

Figure 3.11 Inversion solution of freshwater forcing inferred from paleoclimate data (bottom panel), and model predicted MOCs from the freshwater forcing (top panel). In the model response plot, the MOC remains in the symmetric circulation configuration (red) with the original freshwater forcing in bottom panel; the MOCs will fall into the asymmetric circulation configurations if the forcing is imposed with a larger rate (three times larger); constant diffusivity (blue) and constant energy (green) vertical mixing assumptions are used in the tests.

3.6 Conclusion Remarks

The paleo data inferred freshwater forcing inversion solutions are independent of uncertainties in the treatment of vertical mixing in the low latitude ocean, because in both symmetric and asymmetric circulation configurations, the model's transient responses to freshwater forcing perturbation are independent of vertical mixing physics. The paleo data inferred freshwater forcing solution remains in the symmetric circulation configuration, because the asymmetric circulation can't sustain the cold stadials similar to what is observed in the paleo data. This is due to the asymmetric circulation configuration's large amplitude transient response to sudden changes in high latitude freshening.

Chapter 4 Consistent Observational and Modeling Support for Ice Sheet Forcing of Abrupt Climate Change

4.1 Introduction

Geologic records and climate model simulations suggest that changes in the meridional heat transport in the Atlantic Ocean were involved in the abrupt warming events – the so-called Dansgaard-Oeschger Interstadials (DOIs) – that punctuated an otherwise cold Greenland climate during the last glacial period. However, the role of Northern Hemisphere (NH) ice sheets in these events remains a subject of controversy. Here I report on the first attempt to combine quantitatively a paleoclimate series with a climate model, with the specific purpose of extracting information about the changes in mass balance of the NH ice sheets during the last glaciation. A Greenland paleotemperature record is combined with a simple climate model using Bayesian Stochastic Inversion in order to estimate the changes that would be required to alter the Atlantic Ocean mass and heat transports between ~34 and 39 thousand years ago. The implied changes in NH ice sheet mass balance and SH air temperature are then compared to independent evidence provided by proxy records of sea level and Antarctic air temperature. I find that the inversion reproduces the gradual changes in sea level and Antarctic temperature inferred from these records. The Greenland warm event lasting over 3000 years (DOI 8) can be explained by sustained growth of NH ice sheet and reduced supply of icebergs to the North Atlantic. Our results indicate a more involved role of the NH ice sheets than previously thought, in which both collapse and subsequent

growth would be required to explain the full series of the long (> 3000 years) warm events recorded in Greenland ice.

Important uncertainties remain concerning the role of NH ice sheets in the series of abrupt climate warmings of the last glacial period – the so-called Dansgaard-Oeschger Interstadials (DOIs). Observations of ice rafted debris in North Atlantic sediments prior to the onset of DOIs have been interpreted as the result of ice sheet instability [*MacAyeal* 1993; *Hemming* 2004]. However, these observations are also consistent with ice sheets that respond passively to changes in external climate, with ice sheet expansion and increased berg production during colder climates [*Marshall and Koutnik*, 2006]. The timing and distribution of oceanic oxygen isotopic anomalies suggest that the ice sheet of Antarctica and the Southern Ocean could also be involved [*Rohling et al.*, 2004].

Different ideas have been put forward to explain abrupt climate change in terms of variations in the Atlantic meridional overturning circulation (AMOC) and its attendant poleward heat transport. These studies differ substantially in the amount, timing, and location of freshwater forcing anomaly that is needed, perhaps in part because of the different forcing sensitivities that exist among ocean models [*Stouffer et al.*, 2006]. The glacial ocean may have been inherently less stable than the modern [*Ganopolski and Rahmstorf*, 2001] so that, under favorable conditions, the freshwater anomaly required to force an abrupt change in the AMOC could be relatively small. Proposed changes in the AMOC could be the result of direct freshwater forcing, internal (unforced) ocean

dynamics [*Timmermann et al.*, 2003; *Marchal et al.*, 2007], a combination of stochastic noise and weak periodic forcing [*Ganopolski and Rahmstorf*, 2001; *Alley et al*., 2001], and/or a strong forcing combined with a millennial-scale oscillatory response [*Timmermann et al.*, 2003].

Among the recent efforts to simulate abrupt climate change using coupled atmosphere-ocean general circulation models is the study of *Liu et al.* [2009]. These authors tested two freshwater flux anomaly scenarios in the North Atlantic for explaining the onset of the Bølling-Allerød warm interval observed in Greenland ice around 14.5 kyr B.P. They found that a freshwater forcing scenario that corresponds to a sudden reduction in the mass of the NH ice sheet just prior to the onset of the Bølling is sufficient to trigger a warming event similar in amplitude to that observed. On the other hand, their experimental design does not attempt to quantify the *range* of alternate forcing scenarios that would be required to explain the onset and long-term evolution of the Bølling-Allerød warm interval, which would be important for testing the ice sheet's role in this event.

Here a test of the ice sheet forcing hypothesis of abrupt climate change is provided. The hypothesis proposes that a collapsing NH ice sheet would increase the amount of freshwater being delivered to the Atlantic Ocean at high northern latitudes. The consequent reduction in surface salinity would cause a decrease in deep water formation and a decrease in the strength of the meridional circulation and meridional heat

flux in this basin, leading to a colder Greenland climate. Conversely, a growing ice sheet would sequester poleward moisture transports, allow the polar ocean to become more saline, and increase the meridional transports of mass and heat in the Atlantic Ocean [*Schmittner et al.*, 2002; *Wang and Mysak*, 2002].

Our test of the ice sheet forcing hypothesis proceeds in two steps. In the first step, Bayesian Stochastic Inversion (BSI) is used to infer fluxes of fresh (glacial) water to the North Atlantic Ocean that would be required to force a simple climate model to reproduce the variations in paleo-temperature interpreted from a Greenland ice core (GISP2) between 34.3 – 39.3 kyr B.P. This time interval includes two abrupt climate events: DOIs 7 and 8 [*Grootes et al.*, 1993; *Meese et al.*, 1997]. Its choice is arbitrary other than the fact that DOI 8 represents one longer (~3 kyr) event and DOI 7 one shorter (~1.5 kyr) event. Moreover, DOI 8 occurred after the deposition of a prominent layer of ice rafted debris in North Atlantic sediments, which is known as Heinrich event 4 [Hemming 2004], suggesting that glacial melt water may have been involved in this specific event. The second step of the hypothesis test is to compare variations in mean sea level (MSL) implied by the fluxes of glacial water (associated to changes in NH ice sheet mass balance) to independent evidence provided by different indicators of sea level estimated from analyses on corals and deep-sea sediments. The evolution of air temperature at high southern latitudes predicted by the model is also compared to a paleo-

temperature record from an Antarctic ice core to further assess the consistency of the hypothesis.

The hypothesis test will have inherent limitations. The ability to infer the overall mass balance of NH ice sheets from a Greenland paleo-temperature record can only be approximate for several reasons. For example, the relationship between Greenland temperature and ocean circulation in the North Atlantic and the circulation response to glacial water fluxes are still poorly understood. On the other hand, using BSI for paleoclimate data interpretation allows us, through a large number of numerical experiments with a climate model, to estimate the uncertainty in the glacial water fluxes that provide an acceptable match between model predictions and observations. While the climate model used here is simplified, it can represent the processes and sensitivities of more complete climate models to freshwater forcing anomalies [*Stouffer et al.*, 2006]. Its computational efficiency permits us to conduct a more comprehensive analysis of the physical implications.

4.2 Methods

4.2.1 Paleoclimate Records

A variety of paleoclimate data are used in this study for three specific purposes: (i) as boundary conditions to the climate model, (ii) as a target for model inversion and constraint on candidate freshwater forcing scenarios, and (iii) as independent tests of the ice sheet forcing hypothesis.

Boundary Conditions

The boundary conditions of the climate model are the following. The change in land ice albedo over the past 21 kyrs is estimated from knowledge of present albedo [*Jackson and Broccoli*, 2003] and the change in expanded ice cover at 1-kyr intervals since the Last Glacial Maximum [*Peltier*, 1994]. For the interval from 120 kyr B.P. to 21 kyr B.P., land ice cover is estimated from a sea level record [*Shackleton*, 1987], assuming that the relationship between land ice cover and sea level during this period is the same as that during the last deglaciation [*Fairbanks*, 1989; *Peltier*, 1994]. The latitudinal and seasonal distribution of solar insolation at the top of the atmosphere is estimated from changes in obliquity, precession, and eccentricity using the equations of *Berger* [1978]. The atmospheric CO_2 concentrations are prescribed according to a composite record obtained from different CO_2 records from Antarctic ice cores: from present (A. D. 1950 yr) to 1020 yr B.P. [*Etheridge et al.*, 1996], from 1020 to 11,195 yr B.P. [*Indermuhle et al.*, 1999a], from 11,195 to 21,433 yr B.P. [*Monnin et al.*, 2001], from 21,433 to 64,675 yr B.P. [*Indermuhle et al.*, 1999b], and from 64,675 to 120,000 yr B.P. [*Petit et al.*,

1999]. Dates for ice from 21,433 to 76,362 yr B.P. are converted to the SFCP timescale of *Shackleton et al.* [2004]. Dates for ice older than 76,362 yr B.P. are on the GT4 timescale of *Petit et al.* [1999].

Target for model inversion

Variations of Greenland annual mean air temperature from 39.3 to 34.3 kyr B.P. are estimated from the $\delta^{18}O$ record for the GISP2 ice core [*Grootes et al*., 1993; *Meese et al.*, 1997] and serve as the target for the model inversion. Whereas $\delta^{18}O$ records can in principle be converted into temperature records with high temporal resolution, measurements of the isotopic composition of air entrapped in Greenland ice have questioned the traditional conversion based on the modern spatial relationship between snow $\delta^{18}O$ and air temperature [*Severinghaus and Brook,* 1998]. Indeed, according to these measurements, the increases in annual mean air temperature at the onset of DOIs are estimated to 12 °- 15 ℃, which is significantly larger than earlier estimates based on the traditional conversion [*Lang et al.,* 1999; *Huber et al*., 2006]. Here they are linearly scaled so that they are assumed to correspond to variations of 4 ℃ in surface temperature between $75^{o}N$ – $80^{o}N$ in the Atlantic Ocean which can be directly compared to predictions from the climate model (the atmospheric component of model is zonally averaged and cannot accurately simulate temperature at specific longitudes such as above Greenland). The assumption is likely only qualitatively correct [*Bond and Lotti*, 1995]. Note that the uncertainty in dating the GISP2 ice core is 2% or ~700 years between 39.3 and 34.3 kyr B.P. [*Meese et al.*, 1997].

Independent Geologic Records

Two types of such records are considered in this study: records of mean sea level (MSL) and a record of air temperature in Antarctica.

Records of MSL include reconstructions based on near-surface dwelling corals [*Thompson and Goldstein*, 2006], deep ocean oxygen isotopes [*Waelbroeck et al.*, 2002], and oxygen isotopes from the Red Sea [*Siddall et al.*, 2003]. Coral data lead to estimates of MSL with the smallest uncertainty of approximately +1 to -3 m [*Thompson and Goldstein*, 2006]. $\delta^{18}O$ records from deep ocean sediments produce MSL estimates with poor temporal resolution (about 1500 yr) and with an uncertainty of ±13 meters. Finally, $\delta^{18}O$ records from Red Sea sediments provide estimates of MSL with an uncertainty of ±5.5 m. This uncertainty reflects in part a smoothing of about 500 yr, which removes some of the random inter-sample variability [*Siddall et al*., 2003; *Rohling et al.*, 2004].

The record of Antarctic air temperature that is used in this study is based on the $\delta^{18}O$ record for the Byrd ice core, West Antarctica [*Johnson et al.*, 1972]. Whereas the $\delta^{18}O$ record is assumed to reflect temperature changes, no formal conversion is assumed, i.e., the comparison with the changes in air temperature simulated by the climate model is purely qualitative. The $\delta^{18}O$ record from the Byrd ice core is placed on the GISP2 time scale by using measurements of methane concentration on entrapped air [*Blunier and*

Brook, 2001]. The correlation between gas ages in the Antarctic and Greenland ice cores has an estimated error of ±300 years [*Blunier and Brook*, 2001].

4.2.2 *Climate Model*

The application of BSI to a long time interval with a large number of uncertain changes in forcing requires that a computationally efficient model be employed. Here a zonally averaged climate model that includes seasonality [*Schmittner and Stocker*, 2001] is used. It comprises three components: (i) an ocean circulation model with three basins (Atlantic, Pacific, and Indian Oceans) connected to a Southern Ocean [*Wright and Stocker*, 1992]; (ii) an zonally averaged energy and moisture balance model of the atmosphere [*Stocker et al.*, 1992], and (iii) a thermodynamic model of sea ice [*Wright and Stocker*, 1993]. The ocean component of the model is governed by six coupled ODEs: momentum (2), mass (1), heat (1), salt (1), and state (1). There are six time-dependent variables: speed (2), pressure (1), temperature (1), salinity (1), and density (1). After tuning, the model is able to capture important features of observed modern climate such as the seasonal variations in surface air temperature, the meridional circulation in different oceanic basins, and the meridional heat and moisture fluxes in the ocean and atmosphere [*Schmittner and Stocker*, 2001; *Stocker et al*., 1992]. Similar models have been intensively used for interpreting records of past climate change on century and longer time scales [*Stocker and Wright*, 1991; *Fichefet et al.*, 1994; *Marchal et al.*, 1999; *Ganopolski and Rahmstorf*, 2001; *Knutti and Stocker*, 2002]. Here the climate model is subject to time-dependent boundary conditions related to changes in Earth's orbital

geometry, atmospheric CO_2 concentration, and land ice cover (section 4.2.1). These variable boundary conditions, however, have minimal effect on our inversions experiments (section 4.4.2).

4.2.3 *Bayesian Stochastic Inversion (BSI)*

The evolution of freshwater flux anomaly in the North Atlantic ocean that enable the climate model to reproduce the paleo-temperature record from GISP2 between 34.3 – 39.3 kyr B.P. is determined by Bayesian inference using an algorithm referred to as Multiple Very Fast Simulated Annealing or MVFSA [Jackson et al., 2004; Jackson et al., 2008; Jackson 2009]. Provided that a sufficient number of numerical experiments with the climate model are available, MVFSA can estimate the joint probability distribution of freshwater flux anomalies in this time interval. MVFSA operates similarly to Markov Chain Monte Carlo (MCMC) algorithms [Jackson et al., 2004; Villagran et al., 2008], whereby information about model-data mismatch from prior experiments is exploited for selecting new solutions that will be effective at quantifying uncertainties in the freshwater flux anomalies. MVFSA also makes use of systematic biases between model and data to broaden the search for "acceptable" solutions [Jackson et al., 2008].

More specifically, BSI is used to estimate a joint probability distribution for 51 unknown freshwater flux anomalies between in the Atlantic Ocean between 50°N – 60°N and between 39.3 – 34.3 kyr B.P. at 100-year intervals. Linear interpolation is used to create a continuous time series from the 51 estimated values. Initially, candidate values of

freshwater flux anomalies are sampled from a prior uniform probability distribution ranging from -0.3 Sv to 0.3 Sv (1 Sv = 10^6 m^3s^{-1}). Thereafter, candidate values are sampled from a Cauchy distribution whose mode is centered on the last accepted freshwater forcing scenario and whose width shrinks slightly with each step. The Markov sampling process continues until the search fails to accept a new forcing scenario after a specified number of attempts. This number is determined to be 5.5 times the number of unknowns in the inversion, 280 in this case [*Jackson et al.*, 2004].

The sampling process continues until it reaches convergence and is repeated 100 times with different initial values of freshwater flux anomalies in order to get statistically robust estimates of the uncertainties in the freshwater flux anomalies. A large number (3 x 10^5) of numerical experiments with the climate model were completed in total. The "maximum likelihood solution" is obtained from an average of the top 100 forcing scenarios from independent convergence attempts that lead to the best match of air temperature at high northern latitudes predicted by the model and observed in the Greenland record. I have checked that each of these scenarios contributes to improving the maximum likelihood solution's match to the Greenland data.

Note that the number of unknown forcing parameters (51) combined with the computational cost of each experiment (~2 hours on a present-day workstation) is large compared to that in earlier applications of BSI [*Jackson et al.*, 2003; *Xia et al.*, 2004; *Wang* 2007; *Jackson et al.*, 2008]. This size puts a practical limit on the length of the 5

kyr-long experiments. Adding more forcing parameters would only increase an already expensive calculation and reduce chances of finding a satisfactory solution. However alternate strategies could be used for extending the calculation to include a longer time-span [e.g. *Hong and Sen*, 2009].

4.2.4 *Experimental design*

Each time series of freshwater flux anomalies ("freshwater forcing scenario") is comprised of positive and negative values that are imposed at the ocean surface between 50 ℕ and 60 ℕ in the Atlantic Ocean. The rationale to impose negative anomalies may not seem immediately obvious owing to the fact that the source of moisture for ice sheet growth comes from regions far way from the North Atlantic. However the point is not where the water evaporates from the ocean surface, which would be independent of ice sheet dynamics, but rather how does a change in the mass budget of the Laurentide ice sheet affect the freshwater supply to the North Atlantic. At equilibrium, an ice sheet will discharge as much mass to the ocean as it receives from the atmosphere. If the ice sheet becomes unstable, it may for a period of time discharge much more mass than it receives, resulting in a positive freshwater flux. Following a period of instability, in contrast, an ice sheet will no longer have sufficient thickness to release a significant mass flux to the ocean. In this case one should expect a reduced rate of iceberg production and would have the reverse effect of an ice sheet collapse. Thus, the appropriate way to represent a reduction in the freshwater supply from the Laurentide ice sheet is a negative freshwater flux anomaly in the North Atlantic.

The selected freshwater forcing is imposed to the climate model at each time step. Each integration of the model starts with the same initial conditions: The model integration starts at 47.3 kyrs B.P., or 8 kyrs before the first freshwater flux anomaly is applied (at 39.3 kyrs B.P.). This procedure allows the model to respond to the prescribed variations in land ice cover, orbital geometry, and atmospheric CO_2 concentration prior to the time interval when freshwater flux anomalies are imposed (section 4.2.1).

The surface temperature between 75 ºN and 80 ºN in the Atlantic Ocean simulated by the climate model in response to freshwater forcing (T_{mod}) is compared at 10-year intervals to the sea surface temperature estimated from the Greenland ice record (T_{obs}, section 4.2.1). The difference between T_{mod} and T_{obs} is measured by a "cost function" *E*. The cost function varies with the freshwater forcing scenario (represented by a vector **m**) through the effects of freshwater on ocean circulation and temperature in the model. More specifically, *E* is the mean sum of squared differences between modeled and reconstructed temperatures at evenly spaced N=500 points in time (t) between 39.3 and 34.3 kyr B.P., weighted according to a temperature uncertainty σ,

$$E(\mathbf{m}) = \frac{1}{2N}\sum_{t=1}^{N}\frac{\left(\left(T_{\mathrm{mod}}(t)-\overline{T}_{\mathrm{mod}}\right)-\left(T_{obs}(t)-\overline{T}_{obs}\right)\right)^2}{\sigma^2} \qquad (4.1)$$

The overbar indicates a time average. Note that the cost function compares modeled and observed temperature anomalies, which eliminates any offset that may exist between the modeled and observed data sets. This form of the cost function assumes Gaussian errors and includes a factor of 2 in the denominator as a part of this assumption. The temperature uncertainty σ is based on the following reasoning. The climate model does not resolve the atmospheric circulation and elements of the oceanic circulation that give rise to variability on decadal time scales. Thus, from the viewpoint of the model, variability at these scales represents "noise". Here I take σ = 0.136 ℃, which corresponds to the standard deviation of the high frequency variability (> $(30\ yr)^{-1}$) of T_{obs} obtained after subtracting a 30-year running average from T_{obs}. Here *E* is appropriately normalized by rescaling equation (4.1) by a factor 'S', as described in Jackson et al. (2008), such that Gaussian "noise" added to the smoothed (frequency > $(30\ year)^{-1}$) Greenland data produces distributions of *E* whose standard deviation is equal to 1 cost unit.

The evolutions of freshwater flux anomaly that are sought by BSI correspond to samples from a solution probability distribution. That is, BSI seeks to find all freshwater forcing scenarios (**m**) that minimize *E* to within a probability $e^{-\Delta E(\mathbf{m})}$, where $\Delta E(\mathbf{m}) = E(\mathbf{m}) - E(\mathbf{m})_{min}$ where $E(\mathbf{m})_{min}$ is the minimum cost value that BSI has identified. Note that, although errors for model-data discrepancies represented in *E* (equation 4.1) are assumed to be Gaussian, the non-linear dynamics of the climate model can affect the high latitude

temperature T_{mod} . Hence the model dynamics can potentially yield solution distributions for **m** that are non-Gaussian, or even multi-modal (multi-peaked).

4.3 Results

4.3.1 Mean Sea Level

I find that the freshwater flux anomalies inferred from the combination of the Greenland record and the climate model using BSI alternate between positive and negative values during times of reduced and strong meridional overturning circulation in the Atlantic Ocean, respectively. In turn, the times of reduced and enhanced circulation correspond, respectively, to cool and warm polar temperatures in the Northern Hemisphere (Figure 4.1). The anomalies at different times tend to be uncorrelated, as indicated by the joint probability distribution of these anomalies estimated by BSI (not shown). Consequently, the time integral of the anomalies and the changes in mean sea level which these anomalies imply are relatively well constrained (Figure 4.2).

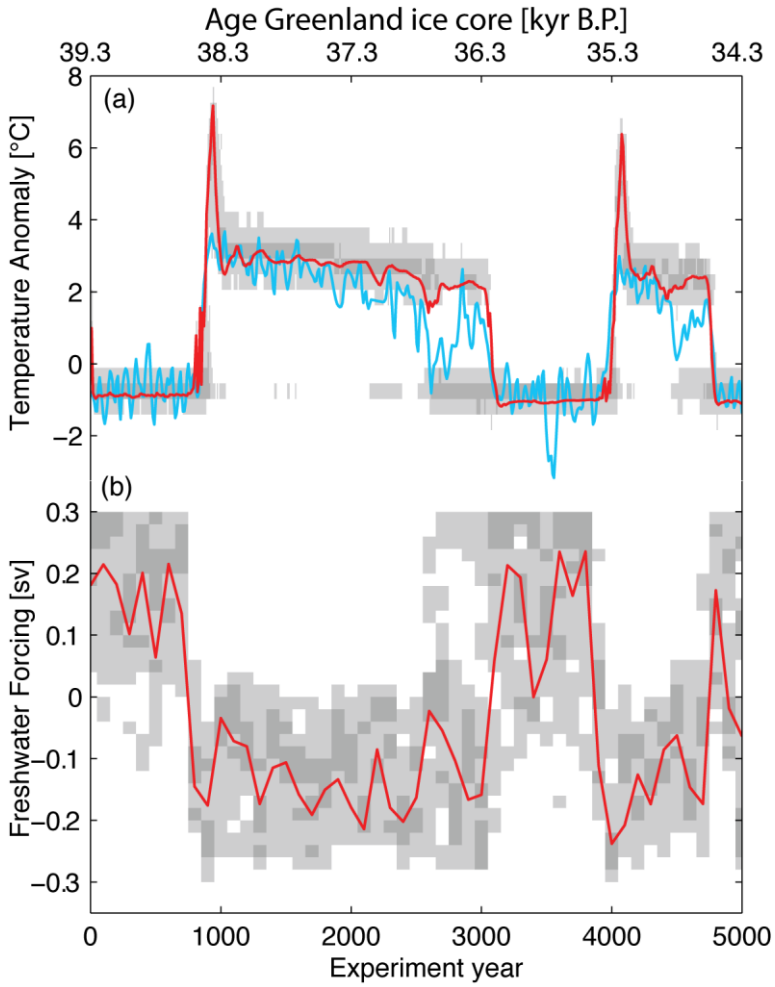

Figure 4.1 *(a) Time series of surface temperature at 72 °N in the Atlantic Ocean obtained from BSI (gray patterns) and inferred from the GISP2 ice core (blue) between 39.3 and 34.3 kyr B.P. [Grootes et al., 1993; Meese et al., 1997]. (b) Time series of freshwater flux anomaly between 50°N and 60°N in the Atlantic Ocean that enables the climate model to follow the GISP2 record in panel (a). In both panels (a-b), red curve represents the maximum likelihood solution and light (dark) gray represents 80% (30%) confidence. DOI 8: experiment year 1000~3000.*

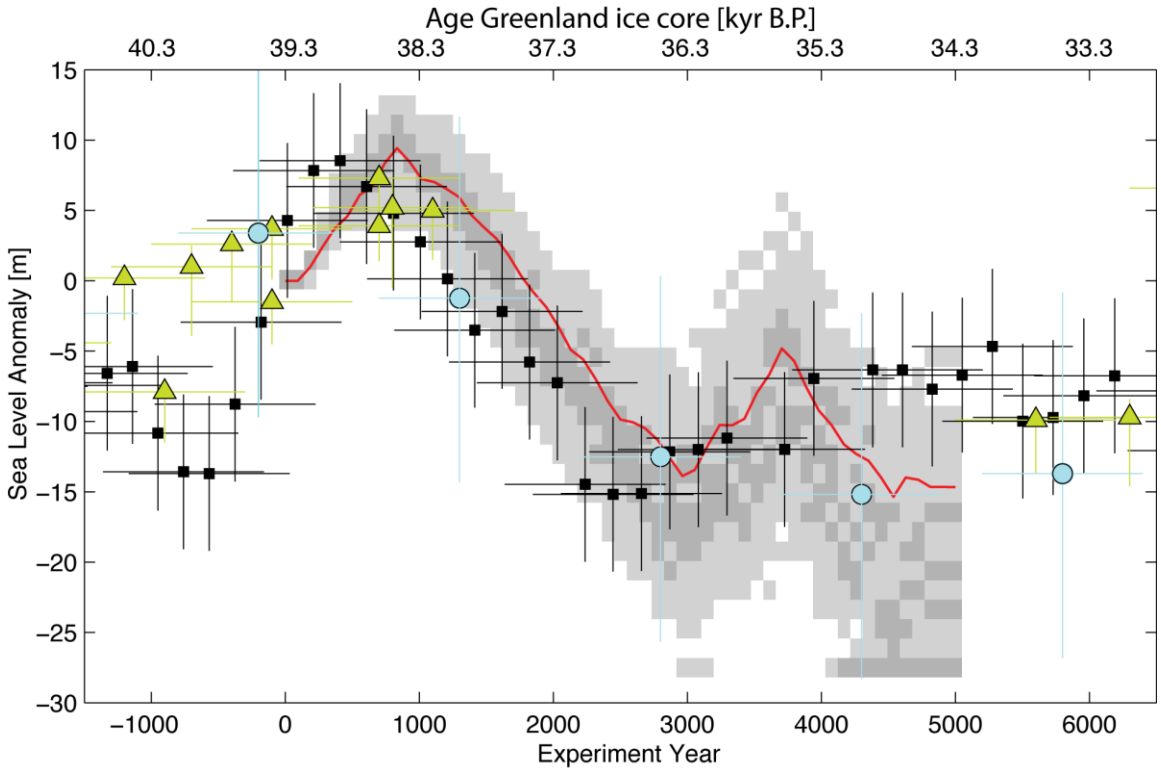

Figure 4.2 *Time series of mean sea level (expressed as an anomaly) implied by the time integral of freshwater flux anomalies (Figure 4.2b). Also shown are independent estimates of sea level anomalies inferred from corals (green triangles) [Thompson and Goldstein, 2006], deep sea oxygen isotopes (blue circles) [Waelbroeck et al., 2002], and oxygen isotopes from the Red Sea (black squares) [Siddall et al., 2003]. The Red Sea data have been smoothed by a three point running mean. The uncertainty of ±5.5 m (1σ) indicated for the Red Sea data reflects a smoothing of about 500-yr, which removes some of the inter-sample variability [Siddall et al., 2003; Rohling et al., 2004]. DOI 8: experiment year 1000~3000.*

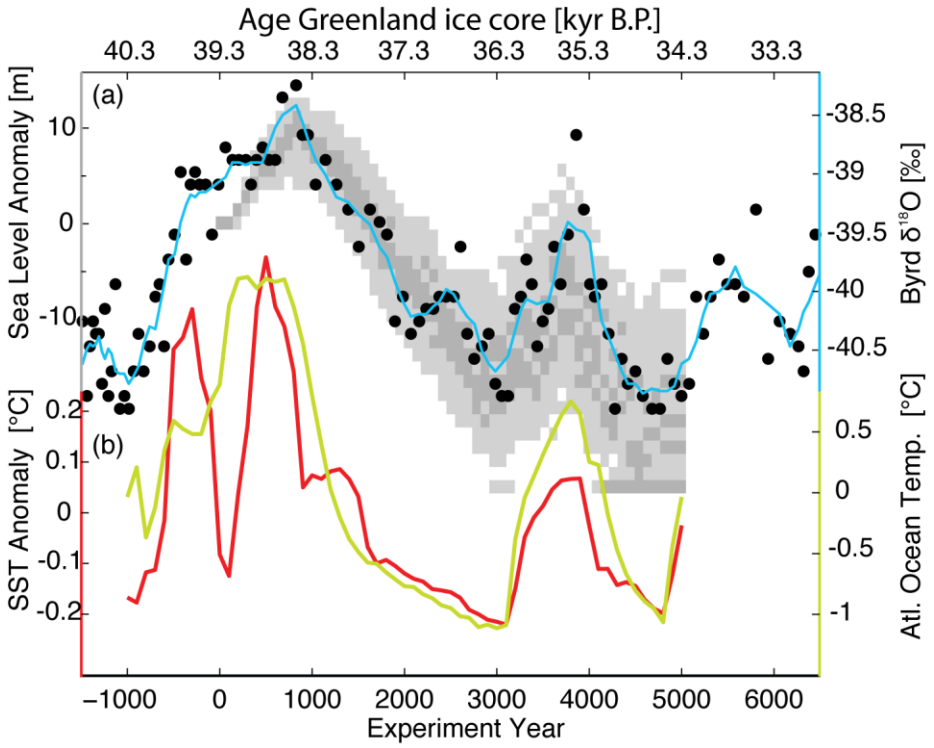

Figure 4.3 *(a) $\delta^{18}O$ proxy record for annual mean air temperature at Byrd Station, West Antarctica [Johnsen et al., 1973; Blunier and Brook, 2001] (raw data: black dots; smoothed record: blue) and time series of mean sea level obtained from BSI (Figure 4.2). (b) Time series of mean temperature in the Atlantic Ocean (between 0 – 4000 m and 70 ℃S – 80 ℃N) (green) and time series of surface temperature at 67 ℃S in the Southern Ocean (red). Note that freshwater anomalies are applied at experiment year 0 through year 5000, implying that the agreement between the model and proxy records prior to year 0 is coincidental. The modeled warming occurs when the AMOC is weak (boundary conditions are time-dependent so whether these oscillations are due to internal model variability or to the boundary conditions is unclear). DOI 8: experiment year 1000~3000.*

The independent reconstructions of mean sea level based on corals and sediment $\delta^{18}O$ records are compared with the changes in MSL inferred from BSI (Figure 4.3). These reconstructions indicate a rise of 10 m near 38 kyr B.P. and a subsequent fall of 20 to 25 m. There is relatively good agreement between the MSL changes reconstructed from coral and sediment records on the one hand and those inferred from BSI on the other hand. The agreement tends to support the NH ice sheet forcing hypothesis for the long DOI 8 that initiated at about 38 kyr B.P, even given the uncertainties in the different estimates of sea level change. Agreement, however, cannot be claimed for the shorter DOI 7. For this event, BSI predicts a 10-meter rise and fall in sea level, which is not apparent in sea level reconstructions [*Siddall et al.*, 2008].

The changes in MSL inferred from BSI agree particularly well with the sea level changes inferred from Red Sea $\delta^{18}O$ data, so the appropriateness of these data for testing the ice sheet forcing hypothesis should be discussed. The MSL drop of about 25 m from ca. 39 kyr B.P. to ca. 36.5 kyr B.P. estimated from the Red Sea $\delta^{18}O$ record is comparable to other estimates based on coral records: 20 m [*Thompson and Goldstein*, 2006], 10-15 m [*Chappell* 2002], and 20 m [*Chappell et al.* 1996]. The similarity between these estimates suggests that sea level is the dominant control on Red Sea $\delta^{18}O$, rather than being a mixed signal of ocean temperature and land ice volume. An implication of our results is that the majority of sea level decrease between 39 and 36 kyrs B.P. would be associated with a net accumulation of continental ice in the NH

4.3.2 Antarctic Temperature

The changes in MSL inferred from BSI display some similarity with the $\delta^{18}O$ proxy for air temperature from the Byrd ice core (West Antarctica) during the time interval 34.3 – 40.3 kyr B.P. (Figure 3a,b). A similarity between MSL and Antarctic air temperature records during this interval has been noted in previous studies and its significance has been the subject of debate [*Siddall et al.*, 2008; *Rohling et al.*, 2004; *Rohling et al.*, 2009]. In our inversion such similarity is a consequence of changes in NH ice sheet mass balance and the seesaw mechanism [*Stocker and Johnsen*, 2003]: a reduced AMOC during times of increased freshwater supply to the North Atlantic and higher MSL leads to a reduction of poleward heat transport in the Atlantic Ocean and hence to an accumulation of heat (warming) in the Southern Hemisphere, particularly at subtropical latitudes in the South Atlantic Ocean.

4.4 Discussion

4.4.1 *Relationship between stadial/interstadial duration and sea level anomaly*

Prior work on mechanisms of abrupt climate change has emphasized ice sheet collapse and ocean non-linear dynamics, such as a hysteresis response of the AMOC to variations in freshwater forcing [e.g. Figure 4.1b; *Stocker and Marchal*, 2000; *Stouffer et al.*, 2006]. The existence of a hysteresis may be one mechanism for locking the system into a particular cold or warm climate state in response to a sufficiently large forcing.

However, our results suggest that ice sheets, through their decay and growth, may have participated in a more direct way to sustaining some stadial/interstadial climates of the last glacial period. Figure 4.2 indicates that the duration of these temperature anomalies would correspond to changes in ice sheet mass balance and sea level, although I acknowledge the case is less certain for changes associated with DOI 7 than DOI 8. Further long-term observational support for this assertion exists for much of marine isotope stage 3 (~60 to 30 ka) [*Siddall et al.,* 2008]. An observational study comparing Antarctic and Greenland climate at high temporal resolution [*EPICA,* 2006] has noted a linear relationship between the duration of Greenland stadial phases and the amplitude of Antarctic temperature perturbations.

The qualitative agreement between modeled and estimated Antarctic temperature within figure 4.3 includes the thousand-year long interval before 39.3 kyr B.P., i.e., prior to the time interval when freshwater flux anomalies are applied to the climate model. Recall that all model experiments begin 8 kyrs prior to 39.3 kyr B.P. Therefore, modeled temperatures for the period prior to 39.3 kyr B.P. can not be related to any freshwater flux anomalies and must, therefore, be dependent on initial conditions and changes in external forcing (atmospheric CO_2 concentration, orbital parameters, and land ice cover). While the model-data agreement prior to 39.3 kyr B.P. may be coincidental, the warming trend found in the model, which accords with the paleotemperature record from Byrd (Figure 4.3), occurs when the AMOC is weak for reasons of internal (unforced) variability (discussed below). It is plausible that in the real ocean, the AMOC could have

been forced to be weak prior to 39.3 kyrs B.P. as a result from a negative NH ice sheet mass balance. Indeed, some sea level indicators show a rising sea during this time interval [*Siddall et al.,* 2008] which, according to the ice sheet forcing mechanism, would have caused a reduction in the AMOC

The difference in sea level evolution between our inversion solutions and the geologic records (corals and marine sediments) for the shorter DOI 7 also leaves open the possibility that some DOI events could be a result of internal ocean dynamics and sustained by non-linearities in the atmosphere-ocean system. Note that geologic records lead to conflicting estimates of MSL during DOI7: MSL increased according to the Red Sea $\delta^{18}O$ record [*Siddall et al.,* 2003] whereas it decreased according to a stack of deep sea $\delta^{18}O$ records [*Waelbroeck et al.,* 2002], although the significance of these MSL variations in both records is unclear given the relatively large uncertainties. The minimum forcing that enables our climate model to capture DOI 7 requires the equivalent of 5-meter amplitude variations in sea level. While the model can produce events similar to DOI 7 without any forcing, it is difficult for the model to produce such an event with the correct timing without interfering with the timing of earlier events. Thus our study also supports the notion that it may be necessary to call on other mechanisms or improved model physics to explain all aspects of what is observed in geologic records

4.4.2 *Role of glacial boundary conditions*

Previous authors have emphasized that glacial boundary conditions (e.g. lower atmospheric CO_2 concentration, expanded land ice cover, and changes in Earth's orbital geometry) may alter the sensitivity of ocean circulation to freshwater forcing [e.g. *Sakai and Peltier*, 1997; *Ganopolski and Rahmstorf*, 2001; *Loving and Vallis*, 2005]. . In order to understand the impact of these conditions in our climate model, two sets of numerical experiments have been performed. In the first experiment, I test the response of the climate model to time-varying glacial boundary conditions over the past 120 kyrs. Figure 4.4a shows the annual mean air temperature between 60°N – 90°N simulated by the model. High frequency oscillations (i.e., at millennial scales) are predicted, even though the model is not perturbed by the application of freshwater flux anomalies (for the displayed simulation, changes in land ice cover occur but these are not connected to the freshwater budget at the ocean surface). These oscillations are most pronounced during the coldest portions of the last glacial period and do not occur during the Holocene. Analyzing the precise mechanism for the modeled climate oscillations is beyond the scope of this paper, however, it is noted that they appear to occur through the alternance of episodes of vertical density stratification and destratification of the water column in the northern Atlantic Ocean and amplified by sea ice feedbacks (oscillations cease when sea ice feedbacks are turned off). While the precise mechanisms may differ in our climate model, previous studies have shown that similar processes can give rise to millennial-scale variability in other models [e.g. *Sakai and Peltier*, 1997; *Loving and Vallis*, 2005].

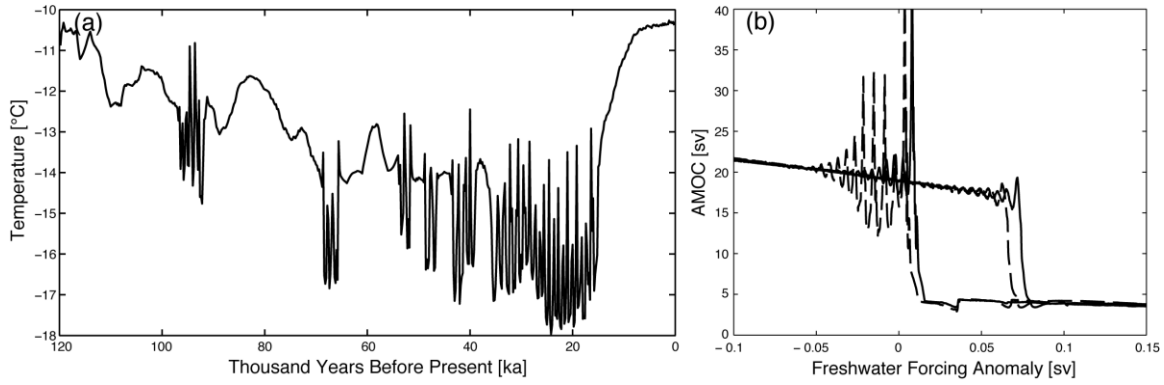

Figure 4.4 *(a) Annual mean air temperature between 60 ℕ – 90 ℕ simulated by the climate model when forced by changes in atmospheric CO_2 concentration, ice sheet albedo, and orbital geometry over the past 120 kyrs. Self-sustained oscillations emerge with 1 to 1.2 kyr periodicity during cooler climates. (b) Equilibrium responses of Atlantic meridional overturning circulation to freshwater forcing between 50 ℕ and 60 ℕ in the Atlantic Ocean simulated by the climate model for modern (solid) and glacial (39 kyr B.P.) boundary conditions (dashed).*

A second set of experiments tests the equilibrium response of the climate model to gradual changes in surface freshwater flux (rate of $\pm 7.5 \times 10^{-6}$ Sv yr^{-1}) between 50 ℕ and 60 ℕ in the Atlantic Ocean under modern (preindustrial) or glacial (i.e. at 39 kyr B.P.) boundary conditions. A hysteresis response is produced in both cases in which either a sluggish or strong circulation states could exist under the same forcing with a transition only occurring until a sufficient amplitude freshwater flux anomaly (> 0.1 Sv) is applied. However, this calculation does not reveal that the glacial ocean circulation

configuration is only weakly stable. Even relatively small changes in freshwater forcing of either sign can cause the system to switch states. Moreover, the millennial scale oscillations that are evident in figure 4.4a may be eliminated by a steady change in freshwater fluxes and keep the AMOC in either its sluggish or strong circulations states depending on the sign of the forcing anomaly.

I have repeated the stochastic inversion with modern boundary conditions to test the sensitivity of the inversion solutions to the nature of external climate forcing. The freshwater forcing scenario that enables our model to comply with the Greenland paleo-temperature record (not shown) is similar to that obtained when the model is subject to glacial boundary conditions (Figure 4.1b). Thus, our results are apparently robust to differences in external climate forcing. A more thorough exploration of this topic is being considered by *Jackson et al.* [submitted].

4.4.3 *Other potential limitations*

In addition to the limitations described above, the BSI can only consider the relative likelihood of different solutions consistent with the paleoclimate series and the climate model being considered. In particular, the amplitude of MSL changes inferred from BSI is likely sensitive to the choice of minimum (–0.3 Sv) and maximum (+0.3 Sv) values in freshwater fluxes that were prescribed. I note, however, that a mean freshwater anomaly of 0.1 Sv is equivalent to a rate of MSL change of 0.9-meter per century, which

is reasonable in light of the rates estimated for the last deglaciation [*Fairbanks*, 1989]. Furthermore, a possible freshwater forcing from the Antarctic ice sheet has not been considered here [*Rohling et al*., 2004].

4.5 Summary

This study shows that paleoclimate records spanning a portion of the last glaciation and from different parts of the globe (Greenland temperature, mean sea level, and Antarctic temperature) can be brought into consistency using a climate model of reduced complexity. The combination of the Greenland record with the model implies sea level changes between 34.3 – 39.3 kyr B.P. which are in accord with reconstructions based on corals and deep-sea sediments. Consequently, our results support a NH ice sheet forcing on abrupt climate change. In particular, they point to the importance of the period of NH ice sheet growth that follows a Heinrich Event to explain the long period of Greenland warmth. Our results are robust against differences in external climate forcing over this time interval Whereas they are encouraging, further investigation with a more comprehensive set of paleoclimate records and more complete climate models is probably desirable.

Appendices

Appendix 1

4-box model formulation

The formulation of a two-hemisphere 4-box model is given here. The box volumes are (for a definition of symbols see Table A1):

$$V_1 = A_1 H\,, \tag{A1.1}$$

$$V_2 = A_2 D, \tag{A1.2}$$

$$V_3 = A_2 (H - D), \tag{A1.3}$$

and

$$V_4 = A_4 H\,. \tag{A1.4}$$

These volumes can vary with time when the depth of the thermocline D or the total depth of the ocean H changes (Figure 1). The equations governing the conservation of heat, salt, and mass for the case when there is sinking in the northern box 1 ($q_1>0$) and upwelling in the southern box 4 ($q_4<0$) (asymmetric circulation) are:

$$\frac{dT_1}{dt} = \frac{1}{V_1}\left[q_1(T_2 - T_1) + \kappa A_1 (T_p - T_1)\right] \tag{A1.5}$$

$$\frac{dS_1}{dt} = \frac{1}{V_1}\left[q_1(S_2 - S_1) - (\varphi_1 + ff) S_1\right] \tag{A1.6}$$

$$\frac{dT_2}{dt} = \frac{1}{V_2}\left[-q_4(T_4 - T_2) + q_m(T_3 - T_2) + \kappa A_2 (T_e - T_2)\right] \tag{A1.7}$$

$$\frac{dS_2}{dt} = \frac{1}{V_2}\left[-q_4(S_4 - S_2) + q_m(S_3 - S_2) + (\varphi_1 + \varphi_4) S_2\right] \tag{A1.8}$$

$$\frac{dT_3}{dt} = \frac{1}{V_3}\left[(q_1 + \varphi_1)(T_1 - T_3)\right] \quad \text{(A1.9)}$$

$$\frac{dS_3}{dt} = \frac{1}{V_3}\left[(q_1 + \varphi_1)(S_1 - S_3)\right] \quad \text{(A1.10)}$$

$$\frac{dT_4}{dt} = \frac{1}{V_4}\left[-q_4(T_3 - T_4) + \kappa A_4(T_p - T_4)\right] \quad \text{(A1.11)}$$

$$\frac{dS_4}{dt} = \frac{1}{V_4}\left[-q_4(S_3 - S_4) - \varphi_4 S_4\right]. \quad \text{(A1.12)}$$

The vertical volume flux q_m only acts to move mass from the sub-thermocline box (box 3) into the thermocline box (box 2) by redefining the depth of the thermocline D. This allows the exchange to be uni-directional while conserving mass and heat in the process.

The heat exchange between the equatorial or polar boxes and the atmosphere is proportional to the temperature difference with respect to reference values T_e and T_p, respectively. The value for the thermal relaxation velocity $\kappa = 1.7 \times 10^{-6}$ m s^{-1} implies a surface heat loss of 6.6 W m^{-2} for each degree difference (the heat loss/gain per degree change in a m^2 column is $\rho \cdot C_p \cdot \kappa$ = 1000 kg m^{-3} · 3850 J kg^{-1} ℃$^{-1}$ · 1.7 x 10^{-6} m s^{-1} = 6.6 W m^{-2} ℃$^{-1}$). This value is smaller than the values of 10 to 80 W m^{-2} ℃$^{-1}$ that are typically associated with this parameter [e.g., *Chu et. al,* 1998]. However it is consistent with other box-type "climate" models [*Scott et. al.,* 1999; *Lucarini and Stone,* 2005].

In equation (A1.6), I choose to impose negative freshwater forcing anomalies to the northern box in the same way as positive anomalies. Note that freshwater fluxes (*ff*) are anomalies on top of the atmospheric moisture flux φ_1. Thus in most cases, the total

flux is still positive, and much reduced during times of ice growth. This choice is consistent with the treatment taken by a number of other authors who have considered ice sheet mass balance influence on the MOC circulation [*Marshall and Clarke*, 1999; *Wang and Mysak*, 2000; *Knutti et al.*, 2004; *Liu et al.*, 2009]. This choice may seem counter-intuitive to some, as there is a number of references in the literature discussing orbital or other climate forcings on ice sheet growth that emphasize the location of moisture for ice sheet growth, which may come from regions far way from the North Atlantic [*Ruddiman and McIntyre*, 1981; *Miller and de Vernal*, 1992; *Jackson and Broccoli*, 2003]. However, the question here is how do changes in ice mass balance affect the climate system, which, I argue, is not a question of where water evaporates from the ocean surface. Rather the question is how does a change in the mass budget of the Laurentide ice sheet affect the freshwater supply to the North Atlantic. At equilibrium, the Laurentide ice sheet will discharge as much mass to the ocean as it receives from the atmosphere. If the ice sheet becomes unstable, it may, for a period of time, discharge much more mass than it receives (positive freshwater forcing). After a period of instability, an ice sheet no longer has the potential energy to drive significant mass flux to the ocean. The reduced rate of iceberg production would have the reverse effect of an ice sheet collapse. The appropriate way to represent this reduction in mass loss to the ocean is a negative freshwater forcing to the North Atlantic. The processes that govern subtropical evaporation may be modeled through a "bulk" formulation that includes terms including the difference in specific humidity between the surface and a reference height. The rate of evaporation is modulated by surface wind speeds and the static

stability of the atmosphere. The latter two quantities determine that rate at which drier air in the free atmosphere exchanges with saturated air near the ocean surface. There is a greater evaporation rate from the sub-tropical ocean as this region lies underneath the descending (very dry) branch of the Hadley circulation and is usually accompanied by persistent trade winds. I do not expect any of these processes would be directly affected by changes in the mass balance of the Laurentide or other high latitude ice sheet. Changes in subtropical evaporation should primarily be affected by radiative balances (e.g. through clouds or CO_2) or processes that control the strength of the Hadley circulation.

The rate of change of the thermocline depth is

$$\frac{dD}{dt} = \frac{q_m - q_1 - q_4 - \varphi_1 - \varphi_4}{A_2} \qquad \text{(A1.13)}$$

where the vertical volume flux q_m balances the horizontal volume fluxes q_1, q_4, and the atmospheric moisture fluxes φ_1 and φ_4. On the other hand, the rate of change of total ocean depth H is only affected by fresh water forcing *ff* from ice sheet growth or decay,

$$\frac{dH}{dt} = \frac{ff}{A_o}, \qquad \text{(A1.14)}$$

where A_o is the area of the whole ocean (not just the area over the Atlantic). Because the freshwater forcing and poleward moisture transports are treated as volume fluxes, they appear as damping terms in equations (A1.6), (A1.8), and (A1.12). This is the correct form for conserving mass, although this form is slightly different from what is traditionally done in ocean models where freshwater transports are treated as fluxes of negative salinity. Note that even though the freshwater transports and freshwater forcing

are independent of salinity, their effect on the circulation (via equations A1.6, A1.8, and A1.12) is dependent on the salinity of the boxes where the forcing is being applied.

The volume fluxes between the equatorial and polar boxes are assumed to be proportional to the depth-integrated density contrasts relative to a reference '*r*':

$$q_1 = q_{1r}\frac{\left(\rho_1 H - \rho_2 D - \rho_3 (H - D)\right)D}{\left(\rho_{1r} H_r - \rho_{2r} D_r - \rho_{3r}(H_r - D_r)\right)D_r} \qquad \text{(A1.15)}$$

and

$$q_4 = q_{4r}\frac{\left(\rho_4 H - \rho_2 D - \rho_3 (H - D)\right)D}{\left(\rho_{4r} H_r - \rho_{2r} D_r - \rho_{3r}(H_r - D_r)\right)D_r}, \qquad \text{(A1.16)}$$

The density of each box (kg m^{-3}) ρ is a linear function of temperature (T) and salinity (S),

$$\rho = \rho_o(1 + \beta S - \alpha T) \qquad \text{(A1.17)}$$

where ρ_o = 1028 kg m^{-3}, α = 1.5 x 10^{-4} ($^\circ$K)$^{-1}$, and β = 0.8 x 10^{-3} (ppt)$^{-1}$. If vertical density stratification is stable ($\rho_3 > \rho_2$), the vertical volume transport q_m is upwards and a function of both vertical density contrast and thermocline depth,

$$q_m = q_{mr}\left(\frac{\rho_{3r} - \rho_{2r}}{\rho_3 - \rho_2}\right)^{\varsigma}\left(\frac{D_r}{D}\right)^{\eta}. \qquad \text{(A1.18)}$$

This formulation does not represent convective processes that would occur if the lower layer becomes less dense than the upper layer ($\rho_3 \le \rho_2$). However, this unstable situation never occurs in our model experiments. The exponents ς and η in equation (A1.18) can be set to represent different mixing assumptions (see text).

Equations (A1.5 – A1.12) for an asymmetric circulation with sinking in the north and upwelling in the south can be re-expressed in a form that covers all possible

circulation states (asymmetric flow with northern sinking, asymmetric flow with southern sinking, and equatorially symmetric flow):

$$\frac{dT_1}{dt} = \frac{1}{V_1}\left[0.5\left(|q_1| + q_1\right)\left(T_2 - T_1\right) + 0.5\left(|q_1| - q_1\right)\left(T_3 - T_1\right) + \kappa A_1\left(T_p - T_1\right)\right] \quad \text{(A1.19)}$$

$$\frac{dS_1}{dt} = \frac{1}{V_1}\left[0.5\left(|q_1| + q_1\right)\left(S_2 - S_1\right) + 0.5\left(|q_1| - q_1\right)\left(S_3 - S_1\right) - \left(\varphi_1 + ff\right)S_1\right] \quad \text{(A1.20)}$$

$$\frac{dT_2}{dt} = \frac{1}{V_2}\left[0.5\left(|q_1| - q_1\right)\left(T_1 - T_2\right) + 0.5\left(|q_4| - q_4\right)\left(T_4 - T_2\right) + 0.5\left(|q_m| + q_m\right)\left(T_3 - T_2\right) + \kappa A_2\left(T_e - T_2\right)\right]$$

(A1.21)

$$\frac{dS_2}{dt} = \frac{1}{V_2}\left[0.5\left(|q_1| - q_1\right)\left(S_1 - S_2\right) + 0.5\left(|q_4| - q_4\right)\left(S_4 - S_2\right) + 0.5\left(|q_m| + q_m\right)\left(S_3 - S_2\right) + \left(\varphi_1 + \varphi_4\right)S_2\right]$$

(A1.22)

$$\frac{dT_3}{dt} = \frac{1}{V_3}\left[0.5\left(|q_1 + \varphi_1| + q_1 + \varphi_1\right)\left(T_1 - T_3\right) + 0.5\left(|q_4 + \phi_4| + q_4 + \varphi_4\right)\left(T_4 - T_3\right)\right] \quad \text{(A1.23)}$$

$$\frac{dS_3}{dt} = \frac{1}{V_3}\left[0.5\left(|q_1 + \varphi_1| + q_1 + \varphi_1\right)\left(S_1 - S_3\right) + 0.5\left(|q_4 + \phi_4| + q_4 + \varphi_4\right)\left(S_4 - S_3\right)\right] \quad \text{(A1.24)}$$

$$\frac{dT_4}{dt} = \frac{1}{V_4}\left[0.5\left(|q_4| + q_4\right)\left(T_2 - T_4\right) + 0.5\left(|q_4| - q_4\right)\left(T_3 - T_4\right) + \kappa A_4\left(T_p - T_4\right)\right] \quad \text{(A1.25)}$$

$$\frac{dS_4}{dt} = \frac{1}{V_4}\left[0.5\left(|q_4| + q_4\right)\left(S_2 - S_4\right) + 0.5\left(|q_4| - q_4\right)\left(S_3 - S_4\right) - \varphi_4 S_4\right] \quad \text{(A1.26)}$$

Table A1 Parameters of the 4-box ocean model.

Symbol	Description	Value
A_1	Area box 1	0.8×10^{13} m^2
A_2	Area box 2	6.4×10^{13} m^2
A_4	Area box 4	0.8×10^{13} m^2
A_o	Area of global ocean	3.61×10^{14} m^2
D_i	Initial depth box 2	500 m
H	Depth of ocean	4000 m
V_1	Volume box 1	3.2×10^{16} m^3
V_2	Volume box 2	3.2×10^{16} m^3
V_3	Volume box 3	9.6×10^{16} m^3
V_4	Volume box 4	3.2×10^{16} m^3
T_p	Temperature of bath for poles	0 ℃
T_e	Temperature of bath for equator	30 ℃
κ	Thermal exchange velocity	1.7×10^{-6} m s^{-1}
$q_{1\mathrm{r}}$	Reference volume flux box 1	6 Sv
$q_{4\mathrm{r}}$	Reference volume flux box 4	6 Sv
q_{mr}	Reference vertical mixing flux	12.2 Sv
φ_1	NH atmospheric moisture flux	0.1 Sv
φ_2	SH atmospheric moisture flux	0.1 Sv
T_{1i}	Initial temperature box 1	2.75 ℃
T_{2i}	Initial temperature box 2	24.3 ℃
T_{3i}	Initial temperature box 3	2.75 ℃
T_{4i}	Initial temperature box 4	2.75 ℃
S_{1i}	Initial salinity box 1	35.0 psu
S_{2i}	Initial salinity box 2	35.6 psu
S_{3i}	Initial salinity box 3	35.0 psu
S_{4i}	Initial salinity box 4	35.0 psu
ρ_o	Mean ocean density	1028 kg m^{-3}
α	Thermal expansion coefficient	1.5×10^{-4} (℃)$^{-1}$
β	Salinity expansion coefficient	0.8×10^{-3} (ppt)$^{-1}$
dt	Time step	1.58×10^{7} s

Appendix 2

3-box model configuration

The single-hemisphere 3-box ocean model is designed to replicate the scaling arguments about the effects of freshwater forcing on MOC under different mixing assumptions [*Nilsson and Walin*, 2001]. I present those results here. Figure A2 shows the equilibrium responses of MOC to changes in freshwater forcing in the 3-box model (numerical results) as compared to scaling theory. The slight differences in slope in Figure A2 panel (b) come from mathematical simplifications that were used by *Nilsson and Walin* [2001] who assume $q_m = q_1$ in the mass conservation equation, whereas I show the accurate expression is $q_m = q_1 + \varphi_1$.

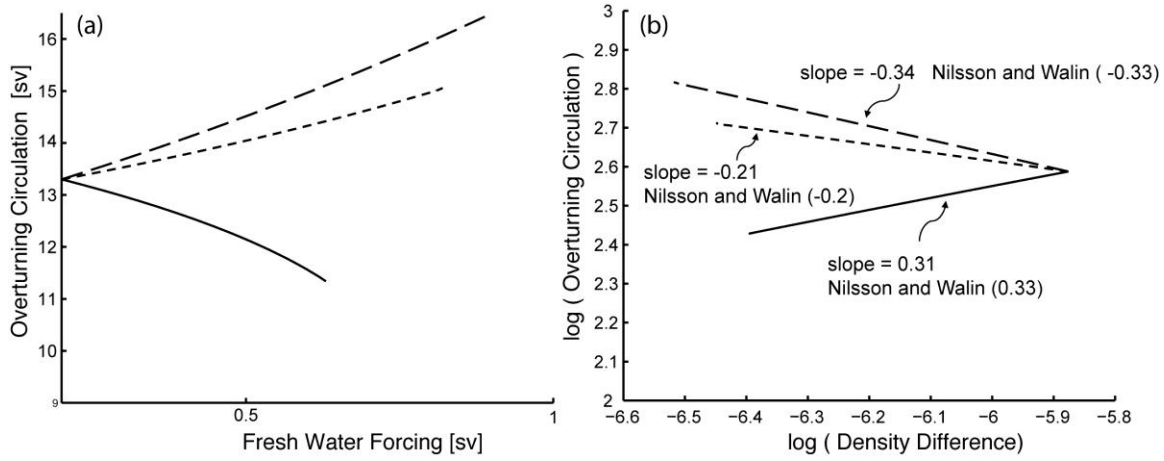

Figure A2. Sensitivity of overturning circulation to freshwater forcing in a single hemisphere 3-box ocean model. Panel (a) compares the equilibrium response to fresh water forcing for different assumptions about vertical mixing: constant vertical mixing (solid line), stability dependent mixing (short dashed line), and constant mixing energy

(long dashed line). Panel (b) compares the responses in the box model to the responses deduced from scaling theory [Nilsson and Walin 2001]. Density contrast shown in panel (b) is that between the polar box and the surface equatorial box.

Appendix 3

4-box model linearization

The overturning circulation can be decomposed into 0th, 1st, 2nd, 3rd order terms by substituting for each quantity a mean "x_{eq}" and a perturbation "dx", e.g. "$x = x_{eq} + dx$"

$$q_1 = q_{1r} \frac{(\rho_1 * H - \rho_2 * D - \rho_3 * (H - D)) * D}{(\rho_{1r} * H - \rho_{2r} * D_r - \rho_{3r} * (H - D_r)) * D_r} \quad . \qquad \text{(A3.1.1)}$$

In equation (A3.1.1), the constant factors are

$$C_1 = q_{1r} \frac{1}{(\rho_{1r} * H - \rho_{2r} * D_r - \rho_{3r} * (H - D_r)) * D_r} \quad . \qquad \text{(A3.1.2)}$$

There are eight terms in total from the 0th to 3rd order. The equations for q_1 also apply for q_4 when switching q_4 for q_1.

The two 0th order terms are

$$q_{10A} = C_1 * (\rho_{3eq} - \rho_{2eq}) * D_{eq} * D_{eq} \qquad \text{(A3.1.3)}$$

$$q_{10B} = C_1 * (\rho_{1eq} - \rho_{3eq}) * H * D_{eq} \quad . \qquad \text{(A3.1.4)}$$

The four 1st order terms are

$$q_{11A} = C_1 * 2 * (\rho_{3eq} - \rho_{2eq}) * D_{eq} * dD \qquad \text{(A3.1.5)}$$

$$q_{11B} = C_1 * (d\rho_1 - d\rho_3) * H * D_{eq} \qquad \text{(A3.1.6)}$$

$$q_{11C} = C_1 * (d\rho_3 - d\rho_2) * D_{eq} * D_{eq} \qquad \text{(A3.1.7)}$$

$$q_{11D} = C_1 * (\rho_{1eq} - \rho_{3eq}) * H * dD \quad . \qquad \text{(A3.1.8)}$$

The 2nd order terms are

$$q_{12A} = C_1 * 2 * (d\rho_3 - d\rho_2) * D_{eq} * dD \qquad \text{(A3.1.9)}$$

$$q_{12B} = C_1 * (d\rho_1 - d\rho_3) * H * dD \qquad \text{(A3.1.10)}$$

$$q_{12C} = C_1 * (\rho_{3eq} - \rho_{2eq}) * dD * dD \quad . \qquad \text{(A3.1.11)}$$

The 3rd order term is

$$q_{13A} = C_1 * 2 * (d\rho_3 - d\rho_2) * dD * dD \quad . \qquad \text{(A3.1.12)}$$

References

Alley, R. B., Anandakrishnan, S. & Jung, P. (2001) Stochastic resonance in the North Atlantic. *Paleoceanography*, **16**, 190 –198.

Alley, R. B., and D. R. MacAyeal (1994), Ice-rafted debris associated with binge/purge oscillations of the Laurentide Ice Sheet, *Paleoceanography*, 9(4), 503-511.

Berger, A., (1978) Long-term variations of caloric insolation resulting from the Earth's orbital elements. *Quat. Res.*, **9**, 139-167.

Blunier, T. & Brook, E. J. (2001) Timing of millennial-scale climate change in Antarctica and Greenland during the last glacial period. *Science* **291**, 109–112.

Bond, G., W. S. Broecker, S. J. Johnsen, J. McManus, L. Labeyrie, J. Jouzel, and G. Bonani (1993), Correlations between climate records from North Atlantic sediments and Greenland ice, *Nature*, 365, 143-147.

Bond, G. C., and R. Lotti (1995), Iceberg discharges into the North Atlantic on millennial time scales during the last glaciation, *Science*, 267, 1005-1010.

Bond, G., B. Kromer, J. Beer, R. Muscheler, M. N. Evans, W. Showers, S. Hoffmann, R. Lotti-Bond, I. Hajdas, and G. Bonani (2001), Persistent Solar Influence on North Atlantic Climate During the Holocene, *Science* 294(5549), 2130, DOI: 10.1126/science.1065680.

Broecker, W. S., G. Bond, and M. Klas (1990), A salt oscillator in the glacial Atlantic? 1. The concept, *Paleoceanography*, 5, 469-477.

Bugnion, V., C. Hill, and P.H. Stone (2006a), An Adjoint Analysis of the Meridional Overturning Circulation in an Ocean Model. *J. Climate*, **19**, 3732–3750.

Bugnion, V., C. Hill, and P.H. Stone (2006b) An Adjoint Analysis of the Meridional Overturning Circulation in a Hybrid Coupled Model. *J. Climate*, **19**, 3751–3767.

Cane, M. (1998) A role for the tropical Pacific, *Science*, 282, 59-60.

Cane, M., and A. C. Clement (1999), A role for the tropical Pacific coupled ocean-atmosphere system on Milankovitch and millennial timescales. Part II: Global impacts, R. Webb, P. U. Clark, and L. D. Keigwin (Eds.), *Mechanisms of Global Climate Change at Millennial Time Scales*, Am. Geophys. Union, Geophysical Monograph vol 12, 373-383.

Chappell, J. (2002), Sea level changes forced ice breakouts in the Last Glacial cycle: new results from coral terraces, *Quaternary Science Reviews*, 21, 1229-1240.

Chappell, J., Omura, A., Esat, A., McCulloch, T., Pandolfi, M. and Pillans, J., (1996) Reconciliation of late Quaternary sea levels derived from coral terraces at Huon Peninsula with deep sea oxygen isotope records. *Earth and Planetary Science Letters* 141, 227–236.

Chu, P.C., Y. Chen, and S. Lu (1998), On Haney-Type Surface Thermal Boundary Conditions for Ocean Circulation Models. *J. Phys. Oceanogr.*, **28**, 890–901.

Clark, P. U., N. G. Pisias, T. F. Stocker, and A. J. Weaver (2002), The role of the thermohaline circulation in abrupt climate change, *Nature*, 415, 863-869.

Curry, W. B., J. C. Duplessy, L. D. Labeyrie, and N. J. Shackleton (1988), Changes in the distribution of d13C of deepwater total CO2 between the last glaciation and the Holocene, *Paleoceanography*, 3, 317-341.

De Boer, A. M., N. R. Edwards, A. J. Watson (2010) Meridional Density Gradients Do Not Control the Atlantic Overturning Circulation. *Journal of Physical Oceanography*, 40(2), 368-380, doi: 10.1175/2009JPO4200.1

Dijkstra, H.A., and W. Weijer (2005): Stability of the Global Ocean Circulation: Basic Bifurcation Diagrams. *J. Phys. Oceanogr.*, 35, 933–948.

Eisenman, E., C. Bitz, and E. Tziperman (2009): Rain driven by receding ice sheets as a cause of past climate change. *Paleoceanography* 24, PA4209.

EPICA community members (2006) One-to-one coupling of glacial climate variability in Greenland and Antarctica. *Nature*, 444, 195-198, doi:10.1038/nature05301.

Etheridge, D.M., L.P. Steele, R.L. Langenfelds, R.J. Francey, J.-M. Barnola, and V.I. Morgan (1996) Natural and anthropogenic changes in atmospheric CO2 over the last 1000 years from air in Antarctic ice and firn. *Journal of Geophysical Research* **101**, 4115-4128.

Fairbanks, R. G. (1989) A 17,000 year glacial euststic sea level record: influence of glacial melting rates on the Younger Dryas event and deep ocean circulation. *Nature* **342**, 637–641.

Fichefet, T., S. Hovine, and J-C. Duplessy (1994) A model study of the Atlantic thermohaline circulation during the last glacial maximum. *Nature*, **372**, 252-255.

Ganopolski, A., and S. Rahmstorf (2001), Rapid changes of glacial climate simulated in a coupled climate model, Nature, 409, 153-158.

Gelman, A., J. B. Carlin, H.S. Stern, and D.B. Rubin (2004), *Bayesian Data Analysis*. 2nd ed. Chapman and Hall, 668 pp.

Gildor, H., E. Tziperman (2003) Sea-ice Switches and abrupt climate change, Phil. Trans. R. Soc. Lond. A, 361, 1935-2944. Doi: 10.1098/rsta.2003.1244

Gnanadesikan, A. (1999), A simple predictive model for the structure of the oceanic pycnocline. Science, 283(5410), 2077-2079.

Grootes, P. M., and M. Stuiver (1997), Oxygen 18/16 variability in Greenland snow and ice with 10^{-3}- to 10^{5}-year time resolution, Journal of Geophysical Research, 102, 26,455-26,470.

Grootes, P., Stuiver, M., White, J. W. C., Johnsen, S. & Jouzel, J. (1993) Comparison of oxygen isotope records from the GISP2 and GRIP Greenland ice cores. *Nature* **366**, 552-554.

Haney, R. (1971), Surface thermal boundary condition for ocean circulation models, *J. Phys. Oceanogr.* 1, 241–248

Hemming, S. R. (2004) Heinrich events: Massive late Pleistocene detritus layers of the North Atlantic and their global climate imprint. *Rev. Geophys.*, **42**, RG1005, doi:10.1029/2003RG000128.

Higdon, D., M. Kennedy, J. C. Cavendish, J. A. Cafeo, and R. D. Ryne (2004) Combining field data and computer simulations for calibration and prediction, SIAM Journal on Scientific Computing, 26, 448-466.

Hong, T., and M. K. Sen (2009) A new MCMC algorithm for seismic waveform inversion and corresponding uncertainty analysis, *Geophys. J. Int.* doi:10.1111/j.1365-246X.2008.04052.x

Huang, R.X., Mixing and energetics of the ocean thermohaline circulation, J. Phys. Oceanogr., 29, 727-746, 1999.

Huber, C., M. Leuenberger, R. Spahni, J. Fluckiger, J. Schwander, T. F. Stocker, S. Johnsen, A. Landais and J. Jouzel (2006), Isotope calibrated Greenland temperature record over Marine Isotope Stage 3 and its relation to CH4, *Earth and Planetary Science Letters*, 243(3-4), 504-519.

Hulbe, C. L. (1997), An ice shelf mechanism for Heinrich layer production, *Paleoceanography*, 12, 711 –717.

Indermühle A., T.F. Stocker, F. Joos, H. Fischer, H.J. Smith, M. Wahlen, B. Deck, D. Mastroianni, J. Tschumi, T. Blunier, R. Meyer, B. Stauffer (1999a) Holocene carbon-cycle dynamics based on CO2 trapped in ice at Taylor Dome, Antarctica. *Nature* **398**, 121-126.

Indermühle, A., E. Monnin, B. Stauffer, T.F. Stocker, M. Wahlen (1999b) Atmospheric CO2 concentration from 60 to 20 kyr BP from the Taylor Dome ice core, Antarctica. *Geophysical Research Letters*, **27**, 735-738.

Jackson, C. (2000), Sensitivity of stationary wave amplitude to regional changes in Laurentide ice sheet topography in single-layer models of the atmosphere, J. Geophys. Res., 105 (D19), 24443-24454.

Jackson, C., and A. J. Broccoli (2003) Orbital Forcing of Arctic Climate: Mechanisms of climate response and implications for continental glaciation, *Climate Dynamics*, 21, 539-557, DOI: 10.1007/s00382-003-0351-3.

Jackson, C. S. (2009) Use of Bayesian Inference and Data to Improve Simulations of Multi-physics Climate Phenomena. *Journal of Physics: Conference Series* 180 doi:10.1088/1742-6596/180/1/012029

Jackson, C., M. Sen, and P. Stoffa (2004) An Efficient Stochastic Bayesian Approach to Optimal Parameter and Uncertainty Estimation for Climate Model Predictions, *Journal of Climate*, 17(14), 2828-2841.

Jackson, C. S., O. Marchal, Y. Liu, S. Lu, W. G. Thompson "A box-model test of the freshwater forcing hypothesis of abrupt climate change and the physics governing ocean stability" (submitted to Paleoceanography).

Jackson, C. S., M. K. Sen, G. Huerta, Y. Deng, and K. P. Bowman (2008) Error Reduction and Convergence in Climate Prediction. *Journal of Climate*, 21(24), 6698-6709.

Jackson, C., Y. Xia, M. Sen, and P. Stoffa (2003) Optimal parameter and uncertainty estimation of a land surface model: A case example using data from Cabauw, Netherlands, *Journal of Geophysical Research*, 108 (D18), 4583 10.1029/2002JD002991.

Johnsen, S. J., W. Dansgaard, H. B. Clausen, C. C. Langway Jr. (1972) Oxygen isotope profiles through the Antarctic and Greenland ice sheets. *Nature* **235**, (5339), 429-434.

Keeling, C. D., and T. P. Whorf (2000), The 1,800-year oceanic tidal cycle: A possible cause of rapid climate change, Proceedings of the National Academy of Sciences, 97, 3814-3819.

Kennedy, M. C., and A. O'Hagan (2001) Bayesian calibration of computer models, Journal of the Royal Statistical Society. Series B, Statistical Methodology, 63, 425-464.

Knutti, R., J. Fluckinger, T. F. Stocker, A. Timmermann (2004) Strong hemispheric oupling of glaicial climate through freshwater discharge and ocean circulation. Nature. 430(7002), 851-856, doi: 10.1038/nature02786

Knutti, R., and T.F. Stocker (2002) Limited Predictability of the Future Thermohaline Circulation Close to an Instability Threshold. *J. Climate*, **15**, 179–186.

Kuhlbrodt, T., A. Griesel, M. Montoya, A. Levermann, M. Hofmann, and S. Rahmstorf (2007), On the driving processes of the Atlantic meridional overturning circulation, Rev. Geophys., 45, RG2001, doi:10.1029/2004RG000166.

Landais, A., J. M. Barnola,V. Masson-Delmotte, J. Jouzel, J. Chappellaz, N. Caillon, C. Huber, M. Leuenberger, and S. J. Johnsen (2004), A continuous record of temperature evolution over a sequence of Dansgaard-Oeschger events during Marine Isotopic Stage 4 (76 to 62 kyr BP), Geophys. Res. Lett., 31, L22211, doi:10.1029/2004GL021193.

Lang, C., M. Leuenberger, J. Schwander, and S. Johnsen (1999), 16 ℃ rapid temperature variation in Central Greenland 70,000 years ago, Science, 286, 934-937.

Liu, Z., B. L. Otto-Bliesner, F. He, E. C. Brady, R. Tomas, P. U. Clark, A. E. Carlson, J. Lynch-Stieglitz, W. Curry, E. Brook, D. Erickson, R. Jacob, J. Kutzbach, and J. Cheng (2009) Transient Simulation of Last Deglaciation with a New Mechanism for Bølling-Allerød Warming. *Science* 325 (5938), 310. DOI: 10.1126/science.1171041

Loving, J. L., and G. K. Vallis (2005), Mechanisms for climate variability during glacial and interglacial periods, *Paleoceanography*, 20, PA4024, doi:10.1029/2004PA001113.

Lu, S., C. S. Jackson, O. Marchal "Box model perturbation analysis of Atlantic Ocean's response to freshwater forcing" (In prep to be submitted to Tellus A).

Lu, S., C. S. Jackson, O. Marchal, W. G. Thompson, L. E. Gulden, T. F. Stocker Consistent Observational and Modeling Support for Ice Sheet Forcing of Abrupt Climate Change (submitted to *Paleoceanography*).

Lucarini V, and P. H Stone (2005a), Thermohaline circulation stability: A box model study. Part I: Uncoupled model. *J. Climate*, **18**, 501–513.

Lucarini, V., and P.H. Stone (2005b), Thermohaline Circulation Stability: A Box Model Study. Part II: Coupled Atmosphere–Ocean Model. *J. Climate*, **18**, 514–529.

MacAyeal, D. R. (1993), Binge/purge oscillations of the Laurentide ice sheet as a cause of the North Atlantic Heinrich events, *Paleoceanography*, 8, 775-784.

Manabe, S., and R. J. Stouffer (1988), Two stable equilibria of a coupled ocean-atmosphere model, *Journal of Climate*, 1, 841-866.

Manabe, S., and R. J. Stouffer (1994), Multiple-Century Response of a Coupled Ocean-Atmosphere Model to an Increase of Atmospheric Carbon Dioxide, J. Climate, 7, 5–23.

Manabe, S., and R. J. Stouffer (1999), Are two modes of thermohaline circulation stable? *Tellus* 51A, 400-411.

Marchal, O., T. F. Stocker, and F. Joos (1998), Impact of oceanic reorganizations on the ocean carbon cycle and atmospheric carbon dioxide content, *Paleoceanography*, 13, 225-244.

Marchal, O., T. F. Stocker, and F. Joos (1999a), Physical and biogeochemical responses to freshwater-induced thermohaline variability in a zonally averaged ocean model, in *Mechanisms of Global Climate Change at Millennial Time Scales*, *Geophysical Monograph*, vol. 112, edited by R. Webb, P. U. Clark, and L. D. Keigwin, pp. 263-284, AGU, Washington, D. C.

Marchal, O., T. F. Stocker, F. Joos, A. Indermuhle, T. Blunier, and J. Tschumi (1999b), Modelling the concentration of atmospheric CO2 during the Younger Dryas climate event, *Climate Dynamics*, 15, 341-354.

Marchal O., Jackson C., Nilsson J., Paul A., and Stocker T. F. (2007), Buoyancy-driven flow and nature of vertical mixing in a zonally averaged model, in "Ocean Circulation: Mechanisms and Impacts ", A. Schmittner, J. C. H. Chiang, and S. R. Hemming (editors), American Geophysical Union, Washington, DC, Geophysical Monograph 173, 33-52.

Marotzke, J., and J. Willebrand (1991), Multiple equilibria of the global thermohaline circulation, *Journal of Physical Oceanography*, 21, 1372-1385.

Marshall, S. J., G. K. C. Clarke (1999) Modeling North American Freshwater Runoff through the Last Glacial Cycle, *Quaternary Research*, 52, 3, 300-315, DOI: 10.1006/qres.1999.2079.

Marshall, S. J. & Koutnik, M. R. (2006) Ice sheet action versus reaction: Distinguishing between Heinrich events and Dansgaard-Oeschger cycles in the North Atlantic. *Paleoceanography*, **21**, PA2021, doi:10.1029/2005PA001247.

Marchal O., Jackson C., Nilsson J., Paul A., and Stocker T. F., Buoyancy-driven flow and nature of vertical mixing in a zonally averaged model, in "Ocean Circulation: Mechanisms and Impacts ", A. Schmittner, J. C.H. Chiang, and S. R. Hemming (editors), American Geophysical Union, Washington, DC, Geophysical Monograph 173, 33-52, 2007.

Marzeion, B., A. Levermann, J. Mignot (2007) The role of stratification-dependent mixing for the stability of the Atlantic overturning in a global climate model. Journal of Physical Oceanography. 37, 2672-2681, doi:10.1175/2007JPO3641.1

Marzeion, B., and H. Drange, 2006: Diapycnal mixing in a conceptual model of the Atlantic Meridional Overturning Circulation. Deep-Sea Res. II, 53, 226–238.

Meehl, G.A., T.F. Stocker, W. Collins, P. Friedlingstein, A. Gaye, J. Gregory, A. Kitoh, R. Knutti, J. Murphy, A. Noda, I. Watterson, A.J. Weaver, and Z.-C. Zhao, Global Climate Projections, in *Climate Change 2007: The Physical Science Basis. Contribution of Working Group I to the Fourth Assessment Report of the Intergovernmental Panel on Climate Change*, edited by S. Solomon, *et al.*, pp. 747-845, Cambridge University Press, 2007.

Meese, D. A. et al. (1997) The Greenland ice sheet project 2 depth-age scale: methods and results. *J. Geophys. Res.*, **102** (C12), 26411–26423.

Meissner, K. J., A. Schmittner, E. C. Wiebe, and A. J. Weaver (2002) Simulations of Heinrich Events in a coupled ocean-atmosphere-sea ice model. *Geophys. Res. Letters*, 29(14) 10.1029/2001GL013514

Mikolajewicz, U., and E. Maier-Reimer (1994), Mixed boundary conditions in ocean general circulation models and their influence on the stability of the model's conveyor belt, *Journal of Geophysical Research*, 99, 22633-22644.

Miller GH, de Vernal A (1992) Will greenhouse warming lead to Northern Hemisphere ice-sheet growth? *Nature* 355, 244–246.

Mohammad, R., and J. Nilsson, The role of diapycnal mixing for the equilibrium response of the thermohaline circulation, *Ocean Dynamics*, 54, 54-65, 2004.

Mohammad, R., and J. Nilsson, Symmetric and asymmetric modes of the thermohaline circulation, *Tellus, Ser. A*, 58, 616-627, 2006.

Monnin, E., A. Indermühle, A. Dallenbach, J. Fluckiger, B. Stauffer, T. F. Stocker, D. Raynaud, and J-M, Barnola (2001) Atmospheric CO2 Concentrations over the Last Glacial Termination. *Science* **291**(5501) 112-114 [DOI:10.1126/science.291.5501.112]

Nilsson, J., and G. Walin (2001), Freshwater forcing as a booster of thermohaline circulation. Tellus, 53A, 629-641.

Nilsson, J., G. Broström, and G. Walin (2003), The thermohaline circulation and vertical mixing: Does weaker density stratification give stronger overturning?, *J. Phys. Oceanogr.*, 33, 2781-2795.

Ottera OH, Drange H, Bentsen M, Kvamst NG, Jiang D (2003), The sensitivity of the present-day atlantic meridional overturning circulation to freshwater forcing. Geophys Res Lett 30(17): 1898

Peltier, W. R. (1994) Ice age paleotopography. *Science* **265**, 195–201.

Petit J.R., Jouzel J., Raynaud D., Barkov N.I., Barnola J.M., Basile I., Bender M., Chappellaz J., Davis J., Delaygue G., Delmotte M., Kotlyakov V.M., Legrand M., Lipenkov V., Lorius C., Pépin L., Ritz C., Saltzman E., Stievenard M., (1999) Climate and Atmospheric History of the Past 420,000 years from the Vostok Ice Core, Antarctica, **Nature**, **399**, pp.429-436.

Prahl, M., G. Lohmann, and A. Paul (2003), Influence of vertical mixing on the thermohaline hysteresis: Analysis of an OGCM. *J. Phys. Oceanogr.*, 33, 1707–1721.

Rahmstorf, S. (2003), Timimg of abrupt climate change: A precise clock, Geophys. Res. Lett., 30(10), 1510, doi:10.1029/2003GL017115.

Roche, D., D. Paillard, and E. Cortijo (2004) Constraints on the duration and freshwater release of Heinrich event 4 through isotope modeling. *Nature*, 432, 379-382. Doi:10.1038/nature03059.

Rohling, E. J., K. Grant, M. Bolshaw, A. P. Roberts, M. Siddall, Ch. Hemleben and M. Kucera (2009) Antarctic temperature and global sea level closely coupled over the past five glacial cycles. *Nature Geoscience*, **2**, 500-504, doi:10.1038/ngeo557.

Rohling, E.J., R. Marsh, N.C. Wells, M. Siddall and N.R. Edwards (2004), Similar 1885 meltwater contributions to glacial sea level changes from Antarctic and northern ice 1886 sheets, Nature, 430, 1016-1021.

Ruddiman WF, McIntyre A (1981) Oceanic mechanisms for amplification of the 23,000-

year ice-volume cycle. *Science*, 212, 617–627.

Sakai, K., and W. R. Peltier (1997) Dansgaard-Oeschger oscillations in a coupled atmosphere-ocean climate model, *Journal of Climate*, **10**, 949-970.

Saenko, O. A., and A. J. Weaver (2003), Southern Ocean upwelling and eddies: sensitivity of the global overturning to the surface density range, *Tellus*, **55**A, 106-111.

Schmittner, A. and T. F. Stocker (2001) A seasonally forced ocean-atmosphere model for paleoclimate studies. *J. Climate* **14**, 1055-1068.

Schmittner, A., and A. J. Weaver (2001), Dependence of multiple climate states on ocean mixing parameters, Geophysical Research Letters, 28(6), 1027-1030.

Schmittner, A., M. Yoshimori, and A. J. Weaver (2002), Instability of glacial climate in a model of the ocean-atmosphere-cryosphere system, Science, 295, 1489-1493.

Schulz, M., W. H. Berger, M. Sarnthein, and P. M. Grootes (1999) Amplitude variations of 1470-year climate oscillations during the last 100,000 years linked to fluctuations of continental ice mass. *Geophys. Res. Lett.*, 26, 3385-3388.

Schulz, M. (2002) The tempo of climate change during Dansgaard-Oeschger interstadials and its potential to affect the manifestation of the 1470-year climate cycle. *Geophys. Res. Lett.*, 29 (1), 10.1029/2001GL013277.

Schulz, M., A. Paul, and A. Timmermann (2002) Relaxation oscillators in concert: A framework for climate change at millennial timescales during the late Pleistocene. *Geophys. Res. Lett.*, 29 (24), 10.1029/2002GL016144.

Sen, M.K., and P.L. Stoffa, (1996) Bayesian inference, Gibbs' sampler and uncertainty estimation in geophysical inversion, *Geophysical Prospecting*, 44, 313-350.

Severinghaus, J. P., T. Sowers, E. J. Brook, R. B. Alley, and M. L. Bender (1998), Timing of abrupt climate change at the end of the Younger Dryas interval from thermally fractionated gases in polar ice, Nature, 391, 141-146.

Shackleton, N. J. (1987) Oxygen isotopes, ice volume and sea level. *Quat Sci Rev* **6**: 183-190.

Shackleton, N. J., R.G. Fairbanks, T.-C. Chiu, and F. Parrenin (2004) Absolute calibration of the Greenland time scale: implications for Antarctic time scales and for $\Delta^{14}C$, *Quaternary Science Reviews* **23**, 1513–1522.

Siddall, M., E. J. Rohling, A. Almogi-Labin, Ch. Hemleben, D. Meischner, I. Schmelzer, D. A. Smeed (2003), Sea-level fluctuations during the last glacial cycle, Nature, 423, 853-858.

Siddall, M., Rohling, E. J., Thompson, W. G. & Waelbroeck, C. (2008) Marine isotope stage 3 sea level fluctuations: data synthesis and new outlook. *Rev. Geophys.*, **46**, RG4003, doi:10.1029/2007RG000226.
Sima, A., A. Paul and M. Schulz (2004) The Younger Dryas -- an intrinsic feature of late Pleistocene climate change at millennial timescales. *Earth Planet. Sci. Lett*., 222, 741-750.

Stocker, T. F. & Johnsen, S. J. (2003) A minimum thermodynamic model for the bipolar seesaw. *Paleoceanography* **18**, doi:10.1029/2003PA000920.

Stocker, T.F., and O. Marchal (2000) Abrupt climate change in the computer: is it real?, *Proceedings of the U.S. National Academy of Sciences*, *97*, 1362-1365.

Stocker, T. F., and D. G. Wright (1991) Rapid transitions of the ocean's deep circulation induced by changes in surface water fluxes. *Nature*, *351*, 729-732.

Stocker, T. F., Wright, D. G. & Mysak, L. A. (1992) A zonally averaged, coupled ocean-atmosphere model for paleoclimate studies. *J. Climate*, **5**, 773-797.

Stouffer, R., et al. (2006), Investigating the Causes of the Response of the Thermohaline Circulation to Past and Future Climate Changes, Journal of Climate, 19, 1365-1387.

Thual, O., and J. C. McWilliams (1992), The catastrophe structure of thermohaline convection in a two-dimensional fluid model and a comparison with low-order box models, Geophys. Astrophys. Fluid Dynamics, 64, 67-95.

Timmermann, A., Gildor, H., Schulz, M. and Tziperman, E. (2003): Coherent resonant millennial-scale climate oscillations triggered by massive meltwater pulses. *Journal of Climate*, 16, 2569-2585.

Toggweiler, J. R., and B. Samuels (1998), On the Ocean's Large-Scale Circulation near the Limit of No Vertical Mixing, Journal of Physical Oceanography, 28, 1832-1852.

Thompson, W. G., and S. L. Goldstein (2006), A radiometric calibration of the SPECMAP timescale, *Quaternary Science Reviews*, 25(23-24), 3207-3215.

van Geel, B., O. M. Raspopov, H. Renssen, J. van der Plicht, V. A. Dergachev, and H. A. J. Meijer, (1999) The role of solar forcing upon climate change, Quaternary Science Reviews, 18, 331-338.

van Kreveld, S., N. Sarnthein, H. Erlenkeuser, P. Grootes, S. Jung, M. J. Nadeau, U. Pflaumann, and A. Voelker (2000), Potential links between surging ice sheets, circulation changes, and the Dansgaard-Oeschger cycles in the Irminger Sea, Paleoceanography, 15, 425-442.

Villagran, A., G. Huerta, C. S. Jackson, M. K. Sen (2008) Parameter Uncertainty Estimation in Climate Models. *Bayesian Analysis* 3(4), 823-850. DOI:10.1214/08-BA331

Voelker, A. H. L., (2002), Global distribution of centennial-scale records for Marine Isotope Stage (MIS) 3: a database, *Quaternary Science Reviews*, **21**(10), 1185-1212.

Waelbroeck, C., L. Labeyrie, E. Michel, J. C. Duplessy, J. F. McManus, K. Lambeck, E. Balbon, and M. Labracherie (2002), Sea-level and deep water temperature changes derived from benthic foraminifera isotopic records, Quaternary Science Reviews, 21(1-3), 295-305.

Wang, F. (2007), Investigating ENSO sensitivity to mean climate in an intermediate model using a novel statistical technique, *Geophys. Res. Lett.*, **34**, L07705, doi:10.1029/2007GL029348.

Wang, Z., and L. A. Mysak (2000) A simple coupled atmosphere-ocean-sea ice-land surface model for climate and paleoclimate studies. *Journal of Climate*, **13**(6), 1150-1172.

Wang, Z., and Mysak, L. A. (2002) Simulation of the last glacial inception and rapid ice sheet growth in the McGill Paleoclimate Model. *Geophys. Res. Lett*., **29** (23), 2102, doi:10.1029/2002GL015120.

Weaver, A. J., and T. M. C. Hughes (1992), Stability and Variability of the thermohaline circulation and its links to climate, Trends in Physical Oceanography, 1, 15-70.

Weinelt, M., E. Vogelsang, M. Kucera, U. Pflaumann, M. Sarnthein, A. Voelker, H. Erlenkeuser, and B. A. Malmgren (2003), Variability of North Atlantic heat transfer during MIS 2, Paleoceanography, 18(3), 1071, doi:10.1029/2002PA000772.

Welander, P. (1982) A simple heat-salt oscillator. Dynamics of Atmospheres and Oceans, 6(4), 233-242.

Wright, D. G. & Stocker, T. F. (1992) Sensitivities of a zonally averaged global ocean circulation model. *J. Geophys. Res.*, **97**, 12707-12730.

Wright, D. G., and Stocker, T. F. (1993) Younger Drayas experiments. Ice in the Climate System. W. R. Peltier, Ed., NATO ASI Series, Vol. 12, Springer-Verlag, 395-416.

Wunsch, C. (2003), Greenland-Antarctic phase relations and millennial time-scale climate fluctuations in the Greenland cores, Quaternary Science Reviews 22, 1631–1646.

Wunsch, C., and R. Ferrari (2004), Vertical mixing, energy, and the general circulation of the oceans, *Annual Review of Fluid Mechanics*, **36**, 281-314.

Wunsch, C. (2006), Abrupt climate change: An alternative view, Quaternary Research, 65(2), 191-203.

Xia, Y., M. K. Sen, C. Jackson, and P. L. Stoffa (2004) Multi-dataset study of optimal parameter and uncertainty estimation of a land surface model with Bayesian Stochastic Inversion and multicriteria method, *Journal of Applied Meteorology*, 43 (10): 1477-1497.

Vita

Shaoping Lu was born in Changyi County, Weifang, Shandong Province, China in February, 1980. After graduating from Changyi No.1 Middle School in 1999, he entered University of Science and Technology of China (USTC) in Hefei. In July of 2004, he got the Bachelor of Science degree in Applied Physics from USTC. In August of 2004, he entered the Graduate School at the University of Texas at Austin, the Department of Physics. Since September 2006, he has been working as a Graduate Research Assistant in the University of Texas Institute for Geophysics (UTIG), Jackson School of Geosciences. He got the PhD degree of Physics from UT in August 2010.

Permanent mail address: Yuejia Cun, Dongzhong Xiang, Changyi Xian, Shandong, China, Postcode 261311

Permanent email address: shaoping.lu@gmail.com

This dissertation was typed by Shaoping Lu.